FROZEN ORBITS-NEAR CONSTANT OR BENEFICIALLY VARYING
ORBITAL PARAMETERS(U) AIR FORCE INST OF TECH
WRIGHT-PATTERSON AFB OH   R C MURROW 15 MAY 86

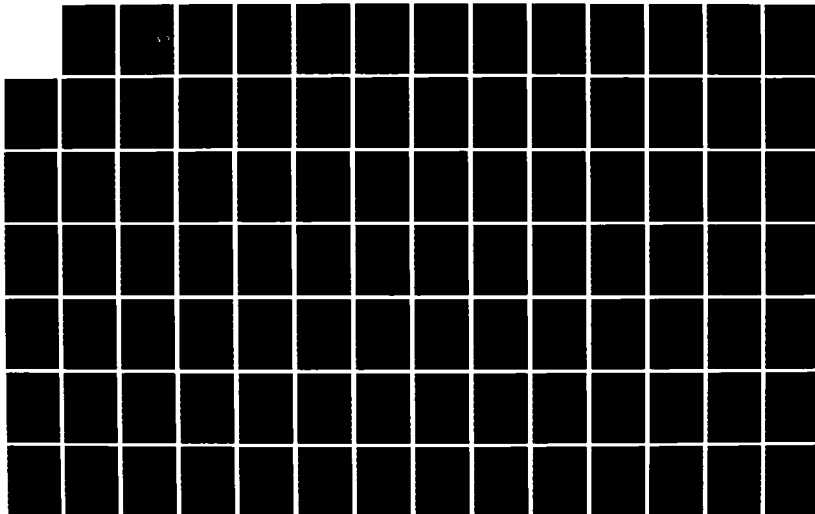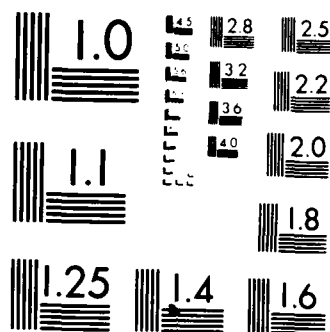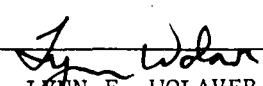MICROCOPY RESOLUTION TEST CHART

NATIONAL BUREAU OF STANDARDS 1963 A

AD-A170 675

REPORT DOCUMENTATION PAGE

READ INSTRUCTIONS
BEFORE COMPLETING FORM

1. REPORT NUMBER	2. GOVT ACCESSION NO.	3. RECIPIENT'S CATALOG NUMBER
AFIT/CI/NR 86-85D		

4. TITLE (and Subtitle)	5. TYPE OF REPORT & PERIOD COVERED
Frozen Orbits-Near Constant or Beneficially Varying Orbital Parameters	THESIS/DISSERTATION
	6. PERFORMING ORG. REPORT NUMBER

7. AUTHOR(s)	8. CONTRACT OR GRANT NUMBER(s)
Richard C. Murrow	

9. PERFORMING ORGANIZATION NAME AND ADDRESS	10. PROGRAM ELEMENT, PROJECT, TASK AREA & WORK UNIT NUMBERS
AFIT STUDENT AT: University of Colorado	

11. CONTROLLING OFFICE NAME AND ADDRESS	12. REPORT DATE
AFIT/NR	1986
WPAFB OH 45433-6583	13. NUMBER OF PAGES
	122

14. MONITORING AGENCY NAME & ADDRESS(if different from Controlling Office)	15. SECURITY CLASS. (of this report)
	UNCLAS
	15a. DECLASSIFICATION/DOWNGRADING SCHEDULE

16. DISTRIBUTION STATEMENT (of this Report)

APPROVED FOR PUBLIC RELEASE; DISTRIBUTION UNLIMITED

DTIC
ELECTE
AUG 1 2 1986
E

17. DISTRIBUTION STATEMENT (of the abstract entered in Block 20, if different from Report)

18. SUPPLEMENTARY NOTES

APPROVED FOR PUBLIC RELEASE: IAW AFR 190-1

LYNN E. WOLAVER 6 Aug 86
Dean for Research and
Professional Development
AFIT/NR

19. KEY WORDS (Continue on reverse side if necessary and identify by block number)

20. ABSTRACT (Continue on reverse side if necessary and identify by block number)

ATTACHED.

DD ₁ FORM ₇₃ 1473   EDITION OF 1 NOV 65 IS OBSOLETE

DTIC FILE COPY

86

FROZEN ORBITS– NEAR CONSTANT OR

BENEFICIALLY VARYING ORBITAL PARAMETERS

by

Richard C. Murrow

B.S., USAF Academy, 1970

M.S., Purdue University, 1971

M.B.A., Rensselaer Polytechnic Institute, 1981

A thesis submitted to the

Faculty of the Graduate School of the

University of Colorado in partial fulfillment

of the requirements for the degree of

Doctor of Philosophy

Department of Aerospace Engineering Sciences

1986

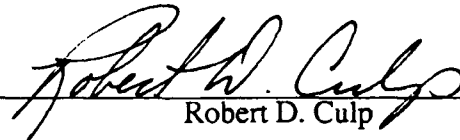This thesis for the Doctor of Philosophy degree by
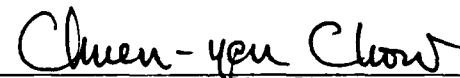
Richard C. Murrow

has been approved for the

Department of

Aerospace Engineering Sciences

by

Robert D. Culp

Chuen–Yen Chow

Date *May 15, 1986*

Murrow, Richard C. (Ph.D., Aerospace Engineering Sciences)

Frozen Orbits—Near Constant or Beneficially Varying Orbital Parameters

Thesis directed by Professor Robert D. Culp

If a satellite were experiencing pure Keplerian motion its orbital elements would remain constant. In actuality, each orbiting body is acted upon by various perturbing forces. Consequently, the orbital elements are continuously subject to change. The forces generating deviation from basic two–body motion consist of, but are not limited to: (1) the Earth's oblateness, (2) atmospheric drag, (3) lunar–solar gravitation, and (4) solar radiation pressure.

Whereas the magnitudes of such perturbing forces are small and varying compared to the gravity effects of the Earth, they are persistent and cause the resulting orbit to depart from its Keplerian counterpart. The variation of the five orbital elements which delineate the size, shape, and orientation of an elliptic orbit, can be determined with reasonable accuracy from existing theory. An understanding of disturbed orbital behavior permits possible control of the elements and exploitation of the inevitable physical effects of perturbations.

The magnitude of the effects of perturbations depends significantly upon the initial values of certain orbital parameters such as semimajor axis, eccentricity, inclination, argument of perigee, and longitude. Achievement of target parameters (passive control) can minimize deviations from the desired orbit. If needed, the employment of onboard propulsion resources (active control) may be implemented. The consequence will be near constant or beneficially varying orbital parameters—a frozen orbit.

This thesis provides physical understanding, theories, and mathematical formulations for different types of frozen orbits. Included in the frozen orbit concept are minimum altitude variation arcs, various categories of low–Earth orbits such as Sun synchronous, and geosynchronous orbits. This study serves as a readily accessible and useful source of information on Earth–orbiting satellites which have near constant or beneficially varying orbital parameters.

v

ACKNOWLEDGEMENTS

I extend my sincere appreciation to Dr. Robert D. Culp, my adviser, for the assistance, counsel, and guidance rendered. For his support I am indeed indebted.

I am grateful to Professors Chuen-Yen Chow, Louis C. Garby, Howard Snyder, Sudhendu K. Datta, and George H. Born for serving on my dissertation committee. I appreciate the constructive comments and guidance given on certain topics by Professor Born.

To the U.S. Air Force I am thankful for the time and financial support making the degree possible. I thank Dr. Felix R. Hoots, Directorate of Astrodynamics at NORAD, and Captain Carl Crockett for information and data that I incorporated in my study.

Two fellow students/friends, Ting-Hua Wang and Rodney Bain, were always available to exchange ideas and feelings. To them I extend my thanks.

Mrs. Kathy James spent countless hours on a word processor/computer producing the final product. For her exacting and exhaustive efforts I express my deepest gratitude.

To my eternal campanion, Marsha, who has constantly supported me in my career decisions and advancements, both in good times and difficult times, I am forever grateful. Words cannot adequately express my feelings and the love I have for her. To my five children, Jennifer, Jeffrey, Kristine, Melanie, and "future arrival", I say "thank you for your love and support."

To my Heavenly Father I express my appreciation for answering my prayers, lifting me up to higher levels, and blessing me constantly.

In appreciation, I dedicate this dissertation to Marsha and my children.

TABLE OF CONTENTS

APPENDIX

TABLES

Table

FIGURES

CHAPTER I

INTRODUCTION

Since October 4, 1957, when the Soviet Union launched the world's first artificial satellite, Sputnik 1, man–made objects have been rotating around the Earth in ever–increasing numbers. Long before this first launch, it was known that the actual path that the satellite would follow would be other than pure Keplerian motion.

Theories endeavoring to describe perturbed motion have been applied since the time of Newton. By his analysis, most of the variations in the Moon's orbit were explained in the "Principia" published in 1687. Newton showed that the observed inequalities in the motion of the Moon were due to perturbations by the Sun. In 1749, Clairaut explained the movement of the perigee of the Moon by using second–order approximations [1,9]. A partial exposition of the method of variations of elements was published by Euler four years later. In 1772, his perturbation theory applied equations of motion referenced to axes rotating with the mean motion of the Moon [1,6,9].

After publishing his technique of initial orbit determination in 1780, Laplace turned his efforts towards the study of perturbed motion. His theory transformed the equations of motion so that the true longitude was the independent variable. His reference orbit was a Keplerian ellipse modified to avoid terms proportional to the time.

In 1783, Lagrange determined that Newton's second–order system of equations could be written in terms of an equivalent first–order system. Generalized

coordinates and Lagrange's equations provide a systematic procedure for solving systems. The resulting equations are equivalent to the equations of motion which would have been obtained by a direct application of Newton's laws. However, the Lagrangian function contains only velocities and displacements, and no accelerations are required. The equations produce a more convenient and manipulable form than a Newtonian formulation. When the total perturbing acceleration can be represented as the gradient of a scalar potential (velocity–independent), the resulting form of the perturbation equations is known as Lagrange's planetary equations [3,4,8,9]. The existence of the perturbing force represented by the scalar potential causes the motion to depart from the unperturbed motion and the orbital elements to change.

Gauss, in 1814, constructed an appropriate generalization for an arbitrary perturbing force. It is not always true that the perturbing forces can be written as the gradient of a velocity–independent scalar. Atmospheric drag is an example of a non–conservative force. The method resolves the perturbing force into three mutually perpendicular components: a component in the direction of the radius vector, a component perpendicular to the radius vector in the orbital plane, and a component perpendicular to the orbital plane [1,3,8].

After twenty years of laboring, Delaunay, in 1860, completed the most exhaustive application of the canonic method in celestial mechanics. The theory involved the analytical removal of the terms of the disturbing function, one by one. Most working procedures based on Hamiltonian dynamics endeavor to eliminate entire classes of variables from the original system of differential equations.While generating suitable transformations, the form of Hamilton's equations must be preserved at all times. This imposes constraints on the selection of variables. These transformations are called *canonical*. The appearance of the mean anomaly in every one of the classical sets of canonic variables forces series expansions, not only to accommodate powers of

the perturbation parameter, but also to allow for the transcendental nature of the coordinate–time relation. The ability to divide the Hamiltonian and treat each term separately, by a succession of canonic transformations, allowed Delaunay to complete his undertaking. The solution extended to include all terms of the seventh order and some of the eighth [2,4,5,8].

Special perturbations refers to the full numerical solution of the appropriate differential equations. One such method was developed in 1857 by Encke. In this approach, the difference between the primary acceleration and all perturbing accelerations is integrated. A reference (or osculating) orbit is established at an epoch. The osculating orbit is the orbit that would result if all perturbing forces were instantly removed. The body at this instant has the same coordinates and the same velocity components as in the unperturbed orbit. At increments of time later the osculating orbit is compared to the actual orbit. When the difference between the coordinates of the two orbits becomes excessive, a new osculating orbit is created by a process known as *rectification*. A new epoch and starting point which coincides with the true orbital path is selected. A new osculating orbit is then calculated from the true position and velocity vector, and the process of comparison is repeated. The advantage of Encke's method is that the difference between the position vector for the disturbed motion and the undisturbed motion and its derivatives is normally small. Consequently, a large integration interval is possible [1,6,7,10].

In the early 1900's, P. H. Cowell developed a perturbation method he used to determine the orbit of Jupiter's eighth satellite. The differential equations of motion contain all the forces acting on the satellite. The acceleration components are integrated step by step to produce velocity and position components. These values are then used with the equations of motion to calculate the acceleration components. The main advantage of Cowell's method is the simplicity of formulation and

implementation. Any number of perturbations can be handled at the same time. The main disadvantage of this method is that as the velocity increases near perigee, smaller integration steps must be taken. This increases the number of calculations and accumulative error due to roundoff [3,6,7].

The mentioned forerunners provided the necessary foundation for modern orbital mechanics. By 1957, the necessary theories were available to amplify and to study and predict the effects of perturbations.

The dominant force acting on an Earth–orbiting satellite is central gravity attraction. Depending upon the altitude, other forces influence the motion in varying degrees. The principal perturbations result from the Earth's oblateness, the longitudinal variations in the gravity field, atmospheric drag, lunar–solar gravitational attractions, and solar radiation. Minor perturbations are also caused by electromagnetic interaction of a charged satellite with the Earth's magnetic field and radiation belts, tidal influences, re–radiation of sunlight from the Earth, and relativistic effects. Although the perturbations depend on the direction and time intervals during which they act, the predominant disturbing force is due to the Earth's oblateness. As the geocentric distance increases, the oblateness effect diminishes, the lunar–solar attraction increases, the drag decreases, and the solar radiation pressure remains relatively constant [11,12,13].

1.1 Related Literatures

Applying the divergence theorem to Gauss' Law and using the fact that the Newtonian gravity field is conservative Poisson's equation is derived. At external points to the main body, where the density function is zero, Laplace's equation is obtained. The gravitational potential satisfying Laplace's equation can be expressed in terms of Legendre's associated polynomials. The external gravity field can be obtained

from the solution by differentiation [4,9,10,12,14].

The gravitational field of the Earth can be expressed as the sum of a series of spherical harmonics. These are of three types: (1)the zonal harmonics which depend on latitude only, (2)the sectorial harmonics, which depend on longitude only, and (3) the tesseral harmonics which depend upon both longitude and latitude. Since the Earth is rotating the tesseral and sectorial harmonics imply a gravitational field which is time dependent. This is manifested as a change in the mean motion.

The artificial satellites that followed Sputnik 1 provided the means to investigate the Earth's gravitational field. With the data that is obtained on the orbital elements of satellites, the harmonics are obtained.

O'Keefe, et al. used data obtained from Vanguard I (1958) to investigate the lower harmonics. Making the assumption that perigee distance is unaffected by drag and calculating the effects of time–integrals of the drag corrections to the semimajor axis and the eccentricity, the effects of drag were removed from the results. It was shown for this high satellite (perigee height = 658 km and apogee height = 3960 km) that the orbital elements at 37 different times over a 297 day period were accurately derived from the zonal harmonics of degrees 0, 2, 3, and 4 together with the six initial elements [15].

Using equations conceived by Tisserand relating the ratio of semimajor axis and radius to an integral of mean anomaly, Kozai (1957) derived the periodic perturbations of the first order and secular perturbations up to the second order using an averaging technique and mean elements. He assumed no air–resistance, a symmetrical density–distribution with respect to the axis of rotation, that the coefficient of the second harmonic of the potential is a small quantity of the first order, and those of the third and fourth harmonics are of the second order [16,17]. Study of the motion of the Explorer 7 and third Vanguard satellites produced coefficients of the second,

third, and fourth harmonics. Differences between the observed and the computed value of the orbital elements implied the importance of the higher harmonics [18].

Care must be taken in defining the constants of integration when handling the Lagrange equations. During the period 1957–1962, a large number of theoretical papers were conceived to solve the problem analytically. The obvious choices are the values of the Keplerian elements at a particular instant of time. It was convenient to define the constants as elements of a fictitious reference or intermediate orbit. In some theories this reference orbit is defined geometrically, while other theories defined the constants dynamically as corresponding to a constant part of the potential function. The more familiar theories include: Musen (1959) adapted the Hansen lunar theory to a form suitable for solution by iteration, Brouwer (1959) applied Von Zeipel's method of canonical transformation with a purely Keplerian intermediary, Vinti (1959,1961) separated the equations of motion by using ellipsoidal coordinates, King–Hele (1958) employed a Keplerian ellipse of fixed inclination and perigee argument as intermediary and solved in successive approximations according to powers of the second harmonic and eccentricity, and Merson (1961) developed a method in a similar manner to King–Hele but started from osculating elements when the satellite is at the node [23]. Merson then integrated the equations for the variation of the osculating elements to yield the complete perturbations of the first order due to the second harmonic. Also, he obtained the secular perturbations of the second order due to the second harmonic and of the first order due to the third to sixth harmonics. A set of smoothed elements was derived in which the perturbations of the even harmonics have no singularities, the semimajor axis and eccentricity have no variation due to the second harmonic, and the other elements have the smallest possible amplitudes of oscillation [50].

Analytical investigations of the oblateness effects showed the argument of perigee, the ascending node, and the mean anomaly experience secular variations or

continously increasing/decreasing changes from the adopted epoch value, as well as periodic variations. Semimajor axis, eccentricity, and inclination experience only periodic variations. Periodic includes both short and long periodic variations [19,24].

King–Hele showed the odd harmonics determine the periodic changes, while the even harmonics give rise to the secular changes. Data from Sputnik 2, Vanguard 1, and Explorer 7 was used to determine values for the second, fourth, and sixth harmonics [19]. In 1963, King–Hele, et al. determined the first seven even zonal harmonics in the Earth's gravitational potential using orbital information from seven satellites covering a wide range of latitude [20]. Transit 2A and Samos 2, two high–inclination satellites, permitted a study of inclinations uniformly distributed between 23° and 96°. King–Hele published the updated values for the even zonal harmonics in 1964 to be: $J_2 = (1082.64 \pm .02) \times 10^{-6}$; $J_4 = (-1.52 \pm .03) \times 10^{-6}$; $J_6 = (.57 \pm .07) \times 10^{-6}$; and $J_8 = (.44 \pm .11) \times 10^{-6}$ [21]. Coefficients of the odd zonal harmonics were evaluated by analyzing the oscillations in orbital eccentricity of fourteen satellites covering the widest and most uniform distribution in inclination and semimajor axis possible [22].

Coefficients of some low order tesseral harmonics in the Earth's gravitational field were successfully evaluated in the 1960s. The first satisfactory comprehensive model was the Smithsonian Standard Earth II published in 1970 by the Smithsonian Astrophysical Observatory, Cambridge, Massachusetts. This model relied largely on 100,000 optical observations of satellites from Baker–Nunn cameras. The expansion of the geopotential was truncated at degree and order 16 which produced about 250 geopotential coefficients to evaluate. The geopotential coordinates and station coordinates were then adjusted so that the observations of 21 satellites from about 30 ground stations achieved the best possible fit to these perturbed orbits while satisfying geometrical constraints for simultaneous observations. Approximately

200,000 equations were solved by least squares [25].

In recent years the Earth's gravitational field has been determined with continually improving accuracy, using hundreds of thousands of observations of Earth satellites, chiefly optical, laser and Doppler, together with surface gravimetry. More recently, altimeter measurements from satellites such as Geo3 have been included [25].

The launching of the first artificial satellite demonstrated the need to be able to estimate lifetime of a satellite and determine air density. Consequently, the studies of atmospheric drag emerged.

Equations expressing the variation of orbital period, perigee distance, and eccentricity were first developed by T. Nonweiler (1958) and by King–Hele (1958). Later King–Hele extended his efforts to include the effects of atmospheric rotation with oblateness and a realistic variation of air density with height [29]. The problem was treated by Brouwer and Hori (1961) on the basis of a non–rotating spherical exponential model atmosphere. The exponential atmosphere function was expanded into a series to the fifth power which limited the eccentricity to a very small quantity. For large eccentricity, a constant coefficient for each term of the series was introduced so that the modified series fit the exponential function. The Brouwer–Hori theory, which combined gravitational and drag effects, was limited to circular orbits [26].

Instead of using an exponential function for the atmospheric density model, Lane (1965) assumed a non–rotating power function atmosphere model. Although Lane found it necessary to expand the velocity in a series in order to perform the necessary integrations, the expansion of the density function was not required. Lane then used the method of successive approximations to complete the integration. His solution excluded orbits of small eccentricity and low inclination [27]. Later, Lane and Cranford (1969) used numerical observations to eliminate the singularity of zero eccentricity and zero inclination. The latter three works used the Von Zeipel method to

obtain the solutions by dealing with Delaunay canonical variables.

Using an asymptotic method, a first–order approximation to the problem was derived by Zee (1971) by dealing directly with the equations of motion in spherical coordinates rather than with the Delaunay canonical variables used in previous investigations [30].

Two classifications of mathematical solution techniques which can be used in the study of drag are numerical and analytical. A numerical method applies numerical integration to the osculating differential equations to obtain the state at a later time. An analytical method generally uses analytical equations to transform from the osculating to a mean set of differential equations. The equations are integrated analytically to predict a future mean state.

Recently, Hoots (1981) used canonical transformations and the method of averaging to obtain transformations of variables. This significantly simplified the transformed differential equations. Analytical integration yields the six osculating orbital elements. The analytical solution is for the motion of an artificial Earth satellite under the influence of the gravitational zonal harmonics through J_4 and any dynamic atmosphere [31].

The importance of determining the lunar and solar perturbations in the motion of an artificial satellite was demonstrated by Kozai's discovery that certain long–period terms in the development of the disturbing function cause large perturbations in the orbital elements. These perturbations may strongly affect the perigee height and the lifetime of a satellite. Modifying A. Cayley's development of the solar perturbative function, Musen et al. generated relations between perigee height variations and launch conditions. Using data from Vanguard I and Explorer VI values of perturbations in the perigee height were computed using a trigonometric expansion of the disturbing function with the angular equatorial elements of the Sun and Moon as

arguments. The disturbing function is then integrated by approximating the equatorial elements as linear functions of time. Kaula adapted the mathematical development of Musen to a form convenient for use in connection with the analysis of satellite orbits affected by a terrestrial gravitational field. Kaula further expressed the disturbing function in terms of osculating Keplerian elements. The formulae use equatorial elements for the Moon. The disturbing function yields all significant first–order lunar–solar effects when used with the equations of motion [12,33]. Neither inclination nor node of the Moon's orbit with respect to the equator of the Earth are simple functions of time. The same elements with respect to the ecliptic are nicely approximated by a constant and a linear function of time respectively. Giacaglia (1973) presented a paper in which he obtained the disturbing function for the lunar perturbations using ecliptic elements for the Moon and equatorial elements for the satellite. The secular, long–period, and short–period perturbations are then computed in closed form in both inclination and eccentricity of the satellite [34].

The motion of a satellite under the influence of the longitude dependent terms of the geopotential and in–plane station–keeping requirements of geosynchronous satellites with nearly zero eccentricity and inclination were investigated by Blitzer et al. (1962,196., Izsak (1961), Frick (1962), Allan (1963), Wagner (1964,1965), Blitzer (1965), and others [39-46]. Their findings regarding equilibrium positions and librational periods are in harmony.

The study of a satellite with a mean motion commensurable with the Earth's rotation was generalized to include the effects of tesseral harmonics on near–circular orbits of arbitrary inclinations in the works of Blitzer (1966), Cook (1966), and Wagner (1966) [47-49].

Ordinarily, the solar radiation pressure has a very small effect on the orbit. This perturbation becomes more important for geosynchronous satellites with large

solar arrays. The major effects are the oscillation of the eccentricity vector and the variation in perigee height.

Kozai (1961) developed closed form analytical expressions to include short–term periodics for first order perturbations. The three components of the disturbing equations were based on three assumptions: (1) the parallax of the Sun is negligible, (2) the solar flux is constant along the orbit of the satellite if there is no shadow, and (3) there is no re–radiation from the surface of the Earth. The resulting expressions are then evaluated over two limits of the independent variable, eccentric anomaly, which must be derived by numerical methods [35].

The short–term secular variations in period resulting from solar radiation pressure were studied by Wyatt (1961). It was shown that the effect of solar radiation is negligible when the satellite is in continuous sunshine. During the time the satellite is in the Earth's shadow, the secular acceleration may attain substantial values, positive or negative depending on the orientation of the orbit relative to the Sun. Wyatt presented a general formula for computing secular accelerations as far as terms in the square of the eccentricity [36].

Based on the assumption that the disturbing acceleration is constant while the satellite is in the sunlight and is zero in the Earth's shadow, Cook (1962) generated equations for the variations in orbital elements. The perturbation expressions are formulated in terms of the radial, transverse, and normal components of the disturbing force evaluated at perigee [38].

An expression which favorably compares to observations was presented by Soop for the mean drift rate of the eccentricity vector as a function of radiation pressure, velocity, mass, cross–sectional area, and sidereal angle of the Sun [37].

1.2 Thesis Outline

Over the last 20–25 years, theories to treat the major perturbations have been developed and used with much success. This study has endeavored to generalize the frozen orbit concept to include types of orbits that have near constant or beneficially varying orbital parameters. To achieve these frozen orbits the effects of perturbations are exploited to maintain the type of orbit desired.

Chapter II presents the equations of motion for a perturbed orbit, the Lagrange Planetary Perturbation Equations explicitly expressed in terms of the disturbing forces, and analytical expressions for the perturbations due to an axially symmetric gravitational field. Secular, long–term periodic, and short–term periodic variations are distinguished. Secular variations of the second order are expanded and a root finder is used on the resulting high order polynomials to find the eccentricity and inclination that freezes the argument of perigee and the ascending node separately. The orbital elements which freeze the perigee along the meridian are studied. Using Bessel expansions the change in radius is investigated at any point on the orbit including the perigee. The chapter concludes with a discussion of a frozen orbit where the change in eccentricity due to the third harmonic is zero as is the change in argument of perigee due to the second and third harmonics.

Atmospheric drag effects are investigated in Chapter III. The force which drains energy from the satellite and causes the orbit to shrink is analyzed for orbits of normal eccentricity $(0 < e < 0.2)$. Changes in orbital elements are handled both analytically and numerically usi, _ a fourth–order Runge–Kutta scheme. Scale height is determined using density values from U.S. Standard Atmosphere tables. Between cardinal altitudes an exponential atmosphere is assumed.

Minimum altitude variation arcs are dealt with in Chapter IV. A least squares method is derived for determining orbital elements for an orbit that closely

follows the contour of the oblate Earth over fixed latitude ranges. Results are included for both drag and no–drag effects. Impulse requirements to maintain the orbit are treated.

Sun synchronism is essential to maintain the same lighting conditions over a particular area of the Earth. Orbital parameters that are necessary to achieve this type of frozen orbit are specified in Chapter V. The chapter considers the ground trace of an artificial satellite. An analytical expression which includes oblateness effects is developed determining the semimajor axis that is needed to give a repeated ground trace in the desired number of days.

The last type of frozen orbit analyzed is the geosynchronous orbit. Chapter VI includes the main perturbing effects on this type of orbit and longitude station keeping requirements. The chapter concludes with a brief discussion of the effects of solar radiation.

1.3 Contribution

This thesis provides physical understanding, theories and mathematical formulations for different types of frozen orbits. It serves as a convenient and useful source of information on Earth orbiting satellites which have near constant or beneficially varying orbital parameters.

CHAPTER II

GRAVITATIONAL PERTURBATIONS ON ORBITAL PARAMETERS

2.1 Equations of Motion

The equations of motion for the classical two–body problem are governed by the inverse square law. The orbit may be determined from the equations of motion and initial values of position and velocity. In the two–body problem, all forces are neglected except the mutual gravitational attraction of two spherically symmetrical bodies. The resulting basic differential equation is

$$\ddot{r} = \frac{-\mu \, r}{r^3} \qquad (2.1)$$

This is equivalent to three second–order differential equations requiring six constants of integration for the complete solution. The solution may be obtained by a variety of methods. The result is the general polar equation for a conic section with the origin at a focus [1,51]:

$$r = \frac{\frac{h^2}{\mu}}{1 + e \cos \, v} \qquad (2.2)$$

Equation (2.2) when combined with the constant angular momentum can provide the last integration, the time relation.

In actuality, forces, in addition to the central gravitational force, act on the system. Other forces include Earth oblateness, atmospheric resistance, lunar–solar attractions, solar radiation, etc. The equation of motion becomes

$$\ddot{r} = \frac{-\mu\, r}{r^3} + f \qquad (2.3)$$

In some cases, it will be convenient to work with the total perturbing force. However, if the force is conservative, it can be represented as the gradient of a scalar function. Equation (2.3) becomes

$$\ddot{r} + \frac{\mu\, r}{r^3} = \nabla R \qquad (2.4)$$

where R is the disturbing function. The form of R will depend on the particular type of perturbing source. For multiple perturbing sources, the respective disturbing functions can be added linearly to yield the total R [2,4,8,10].

2.2 Lagrange's Planetary Equations

If a set of orbital elements (a, e, i, Ω, ω, M) is obtained at a fixed instant, an *osculating* orbit is defined. The osculating ellipse is the path that would be followed by the satellite if the perturbing forces were all suddenly removed. The satellite at this time has the same coordinates and the same velocity components in the perturbed as in the unperturbed orbit. Stated differently, the satellite has the same position and velocity as it would in purely two–body motion. If an osculating ellipse corresponding to a later time is considered, the differences in the orbital elements from those of a previous time are caused by the perturbations. One advantage in expressing actual orbital motion

in terms of osculating elements is that although the position and velocity vectors change rapidly with respect to time, the Keplerian elements vary slowly even in perturbed motion.

The Lagrange planetary equations provide the means for finding the rates of change of the osculating elements. Since any six linearly independent combination of orbital elements provides a valid set, the equations may be written in a variety of forms. For this undertaking the perturbing force f will be expressed in terms of the following three components: (1) f_1 is along r, (2) f_2 is perpendicular to r in the osculating plane and in the direction of increasing anomaly, and (3) f_3 is perpendicular to the osculating plane in the direction of the angular momentum vector. Substituting angular momentum in the equivalent terms, a modified form of Lagrange's planetary equations is [8,50]:

$$\frac{da}{dt} = 2\left(\frac{a^2}{h}\right)\left(f_1 e \sin v + f_2 \frac{p}{r}\right) \tag{2.5}$$

$$\frac{de}{dt} = \left(\frac{h}{\mu}\right)\left[f_1 \sin v + f_2 \cos v \left(1 + \frac{r}{p}\right) + f_2 \frac{er}{p}\right] \tag{2.6}$$

$$\frac{di}{dt} = \frac{r f_3 \cos u}{h} \tag{2.7}$$

$$\frac{d\Omega}{dt} = \frac{r f_3 \sin u}{(h \sin i)} \tag{2.8}$$

$$\frac{d\omega}{dt} = \left(\frac{h}{\mu e}\right)\left[-f_1 \cos v + f_2 \sin v \left(1 + \frac{r}{p}\right) - f_3 e \sin u \cot i \left(\frac{r}{p}\right)\right] \tag{2.9}$$

$$\frac{d\sigma^*}{dt} = \left(\frac{p}{na^2 e}\right)\left[f_1 \left(\cos v - \frac{2er}{p}\right) - f_2 \sin v \left(1 + \frac{r}{p}\right)\right] \tag{2.10}$$

LIST OF SYMBOLS

a = semimajor axis

P_n = Legendre polynomial of order n

e = eccentricity

r = radius vector

E = eccentric anomaly

r = magnitude of r

f = acceleration vector of perturbing force

R = mean equatorial radius of the Earth

f_1, f_2, f_3 = components of f

U = gravitational potential

F = perturbing potential

$u = v + \omega$

$h = (\mu p)^{1/2}$ = angular momentum for an ellipse

μ = gravitational constant = $\dfrac{398601.2 \text{ km}^3}{\text{sec}^2}$

i = inclination angle

Ω = right ascension of the node

J_n = zonal harmonics

v = true anomaly

$k = \sin^2 i$

θ = colatitude

M = mean anomaly = $nt + \sigma$

ω = argument of perigee

n = mean motion = $(\mu/a^3)^{1/2}$

σ = mean anomaly at the node

p = latus rectum = $a(1 - e^2)$

σ^* = modified mean anomaly = $M - \int_0^t n \, dt$
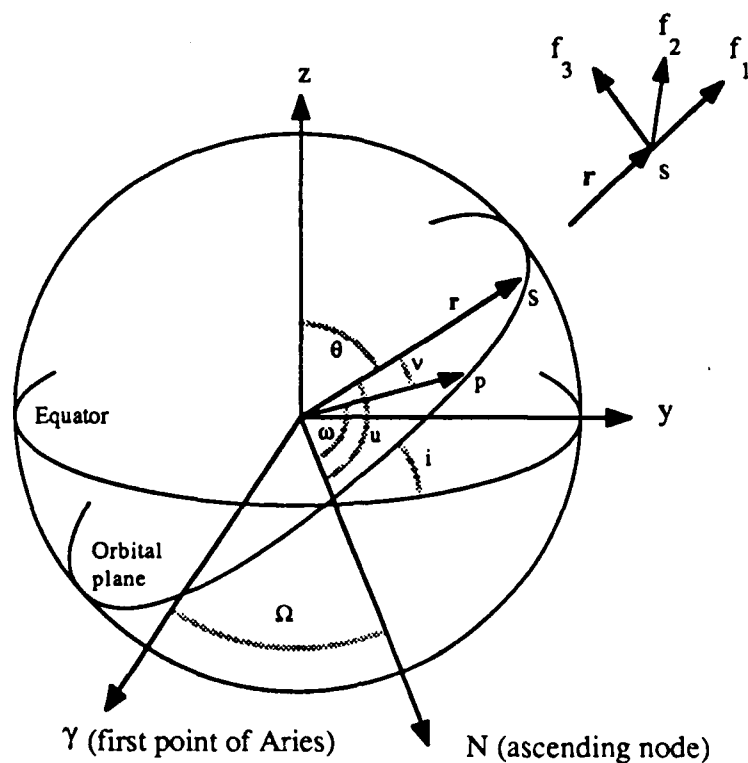
Figure 2.1 ORBITAL PARAMETERS
p = perigee, s = satellite position

2.3 The Gravitational Field

The force exerted by a conservative force field acting on a particle (satellite) can be written as the gradient of gravitational potential U. In terms of equation (2.4), $\nabla U = \nabla R$.

If variations with longitude are ignored and the Earth is assumed to be axially symmetric, the gravitational potential U at an exterior point distance r from the center of the Earth and with a colatitude θ may be written as a series of spherical harmonics in the form [4, 9, 11, 12, 19]

$$U = (\frac{\mu}{r}) [1 - \sum_{n=2}^{\infty} J_n (\frac{R}{r})^n P_n (\cos \theta)] \qquad (2.11)$$

The principal perturbation on a near–Earth satellite is due to the axially–symmetric (zonal) harmonics of the Earth's gravity field. The perturbing potential F for this perturbation becomes:

$$F = U - \frac{\mu}{r} = -(\frac{\mu}{r}) \sum_{n=2}^{\infty} J_n (\frac{R}{r})^n P_n (\cos \theta) \qquad (2.12)$$

The component of the perturbing acceleration $\mathbf{f}$ in any direction is the rate of change of F in that direction. Using spherical trigonometry based on figure 2.1 it follows that

$$f_1 = \partial F / \partial r$$
$$f_2 = -(\cos u \sin i \, / \, r \sin \theta \,) \, \partial F / \partial \theta \qquad (2.13)$$
$$f_3 = -(\cos i \, / \, r \sin \theta \,) \, \partial F / \partial \theta$$

Substituting the explicit formulae for P_n up to n=6, performing the differentiations, then setting $\cos \theta$ = sin i sin u, and using the abbreviations $S \equiv \sin u$ and $k = \sin^2 i$, the result is:

$$
\begin{aligned}
f_1 = (\mu/r^2) \Big[& \tfrac{3}{2} J_2 (^R/_r)^2 (3kS^2 - 1) + 2 J_3 (^R/_r)^3 \sin i (5kS^3 - 3S) \\
& + \tfrac{5}{8} J_4 (^R/_r)^4 (35k^2S^4 - 30kS^2 + 3) \\
& + (\tfrac{3}{4}) J_5 (^R/_r)^5 \sin i (63k^2S^5 - 70kS^3 + 15S) \\
& + \tfrac{7}{16} J_6 (^R/_r)^6 (231k^3S^6 - 315k^2S^4 + 105kS^2 - 5) \Big]
\end{aligned}
\qquad (2.14)
$$

$$
\begin{aligned}
f_2 = -(\mu/r^2) \sin i \cos u \Big[& 3 J_2 (^R/_r)^2 \sin i \sin u + (\tfrac{3}{2}) J_3 (^R/_r)^3 (5kS^2 - 1) + \\
& \tfrac{5}{2} J_4 (^R/_r)^4 \sin i (7kS^3 - 3S) + \\
& \tfrac{15}{8} J_5 (^R/_r)^5 (21k^2S^4 - 14kS^2 + 1) + \\
& \tfrac{21}{8} J_6 (^R/_r)^6 \sin i (33k^2S^5 - 30kS^3 + 5S) \Big]
\end{aligned}
\qquad (2.15)
$$

$$f_3 = - (\mu/r^2) \cos i \times [\, \textit{same as } f_2 \,] \qquad (2.16)$$

To determine the secular and long–period terms equations (2.14), (2.15), and (2.16) are substituted in equations (2.5)–(2.10). The resulting equations are then multiplied by an appropriate equality with $dt/_{du}$ to obtain J_2 to J_6 and J_2^2 terms. This allows the argument of latitude to be used as the independent variable. Expressing the derivative of the orbital elements with respect to the argument of latitude as the sum of a number of terms of a general function, utilizing appropriate identities, and integrating from one ascending node to the next (u=0 to u=2π), the desired equations were obtained (for details see ref. 50, p 23-31).

These analytical expressions reveal that the elements ω, Ω, and M experience secular variations from the adopted epoch values as well as periodic variations. The elements, a, i, and e possess only periodic variations and oscillate about their mean values. The long–period variations are caused by the continuous variance of ω. The strictly secular terms contain only even J_n terms while the odd zonal harmonics contribute to periodic terms. Since the changes in orbital elements over one period are to be studied here, the secular variations are of primary concern. Consequently, the following equations are absent of any odd J_n terms since they all have products of trigonometric functions of ω or multiples of ω.

$$\Delta a_{sec} = \Delta e_{sec} = \Delta i_{sec} = 0$$

$$\Delta \Omega_{sec} = 2\pi[\sum_n J_n (R/p)^n \Omega_n + J_2^2 (R/p)^4 \Omega_{22}] \qquad (2.17)$$

$$\Omega_2 = -^3/_2 \cos i$$

$$\Omega_4 = {}^{15}/_4 \cos i [(1 - {}^7/_4 k) (1 + {}^3/_2 e^2)]$$

$$\Omega_6 = -^{105}/_{16} \cos i [(1 - {}^9/_2 k + {}^{33}/_8 k^2) (1 + 5e^2 + {}^{15}/_8 e^4)]$$

$$\Omega_{22} = {}^3/_2 \cos i [{}^3/_4 - 5k - ({}^1/_4 + {}^5/_{16} k) e^2]$$

$$\Delta\omega_{sec} = 2\pi \left[\sum_n J_n (R/p)^n \omega_n + J_2^2 (R/p)^4 \omega_{22}\right] \qquad (2.18)$$

$$\omega_2 = 3 (1 - {}^5/_4 k)$$

$$\omega_4 = - {}^{15}/_{32} \left[(16 - 62 k + 49 k^2) + (18 - 63 k + {}^{189}/_4 k^2) e^2 \right]$$

$$\omega_6 = {}^{525}/_{64} \left[{}^8/_5 (1 - 8 k + {}^{129}/_8 k^2 - {}^{297}/_{32} k^3) \right.$$

$$+ 6 (1 - {}^{43}/_6 k + {}^{109}/_8 k^2 - {}^{121}/_8 k^3) e^2$$

$$\left. + (2 - {}^{27}/_2 k + {}^{99}/_4 k^2 - {}^{429}/_{32} k^3) e^4 \right]$$

$$\omega_{22} = ({}^9/_4) \left[({}^{95}/_{12} k - {}^{445}/_{48} k^2) + ({}^7/_{12} - {}^3/_8 k - {}^{15}/_{32} k^2) e^2 \right]$$

$$\Delta M_{sec} = n + 2\pi \left[\sum_n J_n (R/p)^n \sigma_n^* + J_2^2 (R/p)^4 \sigma_{22}^*\right] \qquad (2.19)$$

$$\sigma^*_2 = {}^3/_2 (1 - e^2)^{1/2} (1 - {}^3/_2 k)$$

$$\sigma^*_4 = {}^{45}/_{16} (1 - e^2)^{1/2} \left[(-1 + 5k - {}^{35}/_8 k^2) e^2 \right]$$

$$\sigma^*_6 = {}^{-35}/_{16} (1 - e^2)^{1/2} \left[(1 - {}^{21}/_2 k + {}^{189}/_8 k^2 - {}^{231}/_{16} k^3) \right.$$

$$\left. \times (1 - {}^5/_2 e^2 - {}^{15}/_8 e^4) \right]$$

$$\sigma^*_{22} = {}^9/_2 (1 - e^2)^{-1/2} \left[({}^{25}/_{12} k - {}^{131}/_{48} k^2) \right.$$

$$\left. + ({}^5/_{12} - {}^{49}/_{12} k + {}^{67}/_{48} k^2) e^2 \right]$$

2.4 Method of Averaging

A current procedure that is used to simplify a system of nonlinear differential equations is the method of averaging. By proper selection of new variables the original equations are transformed into a simpler form, free of certain variables. The normal form for averaging includes a set of slow variables with time variations proportional to a small parameter. The fast variables have dominant parts with time variations proportional to time. The transformation of variables removes the dependence on mean anomaly, the fast variable. Since the method of averaging requires perturbations to be continuous and periodic in the fast variable, it is an ideal

technique to use to analyze orbital motion. The solution for these transformed equations permits the calculation of the six osculating orbital elements.

Expressing the disturbing function explicitly in terms of the orbital elements, the slow variable perturbation equations have the form:

$$\dot{n} = \varepsilon g_1(n, e, i, \omega, \Omega, M)$$

$$\dot{e} = \varepsilon g_2(n, e, i, \omega, \Omega, M)$$

$$\frac{di}{dt} = \varepsilon g_3(n, e, i, \omega, \Omega, M)$$

$$\dot{\omega} = \varepsilon g_4(n, e, i, \omega, \Omega, M)$$

$$\dot{\Omega} = \varepsilon g_5(n, e, i, \omega, \Omega, M)$$

ε is a small parameter of order J_2.

The fast variable equation is of the form:

$$\dot{M} = n + \varepsilon u_1(n, e, i, \omega, \Omega, M)$$

g_1 thru g_5 and u_1 are continuous functions of the orbital elements as well as periodic functions of mean anomaly with a period of 2π. The equations are in the normal form for the method of averaging and the procedure outlined in references 52 and 54 can be employed.

Using

$$F = \frac{-\mu}{r} \sum_{n=2}^{4} J_n \left(\frac{R}{r}\right)^n P_n(\cos \theta)$$

and adhering to the prescribed approach, the periodics can be eliminated and the following secular variations of the first–order harmonic J_2 and the second–order harmonics J_3 and J_4 result:

$\dot{n} = 0$ (Since $\dot{n} = -\frac{3n}{2a}\,\dot{a}$, $\dot{a} = 0$.)   (2.20)

$\dot{e} = 0$

$\frac{di}{dt} = 0$

$\dot{\omega} = \frac{3}{4} n J_2 (R/p)^2 (4 - 5k)$

$\qquad - \frac{15}{32} n J_4 (R/p)^4 [\, 16 - 62k + 49 k^2 + \frac{3}{4} (24 - 84 k + 63 k^2) e^2 \,]$

$\qquad + (\frac{3}{16}) n J_2{}^2 (R/p)^4 [72 - 169k + \frac{395}{4} k^2 + (-5 + \frac{57}{2}k - \frac{225}{8} k^2)e^2]$

$\dot{\Omega} = -\frac{3}{2} n J_2 (R/p)^2 \cos i + \frac{15}{16} n J_4 (R/p)^4 \cos i [(4 - 7k)(1 + \frac{3}{2} e^2)]$

$\qquad - \frac{3}{2} n J_2{}^2 (R/p)^4 \cos i [\frac{9}{4} + \frac{3}{2}(1-e^2)^{1/2} - k(\frac{5}{2} + \frac{9}{4}(1 - e^2)^{1/2})$

$\qquad + \frac{e^2}{4}(1 + \frac{5}{4}k)\,]$

$\dot{M} = n [\, 1 + \frac{3}{2} J_2 (R/p)^2 (1 - \frac{3}{2} k (1-e^2)^{1/2})]$

$\qquad - \frac{45}{128} n J_4 (R/p)^4 (8 - 40k + 35k^2) e^2 (1-e^2)^{1/2}$

$\qquad + \frac{9}{2} n J_2{}^2 (R/p)^4 (1-e^2)^{-1/2} [\, \frac{3}{2} - \frac{47}{12} k + \frac{139}{48} k^2$

$\qquad + (\frac{-3}{24} + \frac{13}{12} k + \frac{10}{96} k^2) e^2 \,]$

Although the $J_2{}^2$ term is slightly different, these results corroborate those formulated by Merson.

2.5 The Argument of Perigee

One of the most important perturbations is the rotation of the major axis of an orbit in its own plane. From equation (2.18) it is seen that on the $O(J_2)$ the change in argument of perigee over one period is:

$$\Delta\omega = (\frac{3\pi}{2}) J_2 R^2 (4 - 5 \sin^2 i) / (a^2 (1 - e^2)^2) \qquad (2.21)$$

The angle at which the argument of perigee freezes is normally referred to as the *critical inclination*. For $\Delta\omega = 0$, $4 - 5 \sin^2 i = 0$. This occurs at an inclination angle of $63.4°$ for prograde orbits and $116.6°$ for retrograde orbits. For $i < 63.4°$ the perigee moves in the same direction as the satellite's motion; for $63.4° < i < 116.6°$ the perigee moves in the opposite direction; and for $i > 116.6°$ the perigee moves in

the same direction.

If gravitational perturbations due to the geopotential alone are considered and if tesseral and sectorial harmonic resonances are avoided, only the zonal harmonics cause secular and long-period perigee fluctuations. Studies where the averaged Hamiltonian was expanded about critical inclinations revealed very slow (on the order of a century) simple pendulum–type oscillations in argument of perigee [53].

To improve the accuracy to $O(J_2^2)$ the entire equation (2.18) can be set equal to zero. Since there is no secular change in a, e, and i caused by the Earth's geopotential these values can be assumed constant. Using a binomial expansion the following sixth–order polynomial equation in sin i results:

$$o = [3 \, J_2 \, a^4 \, (e^8 - 4e^6 + 6e^4 - 4e^2 + 1) \qquad\qquad (2.22)$$

$$- (15 \, J_4 \, R^2 \, a^2 \, / \, 32) \, (18 \, e^6 - 20 \, e^4 - 14 \, e^2 + 16)$$

$$+ \, ^{524}/_{64} \, J_6 R^4 \, (^{32}/_{20} + 6e^2 + 2e^4) + ^9/_{384} \, J_2^2 \, a^2 R^2 \, (56e^6 - 112e^4 + 56e^2) \,]$$

$$+ [3J_2 a^4/_4)(-5e^8 + 20e^6 - 30e^4 + 20e^2 - 5) - ^{15}/_{32} \, J_4 R^2 a^2 (-63e^6 + 64e^4 + 61e^2 - 62)$$

$$+ \, ^{524}/_{64} \, J_6 \, R^4 \, (-^{432}/_{32} e^4 - 43e^2 - ^{256}/_{20})$$

$$+ \, ^9/_{384} \, J_2^2 \, a^2 \, R^2 \, (-36e^6 + 832e^4 - 1{,}556e^2 + 760) \,] \, sin^2 i$$

$$+ [\, (-15 \, J_4 \, R^2 \, a^2 \, / \, 32) \, (^{189}/_4 e^6 - ^{91}/_2 \, e^4 - ^{203}/_4 e^2 + 49)$$

$$+ \, ^{524}/_{64} \, J_6 \, R^4 \, (^{792}/_{32} \, e^4 + ^{327}/_4 \, e^2 + ^{516}/_{20})$$

$$+ \, ^9/_{384} \, J_2^2 \, a^2 \, R^2 \, (-45e^6 - 800e^4 + 1{,}735e^2 - 890) \,] \, sin^4 i$$

$$- \, ^{524}/_{64} \, J_6 \, R^4 \, (^{429}/_{32} e^4 + ^{363}/_4 e^2 + ^{297}/_{20}) \, sin^6 i$$

Table 2–1 shows the values of inclination that will freeze the argument of perigee given an eccentricity and semimajor axis. The data reveals that as semimajor axis increases the inclination angle required decreases. The decrease is small when the eccentricity is small. As the eccentricity increases the decrease in inclination is of greater magnitude over the same range of semimajor increase. The other trend that is obvious is that for a given semimajor axis, as the eccentricity increases the inclination

required decreases.

A comparison of computed change in argument of perigee with actual 1984 data from NORAD confirms the contribution of zonal harmonics of $O(J^2)$ to the secular variation (see table 2–2). In all cases the secular equation produces reasonable accuracy. Deviation that occurs is possibly due to periodic variations caused by the gravitational field as well as changes due to other major perturbing forces. The most error per time lapse occurs with the satellite experiencing the most drag effect. Another source of error is the fact that the change is averaged over the entire time as opposed to adding the change that occurs each orbit over the time lapse.

Table 2–3 shows the first and second–order changes in the argument of perigee given a semimajor axis, an eccentricity, and an inclination angle. The data demonstrates that for a given eccentricity, as the semimajor axis increases the rate of change in argument of perigee decreases. Also, at a constant semimajor axis, as the eccentricity increases the rate of change in perigee is insignificantly altered.

Table 2-1. INCLINATION REQUIRED TO FREEZE PERIGEE
(63.° +)

a e	15,000 (km)	12,000 (km)	8,000 (km)	7,500 (km)	7,000 (km)
.02			.4386	.4402	.4440
.04	.4336	.4336	.4374	.4393	.4421
.06	.4335	.4332	.4356	.4369	.4389
.08	.4332	.4327	.4329	.4334	
.10	.4329	.4320	.4293	.4288	
.12	.4325	.4310	.4248	.4231	
.14	.4321	.4299	.4194		
.16	.4315	.4285			
.18	.4308	.4269			
.20	.4300	.4250			
.22	.4290	.4228			
.24	.4279	.4201			
.26	.4266	.4170			
.28	.4251	.4134			
.30	.4233	.4092			
.34	.4187	.3984			
.38	.4124	.3835			
.42	.4036	.3625			
.46	.3909	.3323			
.50	.3723				
.54	.3448				

Table 2-2. ACTUAL VS. COMPUTED CHANGE IN PERIGEE

Satellite #	a (km)	e	i (deg)	Δt (days)	$\Delta\omega_{actual}$ (deg)	$\Delta\omega_{computed}$ (deg)
62 B–P	6864.903	.00105	90.613	1.90128	-5.3478	-7.3246
62 B–M	7506.838	.00702	50.150	4.79179	14.2662	14.1413
77–79 F	7844.892	.0005	74.026	30.42327	-39.8920	-45.5713
79–47 A	6934.313	.0024	55.016	46.06976	120.2862	110.2657
11416 U	7187.775	.0012	98.570	10.11341	-28.8684	-29.4842
12553	7227.384	.00133	99.026	4.39037	-12.9535	-12.3858

Table 2-3 CHANGE IN ARGUMENT OF PERIGEE

$e = .02 \qquad a = 7,000$ km

i (deg)	$O(J_2)$ (deg/day)	$O(J_2^2)$ (deg/day)	diff (deg/day)
30	9.9013	9.9318	-.0304
35	8.4793	8.4939	-.0146
40	6.9637	6.9669	-.0031
45	5.4007	5.3969	.0038
50	3.8736	3.8307	.0069
55	2.3221	2.3149	.0071
60	.9001	.8942	.0058
65	-.3851	-.3891	.0039
70	-1.4946	-1.4969	.0023
75	-2.3945	-2.3957	.0012
80	-3.0576	-3.0583	.0006
85	-3.4637	-3.4642	.0004
90	-3.5983	-3.5984	.0001

$e = .02 \qquad a = 7,500$ km

i (deg)	$O(J_2)$ (deg/day)	$O(J_2^2)$ (deg/day)	diff (deg/day)
30	7.7772	7.8088	-.0316
35	6.6602	6.6734	-.0132
40	5.4698	5.4688	.0009
45	4.2421	4.2317	.0103
50	3.0143	2.9993	.0150
55	1.8239	1.8084	.0155
60	.7070	.6940	.0130
65	-.3025	-.3111	.0086
70	-1.1739	-1.1774	.0034
75	-1.8808	-1.8793	-.0014
80	-2.4016	-2.3962	-.0054
85	-2.7206	-2.7126	-.0080
90	-2.8237	-2.8148	-.0089

e = .08   a = 7,500 km

30	7.8714	7.9208	-.0313
35	6.7409	6.7540	-.0131
40	5.5361	5.5351	.0009
45	4.2935	4.2832	.0102
50	3.0509	3.0359	.0149
55	1.8460	1.8303	.0157
60	.7155	.7019	.0136
65	-.3061	-.3160	.0098
70	-1.1881	-1.1935	.0053
75	-1.9036	-1.9047	.0011
80	-2.4307	-2.4285	-.0022
85	-2.7536	-2.7492	-.0044
90	-2.8579	-2.8528	-.0051

2.6 The Ascending Node

Another strong secular perturbation of major significance is the steady rotation of the orbital plane about the Earth's axis commonly referred to as regression of the nodes. Equation (2.17) shows that all secular terms contain a product of cos i. Because of the major influence of the J_2 term, for i < 90°, the orbital plane rotates about the Earth's axis in the direction opposite to the satellite motion. A 90° inclination (polar) orbit would freeze the ascending node and there would be no secular motion.

Table 2–4 shows the rate of change of the ascending node as a function of eccentricity, semimajor axis, and inclination angle. As the eccentricity increases for a given semimajor axis and inclination, the rate of node change increases. For a given eccentricity and inclination, an increase in semimajor axis causes a decrease in the rate of node change. Finally, the difference between first and second–order solutions becomes smaller when any of the following occurs: eccentricity decreases, semimajor axis increases, or inclination increases.

A comparison is made between actual and computed change in the ascending node in Table 2–5. The 1984 NORAD data is on the same satellites listed in Table 2–2.

An interesting combination of the change in argument of perigee and ascending node is

$$\dot{\Omega} + \dot{\omega} \cos i = 0 \qquad (2.23)$$

When this relationship is satisfied, the perigee is frozen along the meridian. For all possible eccentricities and all semimajor axes as large as 15,000 km the inclination (other than 90°) for which equation (2.23) is true varies between 38° and 39.2°. Figure 2.2 shows the change in ascending node, change in perigee, and $\dot{\Omega} + \dot{\omega} \cos i$ graphically.

Table 2-4 CHANGE IN THE ASCENDING NODE

e = .02   a = 7,000 km

i (deg)	$O(J_2)$ (deg/day)	$O(J_2^2)$ (deg/day)	diff (deg/day)
30	-6.2362	-6.2515	.0153
40	-5.5162	-5.5258	.0095
50	-4.6287	-4.6354	.0066
60	-3.6004	-3.6063	.0058
70	-2.4628	-2.4680	.0051
80	-1.2504	-1.2536	.0031
90	.0000	.0000	.0000

e = .05   a = 7,000 km

i (deg)	$O(J_2)$	$O(J_2^2)$	diff
30	-6.2625	-6.2780	.0155
40	-5.5395	-5.5491	.0096
50	-4.6482	-4.6549	.0067
60	-3.6156	-3.6215	.0058
70	-2.4732	-2.4784	.0052
80	-1.2557	-1.2589	.0032
90	.0000	.0000	.0000

e = .02   a = 7,500 km

i (deg)	$O(J_2)$ (deg/day)	$O(J_2^2)$ (deg/day)	diff (deg/day)
30	-4.8983	-4.9086	.0103
40	-4.3328	-4.3395	.0066
50	-3.6357	-3.6404	.0047
60	-2.8280	-2.8321	.0040
70	-1.9345	-1.9379	.0034
80	-.9821	-.9842	.0020
90	.0000	.0000	.0000

e = .11   a = 7,500 km

30	-5.0150	-5.0261	.0110
40	-4.4361	-4.4431	.0070
50	-3.7223	-3.7272	.0049
60	-2.8954	-2.8996	.0042
70	-1.9806	-1.9842	.0035
80	-1.0055	-1.0077	.0021
90	.0000	.0000	.0000

e = .02   a = 8,000 km

30	-3.9079	-3.9195	.0071
40	-3.4568	-3.4615	.0047
50	-2.9006	-2.9040	.0034
60	-2.2562	-2.2591	.0028
70	-1.5433	-1.5457	.0023

e = .17   a = 8,000 km

30	-4.1407	-4.1491	.0084
40	-3.6626	-3.6681	.0054
50	-3.0733	-3.0771	.0037
60	-2.3906	-2.3937	.0031
70	-1.6352	-1.6379	.0026

e = .06   a = 12,000 km

20	-1.0324	-1.0334	.0009
40	-.8416	-.8422	.0005
60	-.5493	-.5496	.0003
80	-.1907	-.1909	.0001

e = .42   a = 12,000 km

i (deg)	$O(J_2)$ (deg/day)	$O(J_2^2)$ (deg/day)	diff (deg/day)
20	-1.5111	-1.5140	.0028
40	-1.2318	-1.2332	.0013
60	-.8040	-.8046	.0006
80	-.2792	-.2795	.0002

e = .06   a = 15,000 km

20	-.4728	-.4730	.0002
40	-.3854	-.3856	.0001
60	-.2515	-.2516	.00009

e = .54   a = 15,000 km

20	-.9354	-.9371	.0017
40	-.7625	-.7633	.0007
60	-.4977	-.4980	.0003

Table 2-5
ACTUAL VS. COMPUTED CHANGE IN ASCENDING NODE

Satellite #	Δt days	$\Delta \Omega$ (deg) actual	$\Delta \Omega$ (deg) computed
62 B-P	1.40128	.1593	.1639
62 B-M	4.79178	-17.3097	-17.3221
77-79F	30.42327	-58.4060	-40.5017
79-47A	46.06976	-245.7439	-196.6044
11416U	10.11341	9.8689	9.8849
12553	4.39037	4.4278	4.4316

(a, e, i are the same as those in Table 2–2.)
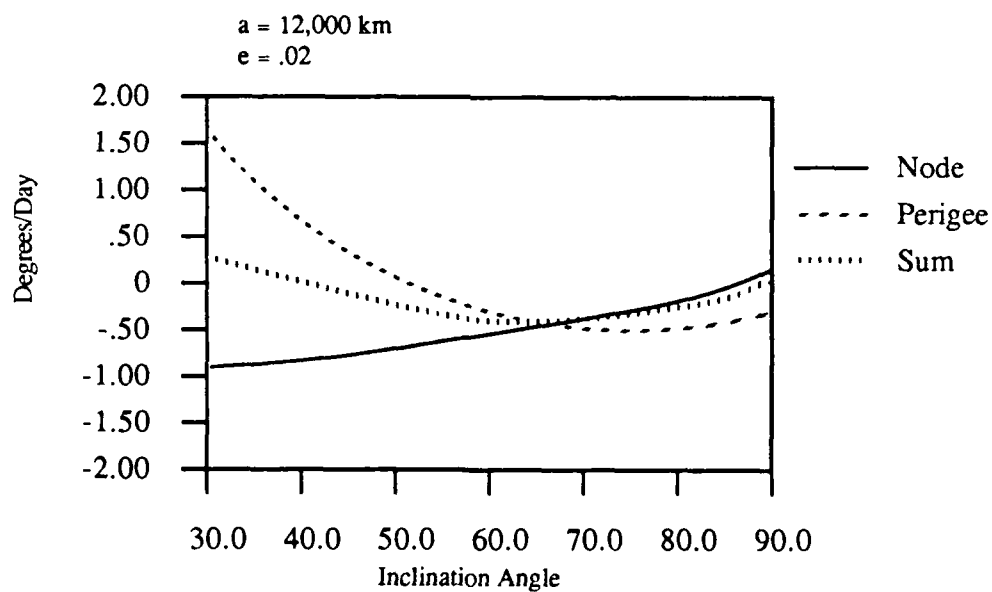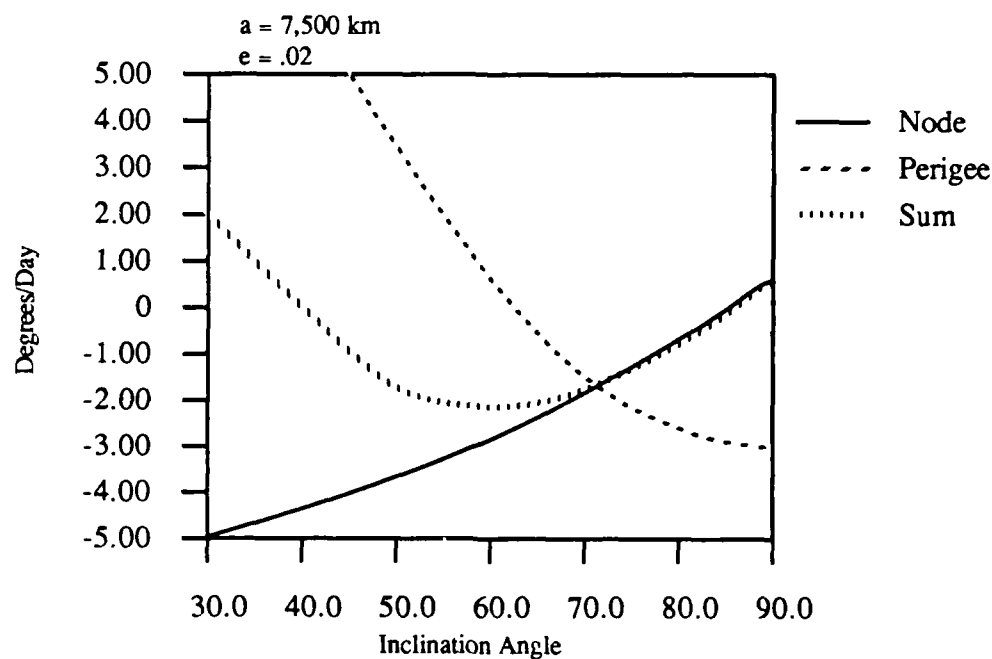
Figure 2.2 SECULAR CHANGES

2.7 Secular Radial Variation

The radial distance to the satellite expressed in terms of orbital elements is

$$r = a(1 - e \cos E) \qquad (2.24)$$

Expressing cos E in terms of a series expansion of derivatives of Bessel coefficients

$$\cos E = -e/2 + 2 \sum_{n=1}^{\infty} \frac{1}{n} \frac{d}{d(ne)} J_n (ne) \cos nM \qquad (2.25)$$

Substituting equation (2.25) in (2.24)

$$r = a + \frac{ae^2}{2} - 2ae \sum_{n=1}^{\infty} \frac{1}{n} \frac{d}{d(ne)} J_n (ne) \cos nM \qquad (2.26)$$

(see Appendix A for derivatives of Bessel coefficients). The differentials of the independent variables a, e, and M are defined by

$$da = \Delta a, \; de = \Delta e, \; dM = \Delta M$$

The differential of the dependent variable r is defined by

$$\Delta r = dr = \frac{\partial r}{\partial a} da + \frac{\partial r}{\partial e} de + \frac{\partial r}{dM} dM \qquad (2.27)$$

If the secular change in radial distance is required and only the perturbation due to the gravitational field is considered then

$$\Delta a_{sec} = \Delta e_{sec} = 0$$

and
$$\Delta r_{sec} = \frac{\partial r}{dM} \Delta M_{sec}$$

Using (2.26)

$$\frac{\partial r}{\partial M} = 2ae \sum_{n=1}^{\infty} \frac{d}{d(ne)} J_n (ne) \sin nM \qquad (2.28)$$

From either (2.26) or (2.28) it is seen that for a given a and e, there is no secular change in r for a given M + 2mπ (m is an integer). Therefore,

$$\left. \frac{\partial r}{\partial M} \right)_{M + 2m\pi} = 0$$

and

$$\left. \Delta r_{sec} \right)_{M + 2m\pi} = 0$$

From orbit to orbit, for a given M, there is no secular change in radial distance if the only force acting on a satellite is due to a gravitational field with axial symmetry.

2.8 Freezing Perigee and Eccentricity

Low altitude near circular orbits are influenced greatly by perturbations caused by the Earth's oblateness. The magnitude of the effects of the perturbations depends on the initial values of certain orbital elements. The appropriate selection of semimajor axis, eccentricity, inclination, and argument of perigee can minimize the variations. A pertinent example consists of stopping the line of apsides and freezing the perigee point [55–57]. If the periodic change in eccentricity is considered and equation (2.18) is modified to include the periodic term of J_3 the resulting equations are:

$$de/_{dt} = -^3/_2 \, nJ_3 \, (^R/_p)^3 \, (1-e^2) \sin i \cos \omega \, (1 - ^5/_4 \, k) \qquad (2.30)$$

$$d\omega/_{dt} = 3nJ_2 \, (^R/_p)^2 \, (1 - ^5/_4 \, k) + ^{3n}/_{2e} \, J_3 \, (^R/_p)^3 \sin \omega \sin i$$

$$\times \, [(1 - ^5/_4 \, k) + (^{35}/_4 \cos^2 i - \text{cosec}^2 i) \, e^2 \,] \qquad (2.31)$$

The idea of this type of frozen orbit is to initially set $\omega = 90°$ causing $de/_{dt}$ due to J_3 to be equal to zero. Finding the root to equation (2.31) yields the value of eccentricity for which $d\omega/_{dt}$ due to J_2 and J_3 equals zero. These values of e and ω will produce a perigee location which remains comparatively constant. The changes in the average argument of perigee and the average eccentricity become zero when $\omega = 90°$ and e approaches some determinable small value. Cutting (1978) asserted that subsequent analysis for the SEASAT-A satellite which included zonals up to degree 21

lowered the appropriate eccentricity only about 20% [56].

The frozen eccentricity for Landsat-5, a Sun synchronous orbit, launched on March 1, 1984, is approximately 0.0012. The averaged argument of perigee and eccentricity will then oscillate within a small range about the frozen condition. Fig. 2.3 shows the evolutions of these parameters over a 116 day period [55].

Some other satellite orbits which would satisfy this type of freezing have the following elements

a (km)	i (deg)	e
7000	97.87	0.00103
7188	98.57	0.00100
7500	100.04	0.00094

The oscillations of ω and e can be observed by plotting the components of the eccentricity vector; the result is a circle centered on the frozen condition (see figure 2.4). The period (T) of the oscillation is related to the secular rate of the change in ω according to

$$T = \frac{2\pi}{\Delta\omega_{sec}}$$

where $\Delta\omega_{sec}$ is obtained from equation (2.18).

MEAN ARGUMENT OF PERIGEE (DEGREES)
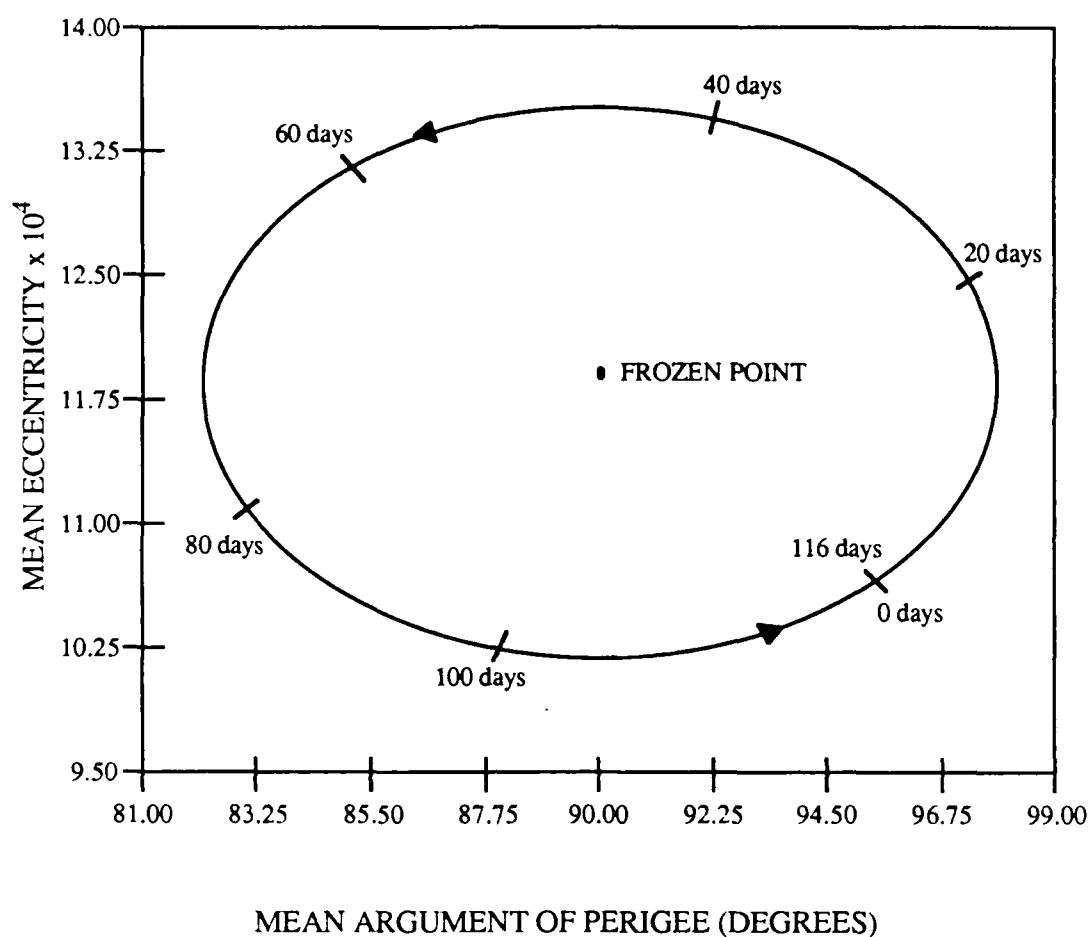
Figure 2.3 EVOLUTION OF $\bar{e}$ AND $\bar{\omega}$ FOR A NEAR-FROZEN
LANDSAT-5 ORBIT [55]
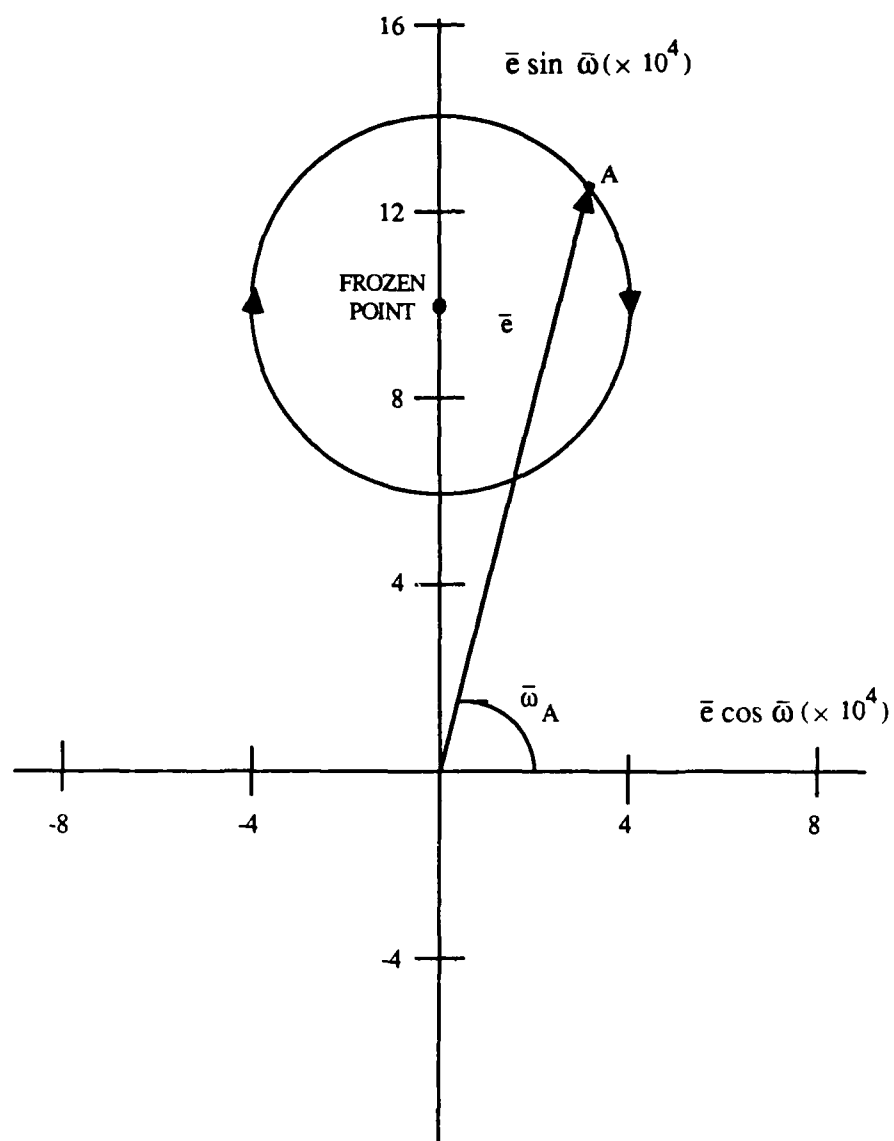
Figure 2.4   OSCILLATION OF $\bar{e}$ AND $\bar{\omega}$ ABOUT FROZEN POINT
FOR A TYPICAL NEAR-FROZEN ORBIT [55]

CHAPTER III

VARIATIONS DUE TO ATMOSPHERIC DRAG

3.1 Aerodynamic Forces

For near-Earth satellites, excluding the Earth's oblateness, the perturbation having the greatest consequences is the resisting force of the atmosphere. This resisting force, called *drag*, is especially predominant from 150 to 600 km. When a satellite with substantial eccentricity is near perigee the drag tends to retard its motion. A decrease in energy causes a reduction in the apogee height; this is called *orbital decay*. The more circular the orbit, the more interminable the energy-draining effect of drag.

The main effects of the force are secular decreases in the orbital elements a and e which in turn cause the orbit to contract. Since the apogee height decreases while the perigee height remains nearly constant, the orbit tends to become more circular. In addition, the rotation of the atmosphere subjects the satellite to small lateral forces which alter slightly the orientation of the orbital plane. The result is a small but steadily increasing change in inclination and limited periodic changes in the line of apsides. Small changes in argument of perigee are caused by the oblateness of the atmosphere [4, 9, 58].

The most common expression for the drag force is

$$D = \tfrac{1}{2} C_D {}^A/_m \, f \, \rho \, |v| \, v \qquad (3.1)$$

where D is the force per unit of mass, m is the mass of the satellite, C_D is a

dimensionless drag coefficient which is empirically determined, and A is the effective cross sectional area of the satellite. $V = v_a - v$, where v is the satellite's inertial velocity and v_a is the inertial velocity of the atmosphere. f represents the effect of atmospheric rotation on drag and is a function of the inclination of the orbit. Since f will usually be between .9 and 1.1, this study will use an average value of 1.0. For details on the development of f, see reference 58.

The *ballistic coefficient*, defined by

$$\beta = \frac{m}{C_D A}$$

is a measure of the ability of the spacecraft to overcome air resistance. For typical spacecraft $1/\beta$ values range from .01 x 10^{-6} to .04 x 10^{-6} km^2/kg.

Therefore,

$$D = \frac{\rho |V| V}{2\beta} \tag{3.2}$$

While drag is acting in the direction opposite to the satellite's motion, there are forces perpendicular to the direction of motion. These forces have components passing through the center of mass which cause lift, and components which produce a turning moment about the center of mass.

The turning moment is normally a destabilizing one for uncontrolled satellites. Consequently, the resultant value of the variant lift force will be zero. For a spinning body, there are moments which affect the orientation, thereby influencing the lift and drag forces. The precise prediction of the orbital motion of elongated bodies of revolution becomes infeasible in the absence of complete information about orientation and spin everywhere on the orbit. For these reasons, for near–spherical and cylindrical satellites with a length/diameter ratio greater than about one, the forces perpendicular to the direction of motion can be ignored [59].

3.2 Density Models

The feature of the atmosphere which has a profound effect upon the satellite is the density (ρ). The density has been investigated over the years by the study of the rate of contraction of satellite orbits as well as with the aid of instruments contained in the satellites.

Research has revealed that the change in density in the upper atmosphere above 250 km can be large and is very time–dependent. Variation in density occurs as the atmosphere responds to solar activity. Fluctuations in density include: (1) irregular diurnal variations resulting from ephemeral solar disturbances, (2) a 27–day variation correlated with the period of axial rotation of the Sun with respect to the Earth, (3) an eleven year variation corresponding to the sunspot cycle, (4) seasonal variations caused by change in the distance from the Sun and the inclination of the Earth's orbit to the Sun's equator, and (5) irregular and impermanent variations affiliated with transient geomagnetic disturbances.

Eliminating the time–dependent variations dictates an approximate model of the atmosphere. Important assumptions provide analytical representations which allow simplification while maintaining reasonable accuracy. A significant simplification is accomplished by assuming that the atmosphere is spherically symmetrical. Consequently, the atmospheric density is a function of the distance from the center of the Earth. The slight inaccuracy introduced by this assumption facilitates the mathematical formulation necessary for determining variations in orbital elements.

The simplest density model assumes that the atmospheric density decreases exponentially with the distance from the center of the Earth. Assuming that the *scale height* (H) is constant over a small altitude interval, the density function can be written as [58,61]:

$$\rho_2 = \rho_1 \exp \left[(r_1 - r_2) / H \right] \qquad (3.3)$$

Consequently,

$$H = \frac{r_1 - r_2}{\ln(\rho_1/\rho_2)}$$

(3.4)

If the oblateness of the atmosphere is to be considered, the same density variation (3.3) can be used as a function of the altitude above the Earth's ellipsoidal surface. The altitude is determined by subtracting the radial distance to the surface of the Earth from the radial distance of the satellite. The radial distance to the surface is found using [12]

$$r_E = R \left[1 - (f + \frac{3}{2} f^2 + ...) \sin^2 \varphi + \frac{3}{2} f^2 \sin^4 \varphi - ... \right]$$

(3.5)

here

f = flattening ratio of the Earth = $1/298.24$

φ = latitude

R = equatorial radius = 6378.163 km

Using *reference* or *cardinal* altitudes (10 km increments) on both sides of the computed altitude (h = r_E - r), a standard atmospheric table such as the *U.S. Standard Atmosphere, 1976* (see Appendix B) can be used to compute the density at the two radial distances. Exercising equation (3.4) a scale height can be computed for that particular 10 km interval. If one end point of the interval is now used as position one with the satellite designated as position two, equation (3.3) can be employed to determine the density at that exact altitude. This method for determining density is best utilized when a numerical integration scheme is used to continuously update the values of the osculating orbital elements. The use of tabular values provides the accuracy of a dynamic atmosphere.

A generalization of the exponential density function is the spherical power density function model which assumes the scale height is linear [62]

$$\rho_2 = \rho_1 \left(\frac{r_1 - s}{r_2 - s} \right)^\tau$$

(3.6)

where τ, which is restricted to positive integer values, and s are disposable parameters. For coverage of all reasonable regions averaged over an 11 year cycle, the following values result: (1) τ = 4, (2) r_1 = 6498 km, and (3) s = 6456 km.

3.3 Numerical Computation of Element Change

To examine the change in a and e caused by drag the radial, transverse, and normal force components (same direction as f_1, f_2, and f_3 respectively in figure 2.1) are expressed in terms of a component along the tangent (f_T) and a component normal to the orbit (f_N). If the angle which the tangent to the orbit makes with the transverse component is ψ, then

$$f_1 = f_T \sin \psi - f_N \cos \psi$$

$$f_2 = f_T \cos \psi - f_N \sin \psi$$

These values for f_1 and f_2 can be substituted into the Lagrange planetary equations (2.5) and (2.6). Since the force normal to the orbital plane is extremely small in comparison to the tangential component, it can be ignored for this approach. This yields a modified set of Lagrange equations. The independent variable can be changed from time to true anomaly using two–body relationships and subsequently to eccentric anomaly. The result is

$$\frac{da}{dE} = \frac{-\rho a^2 (1 + e \cos E)^{3/2}}{\beta \ (1 - e \cos E)^{1/2}} \tag{3.7}$$

$$\frac{de}{dE} = \frac{-\rho a (1 + e \cos E)^{1/2} (1 - e^2) \cos E}{\beta \ (1 - e \cos E)^{1/2}} \tag{3.8}$$

For the change in a and e over one revolution

$$\Delta a = -\frac{a^2}{\beta} \int_0^{2\pi} \frac{\rho (1 + e \cos E)^{3/2} \ dE}{(1 - e \cos E)^{1/2}} \tag{3.9}$$

$$\Delta e = -\frac{a}{\beta} \int_0^{2\pi} \frac{\rho (1 + e \cos E)^{1/2} (1 - e^2) \cos E \ dE}{(1 - e \cos E)^{1/2}} \tag{3.10}$$

The change in perigee over one revolution is found in the following manner:

$$r_p = a \ (1 - e)$$

$$dr_p = (1 - e) \ da - a \ de$$

$$\Delta r_p = (1 - e) \ \Delta a - a \Delta e \tag{3.11}$$

Substituting equations (3.9) and (3.10) into (3.11)

$$\Delta r_p = - \frac{a^2 (1 - e)}{\beta} \int_o^{2\pi} \frac{\rho (1 + e \cos E)^{1/2}}{(1 - e \cos E)^{1/2}} \ (1 - \cos E) \ dE \tag{3.12}$$

In like manner the change in apogee is

$$r_A = a \ (1 + e)$$

$$\Delta r_A = (1 + e) \ \Delta a + a \Delta e$$

$$\Delta r_A = - \frac{a^2 (1 + e)}{\beta} \int_o^{2\pi} \rho \frac{(1 + e \cos E)^{1/2}}{(1 - e \cos E)^{1/2}} \ (1 + \cos E) \ dE \tag{3.13}$$

Comparison of equations (3.12) and (3.13) reveals that unless the eccentricity is very small, the apogee change that would be experienced over one revolution is larger than the perigee change.

3.4 Analytical Computation of Element Change

An expression to find the density in an oblate atmosphere is developed by King-Hele [58]. Using equation (3.5) to determine the radial distance from the Earth's center to the surface of an oblate spheroid

$$r = R \ (1 - f \sin^2 \varphi + 0 \ (f^2)) \tag{3.14}$$

The radial distance at the initial perigee is therefore

$$r_p = R \ (1 - f \sin^2 \varphi_{p_o}) \tag{3.15}$$

Solving for R from equation (3.15) and substituting back into (3.14)

$$r = \frac{r_p \, (1 - f \sin^2 \varphi)}{(1 - f \sin^2 \varphi_p)} \qquad (3.16)$$

The spheroid is now defined in terms of latitude of the initial perigee and latitude of the satellite at any position. The density at any point can be defined in terms of the density at the perigee. From equation (3.3)

$$\rho_2 = \rho_P \exp \left[\, (r - r_2) / H \, \right] \qquad (3.17)$$

Using trigonometric identities, the latitude of the satellite can be expressed as a function of the position

$$\sin \varphi = \sin i \sin (\omega + v) \qquad (3.18)$$

Substituting (3.16) and (3.18) into (3.17), the density as a function of radial distance and true anomaly is

$$\rho_2 = \rho_P \exp \left[(r_p - r_2)/H + c \cos 2 \, (\omega + v) - c \cos 2 \, \omega_0 + O(f^2) \right.$$

$$\text{where } c = {}^1\!/_2 \, f \, r_p \sin^2 i \, / H \qquad (3.19)$$

Expanding $\exp(c \cos 2 \, (\omega + v))$ as an exponential series expansion and transforming terms of true anomaly into terms containing eccentric anomaly equation (3.19) can be written as [58]

$$\rho_2 = q \exp\{(a \, e \cos E - a)\} [\, 1 + c \cos 2 \, (\omega + E) - 2ce \sin 2 \, (\omega + E)$$

$$\times \sin E + c^2\!/_4 (1 + \cos 4(\omega + E)) - ce^2\!/_2 (\cos 2\omega + 2\cos 2(\omega + E)$$

$$- 3 \cos 2(\omega + E) \cos 2 \, E) - c^2 e \sin 4 \, (\omega + E) \sin E$$

$$+ O \, (ce^3, c^2 e^2)] \qquad (3.20)$$

$$\text{where } q = \rho_p \exp({}^{r_P}\!/H - c \cos 2\omega_0)$$

$$\omega_0 = \text{initial argument of perigee}$$

By performing the following: (1) substituting (3.20) into a series expansion of the integrands (3.9) and (3.10), (2) utilizing the integral representation of

the Bessel function (i.e. $I_n(z) = {}^2/_\pi \int_0^{2\pi} \exp(z \cos A) \cos n\, A\, dA$, where A is an angle), and (3) eliminating periodic terms the following represent changes over one revolution

$$\Delta a_{sec} = -2\pi a^2/\beta \quad q \exp(^{-a}/_H)[I_o + 2e\, I_1 + {}^3/_4\, e^2\, (I_o + I_2) + e^3/_4\, (3\, I_1 + I_3)$$
$$+ O(e^4, ce^3)] \tag{3.21}$$

$$\Delta e_{sec} = -2\pi a^2/\beta \quad q \exp(^{-a}/_H)[I_1 + {}^e/_2\, (I_o + I_2) + e^2/_8\, (-5\, I_1 + I_3)$$
$$-e^3/_{16}\, (5\, I_o + 4\, I_2 - I_4) + O(e^4)] \tag{3.22}$$

Substituting equations (3.21) and (3.22) into (3.11)

$$\Delta r_{p_{sec}} = -2\pi a^2/\beta \quad q \exp(^{-a}/_H)\, [I_o - I_1 - {}^e/_2\, (3\, I_o - 4\, I_1 + I_2)$$
$$+ e^2/_8\, (6\, I_o - 11\, I_1 + 6\, I_2 - I_3) + e^3/_{16}\, (-7\, I_o + 12\, I_1 - 8\, I_2 + 4\, I_3 - I_4)$$
$$+ O(e^4)] \tag{3.23}$$

The argument of the Bessel functions is $z = {}^{ae}/_H$. I_o and I_1 can be estimated using an asymptotic expansion or polynomial approximation while I_2, I_3, and I_4 can be found using the recurrence relation

$$I_{n+1}(z) = I_{n-1}(z) - {}^{2n}/_z\, I_n(z)$$

For the complete development of the change in the other orbital elements over one revolution see reference 58.

$$\Delta i = \frac{-\pi a^2}{2\beta} w\, (\frac{a}{\mu f})^{1/2} \exp(^{-a}/_H) \sin i\, [\, I_o + (1+c)I_2 \cos 2\omega$$

$$-4eI_1 \cos^2 \omega + \frac{1}{2}\, c\, (I_o + I_4 \cos 4\omega) + O(c^2, e^2)] \tag{3.24}$$

where w = angular velocity of the atmosphere

and $\quad f = (1 - \frac{r_p\, w}{v_p} \cos i)^2$

Substituting the half–angle formula for $\cos^2\omega$ and eliminating the periodic terms

$$\Delta i_{sec} = \frac{-\pi a^2}{2\beta} w\, (\frac{a}{\mu f})^{1/2} \exp(^{-a}/_H) \sin i\, [\, I_o - 2eI_1] \tag{3.25}$$

If (3.25) is written as

$$\Delta i_{sec} = -S [I_0 - 2eI_1]$$

it is evident that for all values of a, e, and i, S > 0. Therefore, the inclination angle decreases as long as $I_0 > 2eI_1$. Using a polynomial approximation [63]

$$I_0(z) = 1 + .24999985 \, z^2 + .01562519 \, z^4 + \ldots$$

$$I_1(z) = z[^1/_2 + .062499978 \, z^2 + .00260419 \, z^4 + \ldots]$$

it is clear that for all feasible values of eccentricity for near Earth satellites $I_0 > 2eI_1$.

Examining a worst possible situation demonstrates that the relationship is satisfied

a = 7000 km	I_0 = 26.868438
H ≈ 72.6	$2eI_1$ = 3.8241799
e = .06	

The other two orbital elements, Ω and ω, experience no secular change due to drag.

CHAPTER IV

MINIMUM ALTITUDE VARIATION ARCS

4.1 Requirement

A satellite which experiences minimum altitude variation over a circumscribed latitude range can be very useful for scientific research and application experiments. Motivation for achieving and maintaining this category of frozen orbit includes: (1) study of the flattening and other dynamic properties of the atmosphere, (2) photo resolution optimization of preset optical systems, and (3) minimization of necessary geometric corrections to satellite–produced images.

A good example of the necessity of this type of arc is the SEASAT–A satellite, launched on June 26, 1978, to provide a global ocean dynamics monitoring system. The instrument used to obtain radar imagery of ocean waves, ice and snow cover, and land surfaces is a Synthetic Aperture Radar (SAR) which has a resolution of 25 meters. Constraints dictate minimum altitude variation over SAR stations which are all located in the Northern Hemisphere [56].

To date, very little literature exists on the subject of minimum altitude variation arcs. Some work was accomplished by Kalil [64] as he studied the first–order effects of oblateness while neglecting entirely atmospheric drag. Since it is near–Earth satellites for which the requirement for minimum altitude deviation may exist, it is essential to include the effects of atmospheric drag to realize a comprehensive study.

Altitude deviations are best minimized by essentially modeling the shape of the Earth over the latitude range of interest. The proper combination of semimajor axis, eccentricity, inclination, and argument of perigee produces the desired arc.

4.2 Latitude Coverage and Eccentricity Required

To determine the minimum altitude variation several approaches can be exercised. One such approach involves the continuous computation of the altitude along the orbit at intervals defined by a predetermined step size. The difference between the continuously updated altitude and the initial altitude is computed until the maximum allowable limit is reached. This procedure becomes a tradeoff between eccentricity and the latitude coverage attainable.

Referring to figure 4.1: r_s is the radial distance from the center of the Earth to the satellite, r_E is the distance from the center to the surface of the Earth, and h is the altitude above the surface of the Earth. The starting position is designated as 1 while 2 represents the position at an interval or multiple of intervals of time later. Each time an interval is covered the new state becomes position 2.
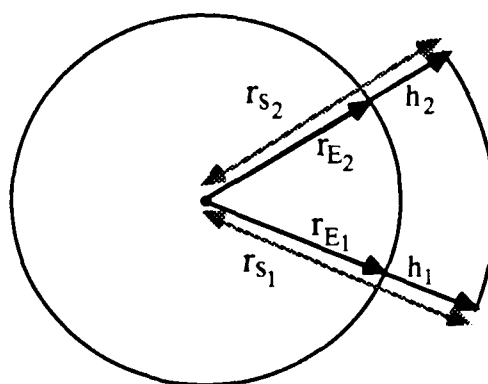
Figure 4.1 RADIAL DISTANCES AND ALTITUDES

The altitudes corresponding to the respective positions are

$$h_1 = r_{s_1} - r_{E_1} \qquad\qquad (4.1)$$

$$h_2 = r_{s_2} - r_{E_2} \qquad\qquad (4.2)$$

Subtracting the above equations

$$h_1 - h_2 = (r_{s_1} - r_{s_2}) - (r_{E_1} - r_{E_2}) \qquad\qquad (4.3)$$

Substituting equation (2.26) for r_s and equation (3.5) for r_E, assuming a secularly constant a and e (no drag), and using (4.3) to include $O(e^3)$ for $e < .1$

$$h_1 - h_2 = a\,[(\cos M_2 - \cos M_1)e + (\cos 2M_2 - \cos 2M_1)e^2$$
$$+ {}^3/8\,(3 \cos 3M_2 - 3 \cos 3M_1 - \cos M_2 + \cos M_1)e^3]$$
$$- R\,[(f + {}^3/2\,f^2)(\sin^2\varphi_2 - \sin^2\varphi_1) + {}^3/2\,f^2(\sin^4\varphi_1 - \sin^4\varphi_2)]$$

$$(4.4)$$

There are two ways in which equation (4.4) can be employed. The first approach is to compute the latitude range that can be achieved prior to exceeding the maximum allowable deviation from the initial altitude given an a and e. The second way is to start with the semimajor axis and latitude range desired and then determine a compatible e which permits $|h_1 - h_2|$ to be a minimum. This method requires an iterative scheme where $|h_1 - h_2| = h_{1-2}$ is defined as the performance index [65]. For a minimum to exist over the range of possible values of eccentricity,

$$\Delta h_{1-2}\,(e) = h_{1-2}\,(e + \Delta e) - h_{1-2}\,(e) > 0$$

where Δe is a small incremental change.

The latitude can be computed at the end of each interval in the following manner:

(1) An initial satellite radial distance and mean anomaly is established.

(2) Recall $\Delta a_{sec} = \Delta e_{sec} = 0$ in the absence of drag. Using equation (2.28) and the secular equation (2.19) for the rate of change of mean anomaly per second, the radial distance can be computed at each new position.

$$dr = \Delta r = \partial r / \partial M \; dM$$

$$r_{s_2} = r_{s_1} + \Delta r$$

(3) The updated mean anomaly is

$$M_2 = M_1 + \Delta M$$

(4) From Kepler's equation, $M = E - e \sin E$, a method of successive approximations can be employed to determine eccentric anomaly.

(5) True anomaly for the elliptic orbit can be calculated from the relation

$$\tan \frac{v}{2} = \left(\frac{1+e}{1-e} \right)^{1/2} \tan \frac{E}{2}$$

(6) Given an argument of perigee ω, the argument of latitude is

$$u = v + \omega \qquad\qquad (4.5)$$

(7) From spherical trigonometry

$$\sin \varphi = \sin i \sin u \qquad\qquad (4.6)$$

(8) All variables are now known for substitution into equation (4.4) to compute the deviation in altitude from the initial position to the next position of the satellite.

(9) If $\in$ is the predetermined maximum allowable altitude deviation, the process is repeated until $|h_1 - h_2| > \in$

4.3 Rate of Change of Altitude

The radial distance measured from the center of the Earth to the satellite in terms of true anomaly is

$$r = \frac{a (1-e^2)}{1+ e \cos v} \qquad\qquad (4.7)$$

Equation (3.5) to $O(f)$ is

$$r_E = R [1- f \sin^2 \varphi] \qquad\qquad (4.8)$$

substituting (4.5) and (4.6) in (4.8)

$$r_E = R \,[1\text{-}f \sin^2 i \sin^2 (v + \omega)] \qquad (4.9)$$

The altitude above the surface of the Earth is

$$h = r - r_E \qquad (4.10)$$

Substituting (4.7) and (4.9) in (4.10), assuming no drag (i.e. a and e are secularly constant), taking the derivative of altitude with respect to true anomaly, and simplifying with trigonometric identities the result is

$$\frac{dh}{dv} = \frac{ae\,(1\text{-}e^2)\,\sin v}{(1+ e \cos v)^2} + Rf \sin^2 i \sin 2(\, v + \omega\,) \qquad (4.11)$$

From (4.11) it is obvious that the change in altitude is a function of the shape of the Earth, the size and shape of the orbit, and the orientation of the orbital plane. For a given a and e the rate of change is highly dependent upon the argument of perigee and inclination angle. For a given ω the change in altitude with respect to the change in true anomaly is a periodic function with period 2π.

The next series of graphs demonstrate the effect of argument of perigee, eccentricity, semimajor axis, and inclination on the rate of change of altitude as determined by equation (4.11). A comparison of figures 4.2 and 4.3 shows that a change of 500 km in semimajor axis has little effect on the rate of change of altitude for a given eccentricity, inclination, and argument of perigee. The maximum change in rate is $\pm\, 5$ km/rad.

A change in eccentricity from .01 to .0024 causes a large change for a given semimajor axis, inclination, and argument of perigee. From figures 4.3 and 4.4 the change in the rate is seen to be as high as 50 km/rad. Figures 4.4, 4.5, and 4.6 show that for a constant a, e, and ω, as the inclination angle increases to 90° the rate of change of altitude increases. From i = 45° to i = 90° the change in the rate is about

10km/rad. Study of the graphs reveals that the minimum rate of altitude change ($^{dh}/dv = 0$) occurs at or around perigee/apogee. Regardless of the argument of perigee as the eccentricity increases the minimum rate progresses closer to the perigee/apogee. Therefore, the minimum altitude variation occurs more closely to perigee/apogee.

Zero rate of change always occurs at the perigee when it is located on the equator (i.e. $\omega = 0°$). As the eccentricity decreases the argument of perigee causes the value of true anomaly for which $^{dh}/dv = 0$ to shift away from perigee/apogee. Figure 4.5 shows that this displacement is as much as 70°.

The latitude range over which the minimum altitude deviation occurs can be determined easily from the figures. All three values of i, v, and ω corresponding to the minimum rate can be obtained from the graph and equation (4.6) used to determine the respective latitude.

Data contained in figures 4.7, 4.8, and 4.9 include oblateness effects. Figure 4.7 demonstrates that the minimum altitude a satellite obtains in an orbit does not necessarily occur at the same latitude at which perigee occurs. The latitude of the perigee φ_p on this plot is 50.77°N. Depending on the eccentricity the minimum altitude deviates from perigee. As the eccentricity increases the secular change in the altitude over the latitude range of interest increases.

Figures 4.8 and 4.9 show a magnified view of the effect of argument of perigee over a latitude range 30° to 60°N. The latitude range of interest can vary depending upon the objective of the satellite mission. Deviation is measured against the altitude at the start of the arc. In this case, study of the entire latitude arc of 30° shows that if the orbit has an eccentricity of .005 and initial argument of perigee of 66° the change in altitude is + 6km. If instead $\omega = 80°$ the deviation over 30° of latitude is less than 1 km. By proper adjustment of argument of perigee the altitude deviation over any latitude range can be minimized for a given semimajor axis and eccentricity.

a = 7000 km   e = .01   i = 63.44°

Values of ω

Figure 4.2

a = 7500 km   e = .01   i = 63.44°

Values of ω
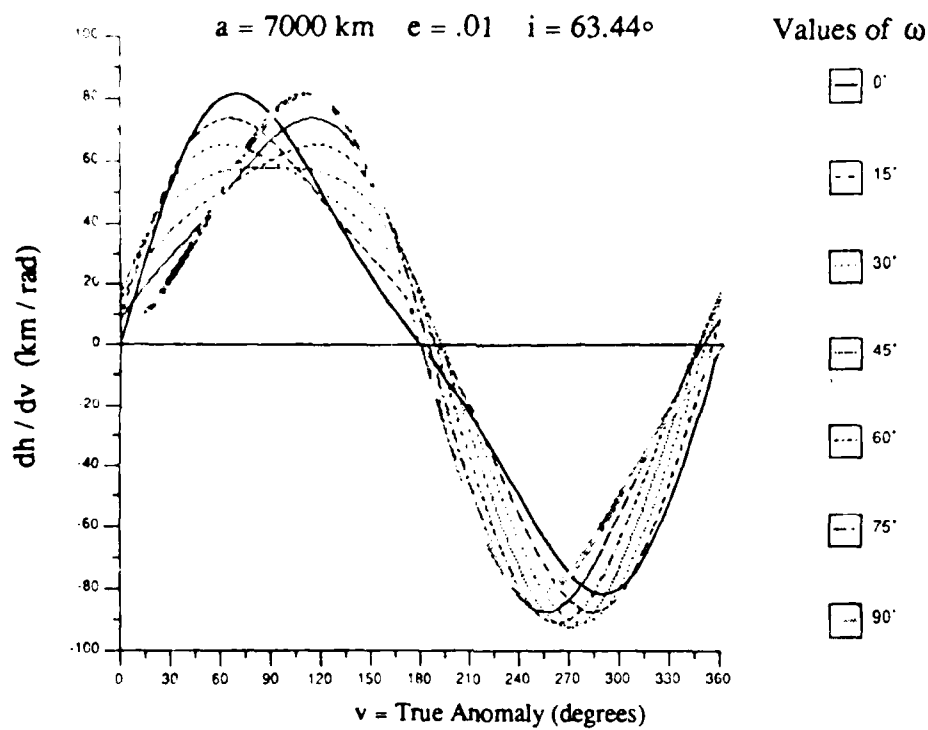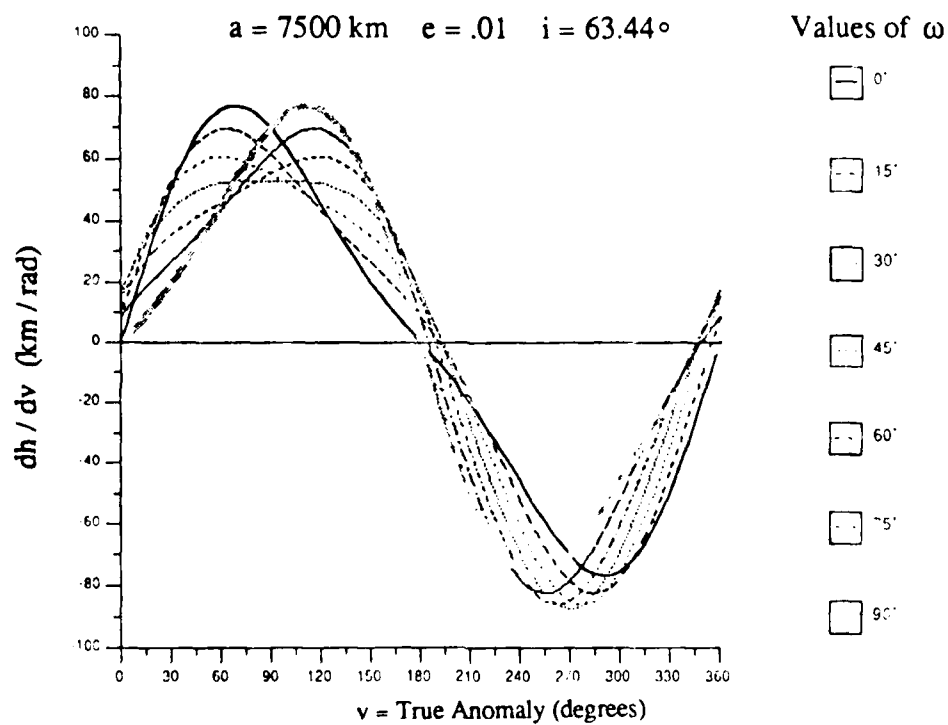
Figure 4.3

Figure 4.4

Figure 4.5

a = 7500 km   e = .0024   i = 90.0°   Values of ω

dh / dv (km / rad)

v = True Anomaly (degrees)

0°
15°
30°
45°
60°
75°
90°

Figure 4.6

a = 7500 km   i = 63.44°   ω = 60°

SECULAR CHANGE IN ALTITUDE (km)

ECC = .02
ECC = .04
ECC = .06
ECC = .08

$\varphi_p = 50.77°$

LATITUDE (degrees)

Figure 4.7

a = 7500 km   i = 63.44°   ω = 66°

Figure 4.8

a = 7500 km   i = 63.44°   ω = 80°
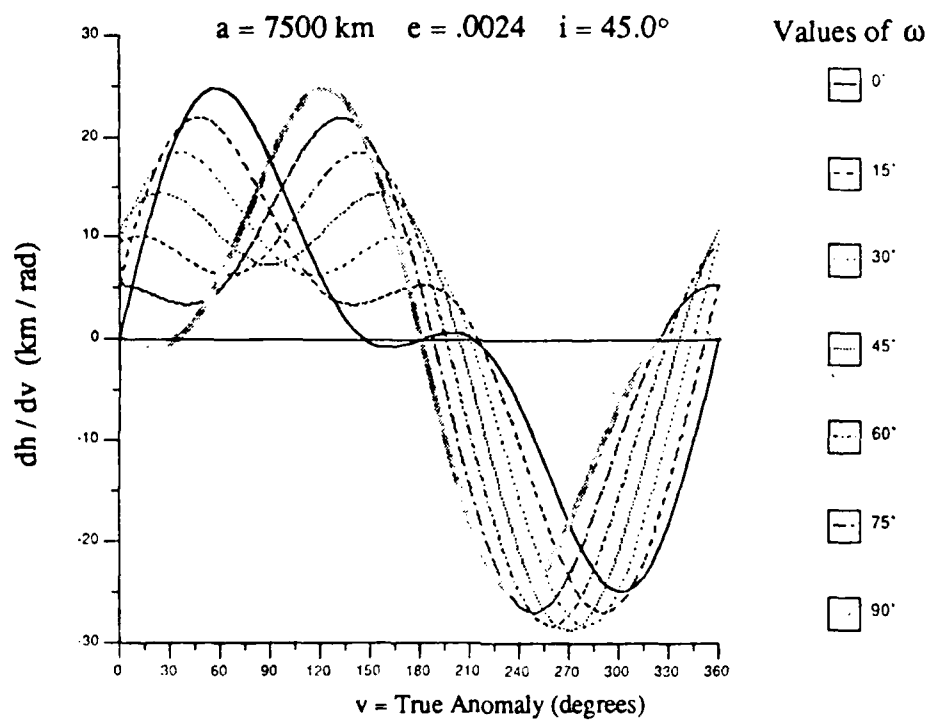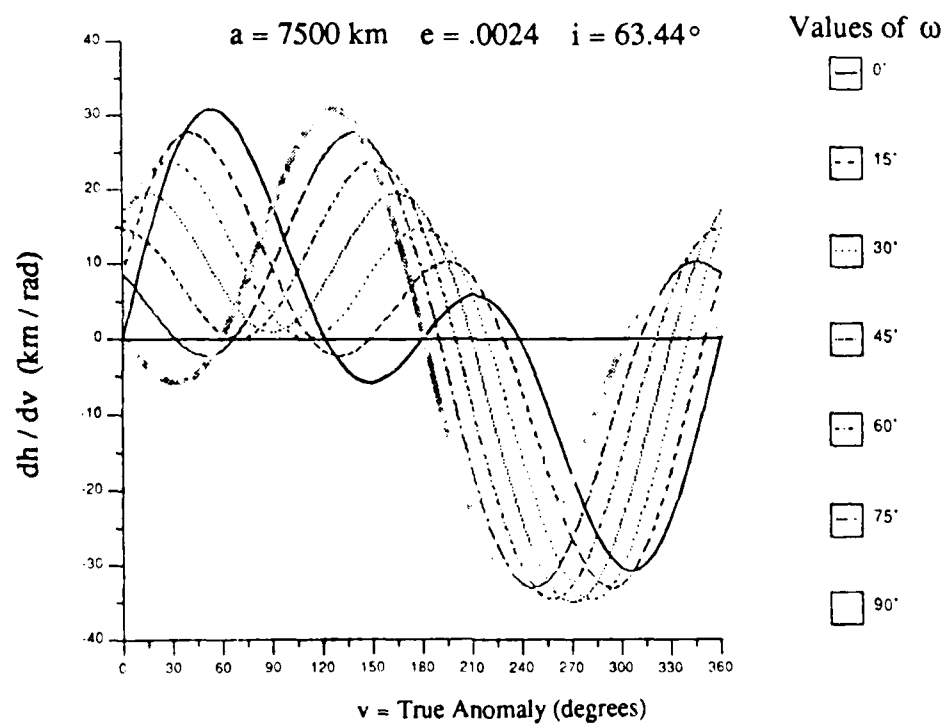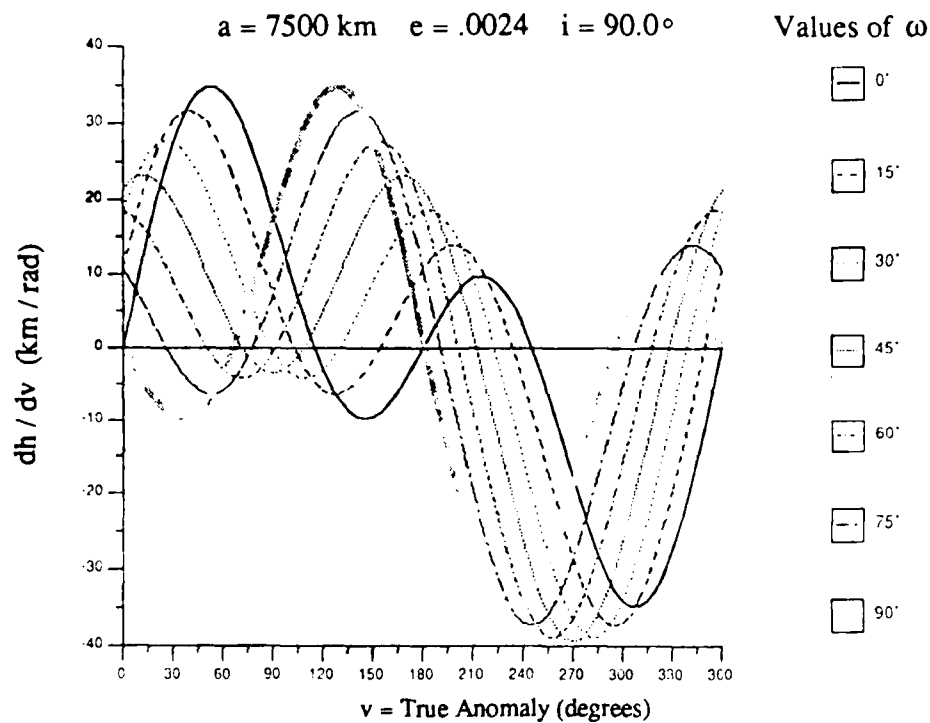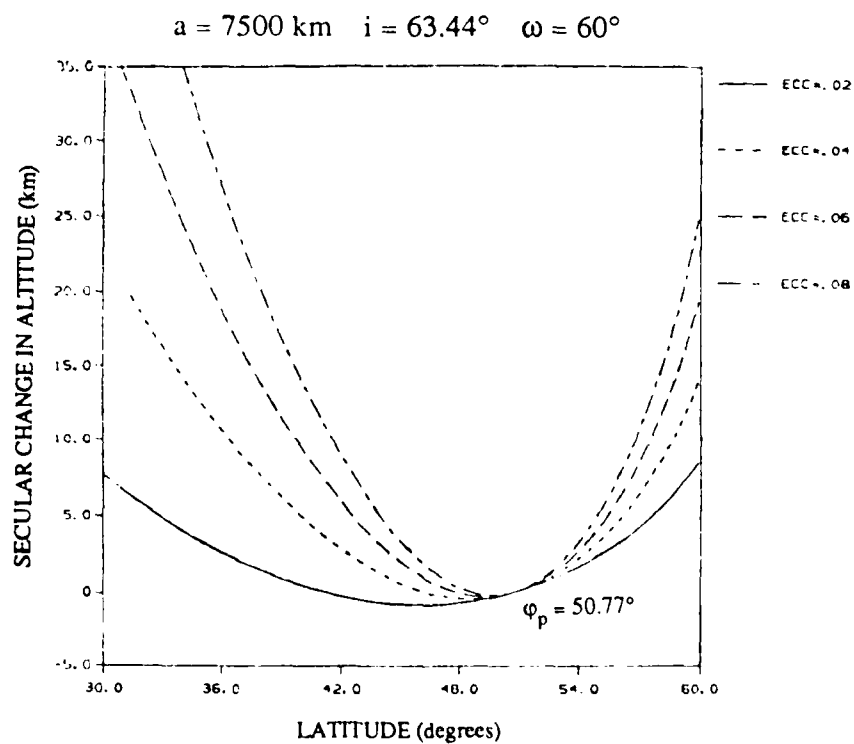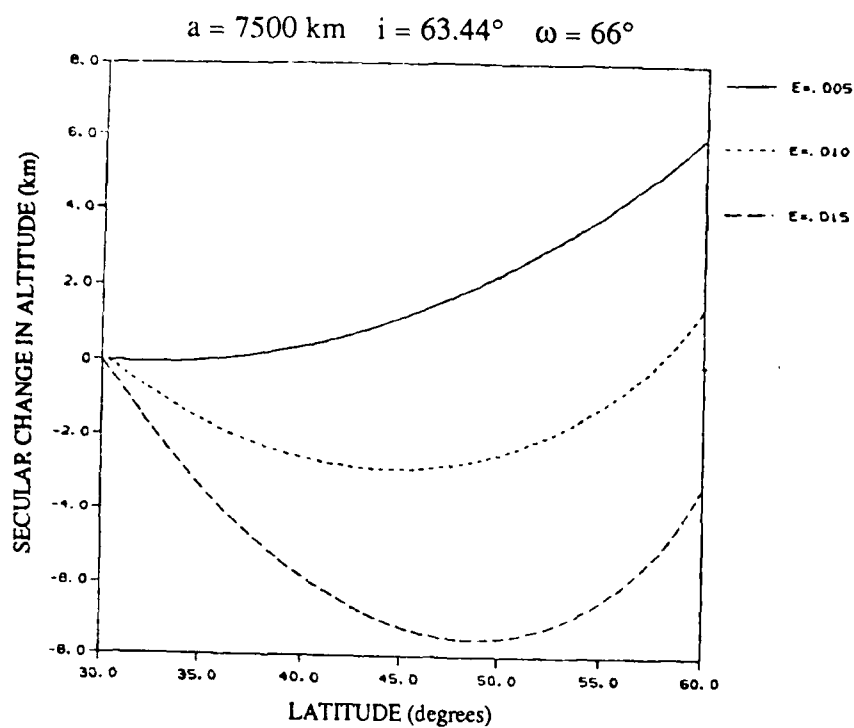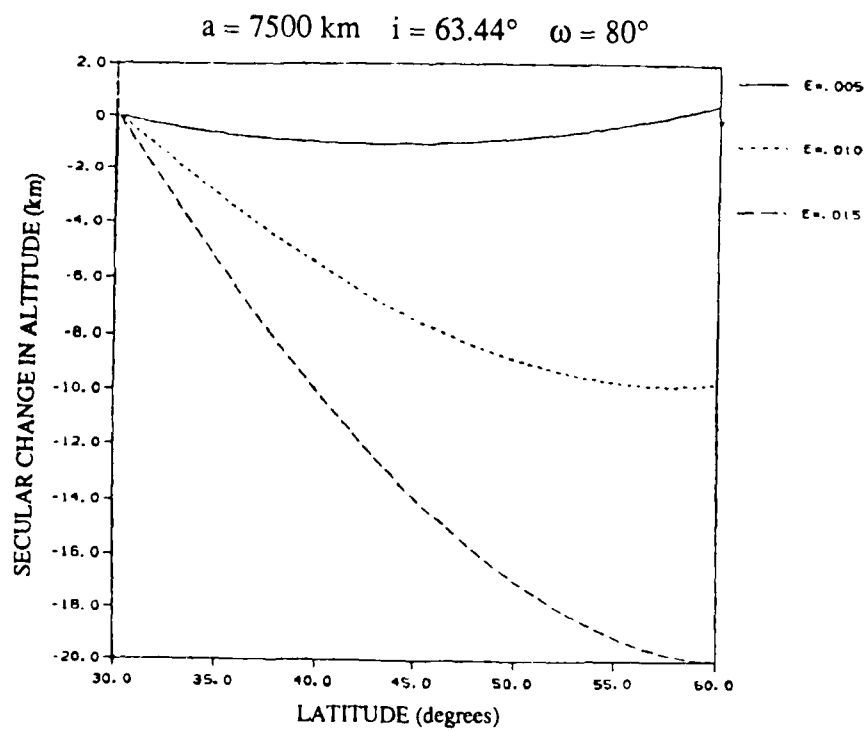
Figure 4.9

4.4 Rate of Change of Perigee Latitude

Starting with the combination of (4.5) and (4.6)

$$\sin \varphi = \sin i \sin (\nu + \omega)$$

Using the trigonometric identity for the sum of angles

$$\sin \varphi = \sin i \left[\sin \nu \cos \omega + \cos \nu \sin \omega\right]$$

Since $\nu = 0$ at the perigee latitude φ_p

$$\sin \varphi_p = \sin i \sin \omega \qquad (4.12)$$

The derivative of (4.12) with respect to time is

$$\cos \varphi_p \, \dot{\varphi}_p = \sin i \cos \omega \, \dot{\omega} + \sin \omega \cos i \; di/dt$$

Recalling $di/dt)_{sec} = 0$

The secular change in the perigee latitude is

$$\dot{\varphi}_p = \frac{\sin i \cos \omega \, \dot{\omega}}{\cos \varphi_p} \qquad (4.13)$$

From (4.13) it is obvious that there are two ways to freeze the perigee latitude. The first is by achieving an argument of perigee of 90°. As discussed in section 2.8 when $\omega = 90°$ the de/dt due to the J_3 term is zero. The eccentricity can then be computed so that $d\omega/dt$ due to the J_2 and J_3 terms is zero. The second way is to establish an orbit having an inclination angle that causes the change in ω to be zero for a given eccentricity and semimajor axis. As discussed in section 2.5 to $O(J_2)$ this occurs when $i = 63.44°$.

4.5 Freezing the Altitude of An Arc
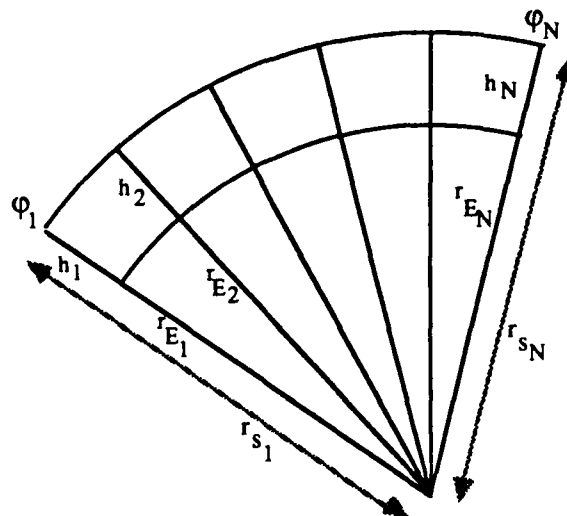
Figure 4.10 THE LATITUDE ARC

If the latitude arc is divided into N equal segments fixed by a predetermined time increment the altitude change at the end of each interval can be determined in the following manner:

$$h_1 = r_{s_1} - r_{E_1} \tag{4.14}$$

$$h_2 = r_{s_1} + \Delta r_{1,2} - r_{E_2} \tag{4.15}$$

Subtracting (4.15) from (4.14)

$$h_1 - h_2 = \Delta h_{1,2} = r_{E_2} - r_{E_1} - \Delta r_{1,2}$$

For the next interval

$$\Delta h_{2,3} = r_{E_3} - r_{E_2} - \Delta r_{2,3}$$

In general terms

$$\Delta h_{N-1,N} = r_{E_N} - r_{E_{N-1}} - \Delta r_{N-1,N}$$

Using (2.27) for $\Delta r_{N-1,N}$ the altitude difference over each interval on the arc is given by

$$
\begin{pmatrix} \Delta h_{1,2} \\ \Delta h_{2,3} \\ \vdots \\ \Delta h_{N-1,N} \end{pmatrix} = \begin{pmatrix} {}^r E_2 - {}^r E_1 \\ {}^r E_3 - {}^r E_2 \\ \vdots \\ {}^r E_N - {}^r E_{N-1} \end{pmatrix} - \begin{pmatrix} \frac{\partial r}{\partial a} \Delta a_{1,2} + \frac{\partial r}{\partial e} \Delta e_{1,2} + \frac{\partial r}{\partial M} \Delta M_{1,2} \\ \frac{\partial r}{\partial a} \Delta a_{2,3} + \frac{\partial r}{\partial e} \Delta e_{2,3} + \frac{\partial r}{\partial M} \Delta M_{2,3} \\ \vdots \\ \frac{\partial r}{\partial a} \Delta a_{N-1,N} + \frac{\partial r}{\partial e} \Delta e_{N-1,N} + \frac{\partial r}{\partial M} \Delta M_{N-1,N} \end{pmatrix}
$$

$$(4.16)$$

The value of the orbital elements can be computed using an Euler type scheme. From the initial values of a, e, M, and E at the beginning latitude the change in mean anomaly over the first interval can be determined from (2.19). The mean anomaly at the start of the next interval is

$$M_2 = M_1 + \Delta M_{1,2}$$

E_2 can be calculated from M_2 using an iterative process. Employing (3.9) and (3.10) the change in semimajor axis ($\Delta a_{1,2}$) and eccentricity ($\Delta e_{1,2}$) due to drag can be computed using E_1 and E_2 as the limits of integration. There is no secular change in these two elements due to the gravitational field. However, secular changes due to gravity occur over the interval to Ω and ω and can be calculated if desired. Therefore,

$$a_2 = a_1 + \Delta a_{1,2}$$

$$e_2 = e_1 + \Delta e_{1,2}$$

$$\Omega_2 = \Omega_1 + (d\Omega/dt)\, \Delta t_{1,2}$$

$$\omega_2 = \omega_1 + (d\omega/dt)\, \Delta t_{1,2}$$

With the new values of a and e an updated value of mean anomaly change $\Delta M_{2,3}$ can be determined. Then

$$M_3 = M_2 + \Delta M_{2,3}$$

The process is repeated until N intervals have been completed and the exit latitude is reached.

Using steps 5 and 6 on page 50 and equation (4.9) r_E can be calculated at the end of each interval. All information is now available for substitution into (4.16). The equation can be ⸱⸱ to compute the altitude deviation over each interval as well as the maximum positive and negative deviation over the entire arc. Additionally, the minimum amount of total altitude deviation over the arc occurs when

$$\sum_{n=2}^{N} (\Delta h_{N-1,N})^2$$

is minimized. In all cases it becomes a matter of selecting the appropriate a, e, and ω to minimize the deviation.

For this study, a fourth-order Runga–Kutta method was used in combination with a tabular density model (see Appendix B) for the integration of (3.9) and (3.10). Three different step sizes of 3, 5, and 10 seconds were exercised; the results varied very little. A fraction of the findings are presented in Tables 4-1 through 4-6.

Max + is the maximum positive altitude deviation for the latitude range studied while Max – is the maximum negative altitude deviation. Both deviations are measured against the altitude at the initial latitude. $h_1 - h_N$ is the altitude difference between the initial altitude and the altitude N intervals later at the exit latitude. In Tables 4-5 and 4-6 Δa is the change in semimajor axis over the latitude range while Δe is the change in eccentricity.

Table 4-2 shows a comparison of minimum altitude deviation for a very small eccentricity (.0022) versus a larger eccentricity (.01). Minimum deviation for the higher eccentricity is approximately 2.7 km versus .36 km for the lower e.

Tables 4-1, 4-2, and 4-3 demonstrate the effect of eccentricity and argument of perigee on minimum altitude deviation for a given semimajor axis and inclination. Tables 4-4 and 4-5 show the effect of semimajor axis on altitude deviation

over a latitude range given an eccentricity, inclination, and argument of perigee. The effect of drag is to decrease the maximum positive deviation while increasing the maximum negative deviation. Table 4-6 shows a comparison of data determined from the same orbital elements but different ballistic coefficients and different integration step sizes. As β increases the maximum positive altitude deviation decreases while the maximum negative deviation increases.

The data in Table 4-3 correlates favorably with figure 4.5. The minimum altitude deviation for e = .0024, a = 7500 km, and i = 63.44° occurs when ω = 69°. Over the latitude range of 30°-60°N the deviation is approximately .18 km. A review of figure 4.5 indicates that when ω = 69° the minimum rate of altitude change is experienced between 35° and 77° true anomaly which corresponds to latitudes 60°N and 30°N respectively. Examination shows that over this range the dh/dv curve rides the zero value for approximately 15°.

The data contained in the tables that follow include secular effects only. The variational equations of the averaged elements were presented without having included the short-periodic variations. The effects contributed by the short-periodic variations can be studied by exercising the corresponding equations developed in reference 54. These equations can be used with (4.16) to predict the altitude deviation due to periodic variations. The procedure outlined in section 4.5 would then be accomplished to determine the combination of orbital elements that would produce minimum altitude deviation over the desired latitude range.

Table 4-1 ALTITUDE DEVIATION OVER LATITUDE RANGE 30° - 60°N
* Least Maximum Deviation at the Corresponding Eccentricity
$.002 \le e \le .005$

a = 6800 km

i = 63.44 °

	e	ω(deg)	Max + (km)	Max - (km)	$h_1 - h_N$ (km)
	.0020	35.0	.4070	1.0686	1.0686
*	.0020	36.0	.3926	1.0554	1.0554
	.0020	36.5	.3972	1.0557	1.0557
	.0022	48.5	.4218	.3806	.3806
*	.0022	49.0	.4187	.3889	.3889
	.0022	49.5	.3930	.4207	.4207
	.0024	60.0	.3015	.1911	.1864
*	.0024	60.5	.2738	.2425	.2390
	.0024	61.0	.2635	.2776	.2734
	.0026	67.0	.2067	.1153	.0464
*	.0026	67.5	.1924	.1627	.0933
	.0026	68.0	.1660	.2239	.1620
	.0028	72.0	.1524	.0638	.1111
*	.0028	72.5	.1254	.1296	.0424
	.0028	73.0	.1100	.1864	.0299
	.0030	76.0	.2538	.0639	-.2538
*	.0030	76.5	.1672	.1247	-.1672
	.0030	77.0	.0903	.1942	.0903
	.0050	78.5	1.0040	.9216	-1.0040
*	.0050	79.0	.8207	.9514	-.8207
	.0050	79.5	.6282	1.0408	-.6282

Table 4-2   ALTITUDE DEVIATION OVER LATITUDE RANGE 30° - 60°N
e = .0022 and .01

a = 7000 km

i = 63.44°

e	ω(deg)	Max + (km)	Max - (km)	h_1-h_N (km)
.0022	50.0	.4790	.1356	.1356
.0022	53.5	.3634	.3283	.3283
* .0022	54.0	.3555	.3527	.3527
.0022	54.5	.3283	.3941	.3941
.0100	62.0	4.4216	1.9143	-4.4216
.0100	64.0	2.7079	2.5605	-2.7079
* .0100	64.5	2.2976	2.6576	-2.2976
.0100	65.0	1.9001	2.8653	-1.9001

Table 4-3   ALTITUDE DEVIATION OVER LATITUDE RANGE 30° - 60°N
.002 ≤ e ≤ .0032

a = 7500 km

i = 63.44°

e	ω(deg)	Max + (km)	Max - (km)	h_1-h_N (km)
* .0020	49.5	.4150	.3798	.3798
* .0023	65.5	.2197	.1736	.1322
* .0024	69.0	.1632	.1781	.0944
* .0025	71.5	.1395	.1298	-.0150
* .0026	74.0	.1055	.1323	-.0771
* .0027	76.0	.1796	.1096	-.1796
* .0028	78.5	.1476	.1956	-.1476
* .0032	85.0	.3059	.3332	-.3059

Table 4-6 ALTITUDE DEVIATION OVER LATITUDE RANGE 30°-60°N
With Drag

$i = 63.44°$ $\omega = 76.0°$ $e = .003$ $\beta = .01 \times 10^{-6}$ Interval Size = 5 sec.

a (km)	Δa (km)	Δe	Max + (km)	Max - (km)	$h_1 - h_N$ (km)
6800	.0007	.0000001	.2526	.0646	-.2526
6750	.0016	.0000001	.1632	.1179	-.1632
6700	.0041	.0000004	.0950	.1671	-.0950
6650	.0118	.0000011	.0647	.2324	.0089
6600	.0429	.0000041	.0501	.3342	.1470
6550	.2523	.0000245	.0156	.7736	.7189

$\beta = .04 \times 10^{-6}$ Interval Size = 5 sec.

a (km)	Δa (km)	Δe	Max + (km)	Max - (km)	$h_1 - h_N$ (km)
6800	.0026	.0000002	.2491	.0667	-.2491
6750	.0063	.0000006	.1624	.1154	-.1624
6700	.0164	.0000016	.0745	.1817	-.0721
6650	.0476	.0000046	.0548	.2790	.0779
6600	.1759	.0000170	.0314	.5335	.4180
6550	1.2844	.0001244	.0000	2.8811	2.8811

$\beta = .01 \times 10^{-6}$ Interval Size = 10 sec.

a (km)	Δa (km)	Δe	Max + (km)	Max - (km)	$h_1 - h_N$ (km)
6800	.0007	.0000001	.2448	.0724	-.2448
6750	.0016	.0000001	.1462	.1179	-.1462
6700	.0041	.0000004	.0783	.1670	-.0783
6650	.0117	.0000011	.0579	.2392	.0158
6600	.0429	.0000041	.0501	.3341	.1469
6550	.2481	.0000241	.0119	.7765	.7298

4.6 Impulse Requirements To Maintain Perigee/Apogee

To maintain the orbit and freeze the apogee and perigee height maintenance maneuvers must be performed. One way of performing the maneuvers is to allow the orbit to decay until one of the elements has changed an amount equal to or greater than a prescribed tolerance for that element. Another way is to apply corrective propulsion at perigee and apogee each orbit. In this study the second approach is used to provide the propulsion for counteracting drag effects. In both cases a two–impulse maneuver is initiated which transfers the satellite back to the original orbit. The transfer is virtually coplanar since the atmospheric velocity is small compared to the satellite velocity and consequently the majority of the perturbing force is in the plane of motion.

To conserve propellant a minimum total ΔV is of particular interest. The associated maneuver which corresponds to the least amount of energy consumed is the Hohmann transfer. This type of transfer represents the minimum total ΔV maneuver for cases where the ratio of large to small orbit radius is less than 11.8 [51,66].

The ΔV required to maintain the apogee height and then the perigee must be computed separately and then added together to determine the total impulse required. The amount of ΔV that is depleted as the satellite moves from the perigee to apogee should be added at the perigee. The amount of ΔV that is dissipated going from apogee back to the perigee should be inserted at the apogee.

Using the vis–viva integral the total ΔV required can be computed in the following manner

Figure 4.11 APOGEE CHANGE
DUE TO DRAG
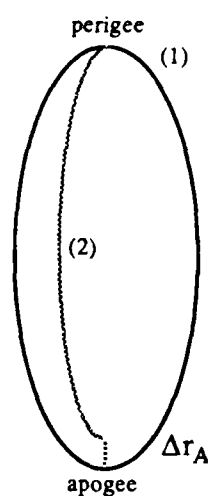
(1) no drag case

(2) actual, if no corrective
propulsion (o < v < 180)

The velocity at apogee if drag were not present

$$V_{1_A}^2 = \mu(\frac{2}{r_{1_A}} - \frac{1}{a_1}) \Rightarrow V_{1_A} = \sqrt{\frac{2\mu}{r_{1_A}} - \frac{\mu}{a_1}}$$

Since drag affects the radius and apogee height

$$V_{2_A} = \sqrt{\frac{2\mu}{r_{1_A} - \Delta r_A} - \frac{\mu}{a_1 - \Delta a_A}}$$

Therefore

$$|V_{1_A} - V_{2_A}| = \Delta V_{@perigee}$$
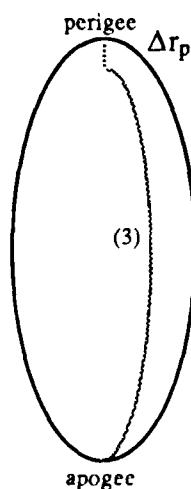
(3) = actual, if no corrective
propulsion (180 < v < 360°)

Figure 4.12 PERIGEE CHANGE
DUE TO DRAG

The velocity at perigee if drag were not present

$$V_{1_p} = \sqrt{\frac{2\mu}{r_{1_p}} - \frac{\mu}{a_1}}$$

Since drag affects the radius and perigee height

$$V_{3_p} = \sqrt{\frac{2\mu}{r_{1_p} - \Delta r_p} - \frac{\mu}{a_1 + \Delta a_p}}$$

Therefore

$$\Delta V_{@apogee} = |V_{1_p} - V_{3_p}|$$

And

$$\Delta V_{Total} = \Delta V_{@perigee} + \Delta V_{@apogee}$$

Table 4-7 shows the ΔV required to maintain the orbit given an initial set of orbital elements. A1, E1, R1P, and R1A are the semimajor axis, eccentricity, radius of perigee, and radius of apogee for an unperturbed orbit. A2, E2 and R2A represent the orbital parameters that exist at apogee if drag is not compensated for at the perigee. A3, E3, and R3P represent the orbital parameters that exist at perigee if drag is not compensated for at the apogee. As would be expected the lower the semimajor axis the more the ΔV required to maintain the orbit.

As is seen from Tables 4-4 and 4-5 the smaller the semimajor axis the more the drag affects the altitude deviation over the latitude range. Corrective propulsion becomes essential to maintaining the minimum altitude variation arc.

Table 4-7 IMPULSE REQUIREMENTS TO MAINTAIN THE ORBIT

E1 = .0026   ω = 76.0°   i = 63.44°   β = .04 x 10^{-6} km^2/kg

A1 (km)	A2 (km)	A3 (km)	E2	E3	R1P (km)	R1A (km)	R2A (km)	R3P (km)	ΔV_P m/sec	ΔV_A m/sec	ΔV_{Total} m/sec
6600	6599.41	6599.38	.00260	.00259	6582.84	6617.16	6616.47	6582.38	.457	.182	.639
6575	6573.74	6573.65	.00257	.00254	6557.91	6592.10	6590.61	6556.94	1.004	.342	1.346
6550	6546.77	6546.39	.00251	.00241	6532.97	6567.03	6563.21	6530.62	2.611	.657	3.269
6525	6511.21	6506.31	.00239	.00113	6508.04	6541.97	6526.79	6498.98	9.867	.912	10.779

E1 = .0036

A1 (km)	A2 (km)	A3 (km)	E2	E3	R1P (km)	R1A (km)	R2A (km)	R3P (km)	ΔV_P m/sec	ΔV_A m/sec	ΔV_{Total} m/sec
6600	6599.38	6599.34	.00358	.00357	6576.24	6623.76	6622.99	6575.79	.530	.140	.670
6575	6573.66	6573.53	.00355	.00352	6551.33	6598.67	6596.98	6550.40	1.200	.230	1.430
6550	6546.48	6545.90	.00345	.00333	6526.42	6573.58	6569.06	6524.12	3.260	.310	3.570
6525	6508.12	6496.84	.00311	.00085	6501.51	6548.49	6528.41	6491.29	13.850	4.570	18.420

CHAPTER V

SUN SYNCHRONOUS ORBITS

5.1 Sun Synchronous Orbits

Since the early 1960s the Sun synchronous orbit has been used for most every meteorological satellite as well as Earth Resources Technology satellites. Data from satellites in this type of orbit will generate most of the Earth resources data in the 1985-1995 time period [67]. This familiar orbit uses the precession of the orbit line-of-nodes caused by the Earth's oblateness to maintain a fixed angular orientation of the orbit plane relative to the Sun. The required precession, which depends upon the inclination and semi-latus rectum, is approximately .9856°/day. The Sun synchronous orbit condition occurs when the orbit nodal motion is equal to the motion of the Earth about the Sun. The orbital orientation is effectively frozen with respect to the Earth–Sun line. By careful execution of final insertion into the desired orbit the angle between the orbit node and the Sun's right ascension will remain nearly constant.

The Sun synchronous orbit is particularly suitable for Earth observation and remote sensing applications for the following reasons: (1) the satellite traverses each latitude at the same local time; the consequence is similar ground lighting conditions on each pass, (2) the majority of the Earth's surface can be mapped with near north–south contiguous swaths in a fixed period with repeatability, and (3) the average spacecraft solar array angle of incidence to the Sun remains within defined limits ensuring continuous electric power.

5.2 Sun Synchronous Degradation

Any perturbation which alters the orbit altitude or the orbit inclination promotes the loss of Sun synchronism. One primary source of synchronism degradation is atmospheric drag. The principal effect of drag is to reduce altitude and thereby cause period reduction. This orbit decay separates the corresponding tracks of two successive repeat cycles. Consequently, the tracks are no longer exactly overlaid. The study presented in reference 69 reports that for a satellite with an average ballistic coefficient initially at 678 km the loss in altitude after three months is .19 km. The loss in altitude induces a nodal sideslip. The sideslip results in a loss of in–orbit phasing of approximately 2.6 minutes which corresponds to an eastward movement in nodal crossing of 72.267 km. If corrections are made every three months, Sun synchronism may be considered as varying ±1.3 minutes about a mean node; an insignificant disturbance. The adjustment can be achieved by the two-impulse Hohmann transfer orbit. The ΔV required every three months would be about .0914 m/sec.

Another source of degradation is the gravitational force. A 1975 Goddard Space Flight Center study indicated that even zonal harmonics through order 4 and solar gravity dominated the nodal motion. For long periods it was shown that the orbit inclination and nodal orientation each exhibited an oscillatory behavior having the same period. The findings revealed a resonance exists between the inclination and the nodal motion [68].

5.3 The Nodal Motion

To study the long term nodal motion of Sun synchronous orbits it is sufficient for this investigation to determine the results to $O(J_2)$. The rate of change of the node from (2.17) is

$$\dot{\Omega} = {}^{-3n}/_2 \cos i \; J_2 \; ({}^{R}e/_p)^2 \qquad\qquad (5.1)$$

Let

Ω_c = the clock angle, the angle between the longitude of the ascending node and the mean Sun used computing the local time.

$\dot{\varnothing}_s$ = the desired precession rate of the longitude of the ascending node; the same rate as the apparent eastward movement of the Sun.

R_e = mean equatorial radius of the Earth

Start with the relationship

$$\dot{\Omega}_c = \dot{\Omega} - \dot{\varnothing}_s \qquad\qquad (5.2)$$

Differentiating (5.2) and remembering $\dot{\varnothing}_s$ = constant

$$\ddot{\Omega}_c = \ddot{\Omega} = {}^{3n}/_2 \sin i \; J_2 \; ({}^{R}e/_p)^2 \; {}^{di}/_{dt} \qquad (5.3)$$

Since the change in inclination due to even zonal harmonics is zero, the next area to investigate is the change due to solar gravitation. The mathematics of the gravitational effects of the Sun and Moon on near–Earth satellites was first developed by Musen, et al. in 1961 [70]. These results were later adapted to a more convenient form which allowed the disturbing function to be expressed in terms of osculating Keplerian elements for use in the equations of motion.

The complete gravitational disturbing function due to a body such as the Sun or Moon orbiting the Earth as derived by Kaula [71] is

$$R = \mu^* \sum_n \frac{a^n}{a^{*n+1}} \sum_{m,p,h,q,j} k_m \frac{(n-m)!}{(n+m)!} F_{nmp}\,(i)F_{nmh}(i^*)H_{npq}(e)G_{nhj}(e^*)$$

$$x \cos[(n-2p)\,\omega + (n-2p+q)M - (n-2h)\,\omega^* - (n-2h+j)M^*$$

$$+ m(\Omega - \Omega^*)] \qquad\qquad (5.4)$$

where F, H, and G are polynomials. For tables of $F_{nmp/h}$ and G_{nhj} see Kaula [12]. A table for H_{npq} is contained in reference 72. The elements of the disturbing body are designated by asterisks (see Figure 5.1). Also,

$$k_o = 1 \quad \text{and} \quad k_m = 2, \; m \neq 0$$

Examining the trigonometric expression, the terms likely to be significant are those of long period. When $n - 2p + q = 0$ the periodics in M are eliminated.

It is sufficient for this examination to restrict n to 2. Since both the G and H functions are power series in e and since the lead terms in both are of order $e^{|q|}$, reasonable accuracy can be achieved for the near circular orbit if $q = 0$. For a detailed discussion see Born [72].

If $q = 0$ and $n = 2$ then from $n - 2p + q = 0$, p must equal 1 considering only zero order terms in e. The controlling terms in the series expansion of the function G are the ones in which $j = 0$ (see table in reference 12).

NORTH VIEW

$$\Omega_c = \Omega^* + \omega^* + M^* - \Omega$$
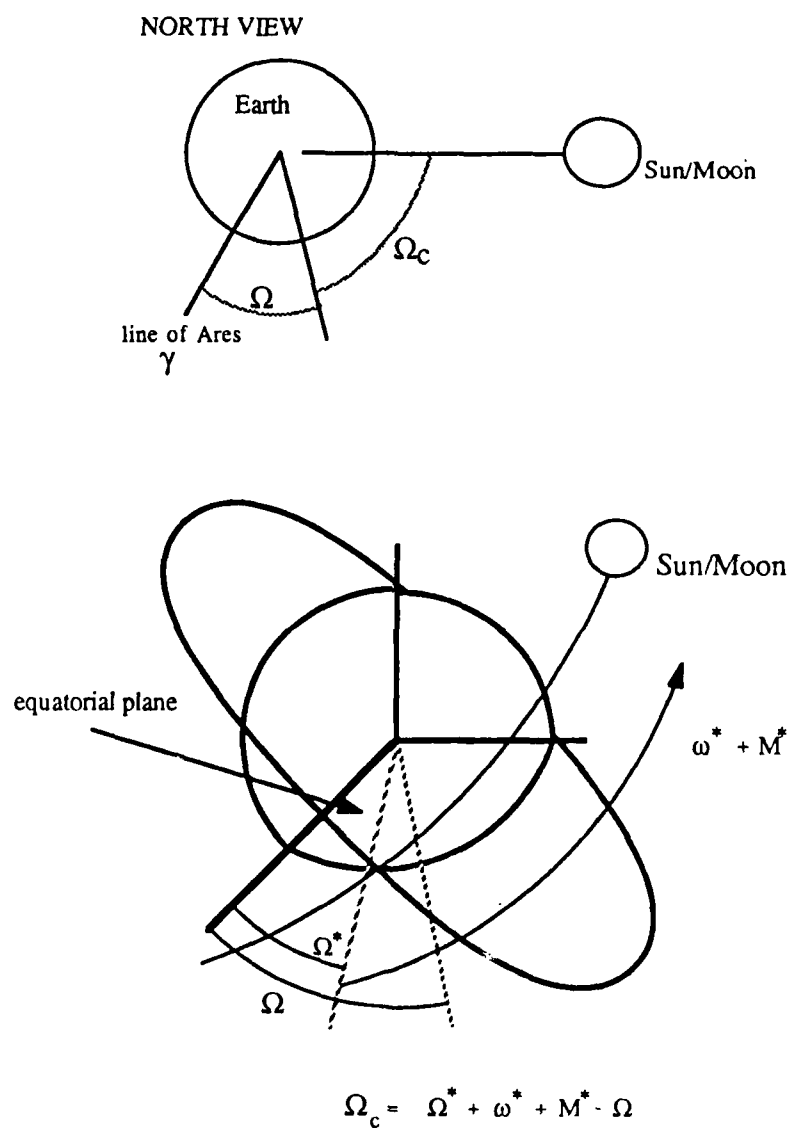
Figure 5.1 ANGLE RELATIONSHIPS WITH DISTURBING BODY

If $\propto$ = the argument of the trigonometric expression in (5.4) with the above values of the n, p, q, and j integers then

$$\dot{\propto} = [-(n - 2h)\dot{\omega}^* -(n - 2h)\dot{M}^* + m\dot{\Omega}] \qquad (5.5)$$

For Sun synchronism when the Sun is the disturbing force

$$(n - 2h) \dot{M}^* = m\dot{\Omega}$$

Therefore from (5.5)

$$n - 2h = m$$

For long term

$$n - 2h + j \neq 0$$

Since $n = 2$ and $j = 0$, $h \neq 1$

If $h = 0$ then $m = 2$

Substituting the determined values of the integers n, p, q, j, h, and m into (5.4)

$$R = \frac{\mu^* a^2}{12a^{*3}} F_{221}(i) F_{220}(i^*) H_{210}(e) G_{200}(e^*)$$

$$x \cos [2\omega^* - 2M^* + 2(\Omega - \Omega^*)] \qquad (5.6)$$

From the tables of F, G, and H

$$F_{220}(i^*) = 3(1 + \cos i^*)^2 / 4$$

$$F_{221}(i) = {}^3/2 \sin^2 i \qquad (5.7)$$

$$G_{200}(e^*) \text{ and } H_{210}(e) \approx 1$$

Expressing the change in inclination in terms of the disturbing function

$$\frac{di}{dt} = \frac{1}{(\mu a)^{1/2}(1 - e^2)^{1/2}\sin i} [\cos i \frac{\partial R}{\partial \omega} - \frac{\partial R}{\partial \Omega}] \qquad (5.8)$$

Substituting (5.7) into (5.6) and taking the appropriate partials

$$\frac{\partial R}{\partial \omega} = 0 \tag{5.9}$$

$$\frac{\partial R}{\partial \Omega} = \frac{-3\mu^* a^2}{16 a^{*3}} \sin^2 i \,(1 + \cos i^*)^2 \sin\,(-2(\omega^* + M^* + \Omega^* - \Omega)) \tag{5.10}$$

From figure 5.1 $\quad \Omega_c = \omega^* + M^* + \Omega^* - \Omega \tag{5.11}$

Substituting (5.9), (5.10), and (5.11) into (5.8) the change in inclination due to solar attraction is

$$\frac{di}{dt} = \frac{3\mu^*}{16 n a^{*3}} \sin i \,(1 + \cos i^*)^2 \sin\,(-2\Omega_c) \tag{5.12}$$

From IAU (1976) System of Astronomical Constants for the Sun

$i^* = $ solar obliquity $= 23.45°$

$\mu^* = 1.32715 \times 10^{11} \text{ km}^3/_{\text{sec}^2}$

$a^* = 1.49467 \times 10^8 \text{ km}$

Equation (5.12) compares exactly with the analytically averaged results found in reference 68 in which the model used consisted of even zonal harmonics through order 4 and solar gravitation.

The libration period of the node can now be found. For regions where drag is negligible and assuming that $\sin^2 i$ is approximately constant substituting (5.12) into (5.3)

$$\ddot{\Omega}_c = A \sin 2\Omega_c \tag{5.13}$$

where $\quad A = \dfrac{-9\mu^*}{32 a^{*3}} J_2 \,(\dfrac{R_c}{p})^2 (1 + \cos i^*)^2 \sin^2 i$

$p = a(1 - e^2)$

Equation (5.13) is in the form of the familiar pendulum equation and can be solved analytically using elliptic functions. The period is found to be

$$T = 2\pi \left[1 + \tfrac{1}{4}\sin^2 \Omega_{co} + \tfrac{9}{64}\sin^4 \Omega_{co} + \tfrac{25}{256}\sin^6 \Omega_{co} + ...\right]/(2c)^{1/2}$$

$$(5.14)$$

where $\quad \Omega_{co}$ = the initial clock angle

$$c = \frac{-9\mu^*}{32a^{*3}} J_2 \left(\frac{R_e}{p}\right)^2 (1 + \cos i^*)^2 \sin^2 i$$

The actual veracity of the findings in this section can be demonstrated by comparison with actual 1985 NORAD data.

Comparison #1: #11416 U- NOAA6   Weather Satellite

$t_1 =$	006.91066734 day	$t_2 =$	364.51214982 day
$i_1 =$	98.5704°	$i_2 =$	98.5375°
$e_1 =$	.0012005	$e_2 =$	.0011415
$a_1 =$	7187.775 km	$a_2 =$	7187.295 km
$\Omega_{C1} =$	110.56°	$\Omega_{C2} =$	106.52°
	(1922.24 L ascending node)		(1906.08 L)

From (5.12) $\quad ^{di}/_{dt} = \quad -.085139 \times 10^{-3}\ ^{deg}/_{day} \quad\quad ^{di}/_{dt} = -.070557 \times 10^{-3}\ ^{deg}/_{day}$

$$\Delta i_{Avg} = \quad -.077848 \times 10^{-3}\ ^{deg}/_{day}$$

$$\Delta t = \quad 357.6014825 \text{ days}$$

$$\langle \Delta i_{comp\ Avg} = -.02784° \quad vs. \quad \Delta i_{actual} = -.0329° \rangle$$

Comparison #2: #12553 - NOAA7   Weather Satellite

$t_1 =$	020.46132110 day	$t_2 =$	365.43820864 day
$i_1 =$	99.0262°	$i_2 =$	99.0747°
$e_1 =$	.001327	$e_2 =$	.0012216
$a_1 =$	7227.384 km	$a_2 =$	7226.827 km

$$\Omega_{C1} = 51.25° \qquad\qquad \Omega_{C2} = 60.25°$$

(1525 L ascending node) \qquad\qquad (1600.54 L)

From (5.12) $\quad di/dt = \quad .127187 \times 10^{-3} \; deg/day \qquad di/dt = .112291 \times 10^{-3} \; deg/day$

$$\Delta i_{Avg} = \quad .119739 \times 10^{-3} \; deg/day$$

$$\Delta t = \quad 344.9768875 \; days$$

$$\langle \Delta i_{comp \; Avg} = .0413° \quad vs. \quad \Delta i_{actual} = .0485° \rangle$$

Table 5–1   CLOCK ANGLE LIBRATION PERIOD
(initial orbital elements for NOAA6 and NOAA7 used)

Ω_{co} (deg)	NOAA6 Period (years)	NOAA7 Period (years)
0	24.070	24.233
15	24.489	24.655
30	25.823	25.997
45	28.219	28.409
60	31.479	31.692
75	34.540	34.774
90	35.823	36.065

To study the long term effect of lunar gravitation on the change in inclination the same steps are taken as were followed for the examination of solar gravitation. Using identical reasoning n = 2, q = 0, p = 1, and j = 0. The argument of the trigonometric expression in (5.4) is

$$\alpha = [(n-2p) \, \omega + (n-2p+q) \, M - (n-2h) \, \omega^* - (n-2h+j) \, M^* + m \, (\Omega - \Omega^*)]$$

$$(5.15)$$

Using these values for n, q, p, and j equation (5.8) becomes

$$\frac{di}{dt} = \frac{\mu^*}{\sin i \left(\frac{\mu}{a^3}\right)^{1/2}(1-e^2)^{1/2}a^{*3}} \sum_{m,h}^{n} m\, k_m \frac{(2-m)!}{(2+m)!}\, F_{2ml}(i)\, F_{2mh}(i^*)$$

$$\times\; H_{210}(e)G_{2h0}(e^*)\sin \propto \qquad\qquad (5.16)$$

where $\propto = [\ (2h-2)(\omega^*+M^*) +m\,(\Omega - \Omega^*)]$ \qquad\qquad (5.17)

Equation (5.16) can be written in the following form

$$\frac{di}{dt} = S \sin \propto$$

where S is the summation over the possible integer values of m and h. From the 1984 Astronomical Almanac the following is data for the Moon:

$e^* = .054900489$

$a^* = 3.84402 \times 10^5$ km

$\mu^* = .0048994 \times 10^6$ km^3/sec^2

$i^* =$ varies over an 18 year period from $18.32°$ to $28.58°$;

average value will be used in this study.

$\Omega^* =$ period of 18.6 years

$\omega^* =$ period of 8.9 years

$\Omega =$ period of 1 year

$M^* =$ period of 27.21222 days

Table 5-2 lists the values of S for the respective long term integers. For a complete listing of values of S containing all possible integer values m, p, h, and j see Appendix C.

Table 5-2 LUNAR GRAVITATIONAL EFFECT ON
NEAR-CIRCULAR ORBITS

n = 2, p = 1, j = 0, q = 0

m	h	S (deg/day)
0	0	0
0	0	0
1	0	$.186543 \times 10^{-4}$
1	2	$-.803530 \times 10^{-6}$
2	0	$.282902 \times 10^{-3}$
2	2	$.524913 \times 10^{-6}$

The only value that has an effect on (5.16) of the order of magnitude of that of the Sun's gravitational effect is $S = .282902 \times 10^{-3} \sin \propto$. From (5.17)

$$\sin \propto = \sin [-2 (\omega^* + M^* + \Omega^* - \Omega)] \qquad (5.18)$$

Since M* has a period of 27.21222 days this is the controlling orbital element and over a long period of time the other elements have little effect on the value of the trigonometric expression. Approximately once a month the value of the trigonometric term will have cycled through one period and the effects will cancel. Therefore, over the long term the effects of lunar gravitation can be ignored in comparison to the effects of the Sun.

5.4 Repeated Ground Track

For altimetry applications it is often desirable for the satellite to periodically repeat its ground track. This was accomplished by SEASAT A during its last month of operation and the Earth Observatory Satellite (EOS). Additionally, repeat ground tracks are planned for many altimeter missions now under consideration. Ground track repeatability is important for satellite science experiments which are correlated to ground measurements or which require multiple samplings over a particular point on the Earth. Repeating the track furnishes a predictable pattern of coverage and permits direct comparison of similar data taken at regular intervals.

Sun synchronous orbits permit the repetition to occur under similar lighting conditions. The interval of time during which Earth coverage is fully completed by a satellite is referred to as the *repeat cycle*, N, which is measured in days. The number of orbits during a repeat cycle is m, an integer. The value of N is constrained to be an integer if the initial track of a repeat cycle is required to be superimposed on the initial track of a previous cycle at the same time of day. Each combination of N and m is valid if it satisfies the requirement for periodicity and similar lighting conditions, complies with altitude restrictions (imposed by launch vehicle, experiment instrumentation, tracking, orbit adjustment, etc.), and achieves full Earth coverage. Full Earth coverage will result if the sensor swath width is adequate for the selected value of m.

If the requirements restrict the semimajor axis to a range of values the bounds on the mean motion and period of the orbit are determined. For this study

$$7115 \text{ km} \leq a \leq 7500 \text{ km. Therefore,}$$

$$n_{max} = \sqrt{\frac{\mu}{a^3}} = 5208.052°/\text{day} \Rightarrow T = 99.546 \text{ minutes}$$

$$n_{min} = 4812.223°/\text{day} \Rightarrow T = 107.734 \text{ minutes}$$

This in turn places limits on the number of revolutions per day.

$$13.367 < \# \text{ of revs} < 14.467$$

The desired range of semimajor axis translates into bounds on the number of revolutions per day.

If there is a requirement for a repeat cycle of N days it should be remembered that an integer number of revolutions are necessary. A fraction with the numerator as the number of revolutions in the repeat cycle time and the denominator as the whole number of days for the repeat cycle should be formed. This fraction which represents the number of revolutions per day must be within the determined limits. If the fraction is reducible, the repeat cycle is actually less than the desired N [73].

5.5 Nodal Distance

The first order gravitational term (J_2) is normally the most significant perturbation to the nodal period for near–Earth satellites. For orbital motion above 400 km (see Tables 4-4 and 4-5) the effect of atmospheric drag is much smaller than that introduced by J_2. Therefore, for the determination of the distance between consecutive ascending nodes in an Earth–fixed frame only the effects of J_2 will be considered here.

The *nodal period*, P_N, is the time necessary for the argument of latitude to go through 2π radians. The *anomalistic period*, P_A, is the time to go from perigee to perigee. Assuming no secular change in a, e, and i

$$\text{let} \qquad P_A = 2\pi \left(a^3/\mu \right)^{1/2} \qquad\qquad (5.19)$$

P_N can be obtained from the proportion

$$P_N = \left(\frac{2\pi}{2\pi + \dot{\omega} P_A} \right) P_A \qquad (5.20)$$

where

$\dot{\omega}$ = change in argument of perigee

$P_N = P_A$ in the absence of perturbations

Also, from references 56 and 74

$$D_N = P_N \; (\omega_e - \dot{\Omega}) \qquad (5.21)$$

where

D_N = distance between consecutive ascending nodes; nodal distance

$\dot{\Omega}$ = inertial nodal precession rate

ω_e = Earth rotation rate

Substituting (5.19) and (5.20) in (5.21) and simplifying

$$D_N = \frac{2\pi \left(\frac{a^3}{\mu}\right)^{1/2} (\omega_e - \dot{\Omega})}{1 + \dot{\omega} \left(\frac{a^3}{\mu}\right)^{1/2}} \qquad (5.22)$$

For this section, let

$p = (1 - e^2)^2$

$f = (1 - {}^5/4 \sin^2 i)$

R = radius of the Earth at the equator

$C = J_2 R^2$

m, N are defined in Section 5.4

Using equations (2.17) and (2.18) for ω and Ω to $O(J_2)$ and making the appropriate substitutions, the nodal distance for a perturbed orbit is

$$D_N = 2\pi \left[\frac{2 \left(\frac{a^7}{\mu}\right)^{1/2} p \, \omega_e + 3 \, C \cos i}{2a^2 p + 6 \, Cf} \right] \quad (5.23)$$

Rearranging (5.23)

$$2 \, D_N \, a^2 p - 4\pi \, (a^7/\mu)^{1/2} \, p \, \omega_e = 6\pi \, C \cos i - 6D_N \, Cf \quad (5.24)$$

Substituting $h^2 = a$ in (5.24)

$$\frac{4\pi p \, \omega_e}{\mu^{1/2}} h^7 - 2D_N \, ph^4 + 6C(D_N f - \pi \cos i) = 0 \quad (5.25)$$

One way to achieve the desired repeat cycle while taking into account the gravitational effects of J_2 is to determine the desired nodal distance for an unperturbed satellite. The semimajor axis that is necessary to achieve the same nodal distance under the influence of the gravitational perturbation can then be computed.

The steps to be taken are:

1. Compute the nodal distance for unperturbed motion as follows

$$P_A \text{ (mins)} = \frac{(24 \times 60)N}{m}$$

The semimajor axis for unperturbed motion is

$$a = (P_A{}^2 \, (60)^2 \, \mu \, / \, 4\pi^2)^{1/3}$$

$$D_N = P_N \, \omega_e = P_A \omega_e$$
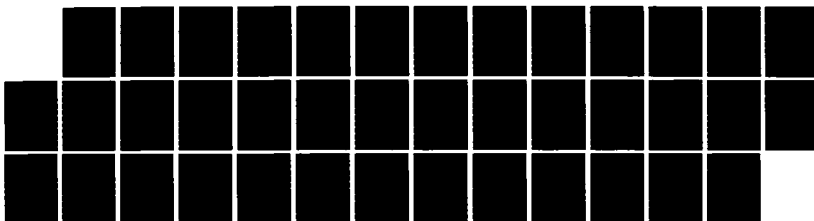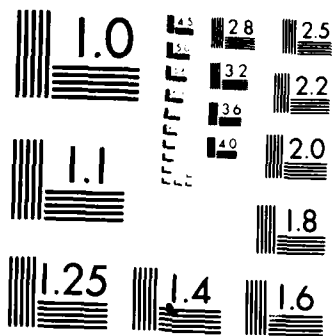
MICROCOPY RESOLUTION TEST CHART
NATIONAL BUREAU OF STANDARDS 1963-A

2. Given an eccentricity and inclination angle and using the required D_N in (5.25) solve the seventh order polynomial to determine the required semimajor axis.

3. If a Sun synchronous orbit is desired an iterative process will be necessary. For step #2 an approximate inclination angle can initially be used in (5.25) to determine a semimajor axis. The inclination angle is then computed using

$$i = \cos^{-1} [-4.7733 \times 10^{-15} (1- e^2)^2 a^{7/2}] \qquad (5.26)$$
$$(\text{assumes } \dot{\Omega} = .9856°/\text{day})$$

This inclination angle is then used in (5.25) and the process is repeated until the semimajor axis and inclination deviations are within desired tolerances.

4. The computed semimajor axis is used in (5.19) to determine the new anomalistic period.

5.6 16-Day Repeat Cycle

For a 16-day repeat cycle the fraction discussed in section 5.4 would have a denominator of 16. To satisfy the orbital semimajor axis criteria the number of revolutions per day must be between 13.367 and 14.467.

$$^{213}/_{16} < 13.367 \text{ revs/day} < {}^{214}/_{16}$$
$$^{231}/_{16} < 14.467 \text{ revs/day} < {}^{232}/_{16}$$

Since 213 revolutions in the 16 day period is less than 13.367 revs/day it is not acceptable. Additionally, 232 revolutions in 16 days would necessitate a lower semimajor axis than is allowable. Therefore,

$$214 \leq m \leq 231$$

Table 5-3 shows each fraction with a numerator between 214 and 231 and a denominator of 16. If the fraction is reducible the orbit does not qualify as a 16 day repeat cycle. Steps 1, 2, and 4 in the previous section are used for Table 5-3. The semimajor axes listed under the perturbed column are those required to yield the desired nodal distance for $e = .002$ and $i = 55.0°$.

Steps 1 through 4 are used to generate Table 5-4. The results show that for a Sun synchronous orbit influenced by gravitational perturbation the semimajor axis required to produce the desired nodal distance is approximately 10 km higher than the unperturbed semimajor axis.

Table 5-3 CHARACTERISTICS OF A 16-DAY REPEAT CYCLE
( ) = valid 16 day cycle   < > = semimajor axis

e=.002   i=55.0°

# Revs /16 days	Fraction	Repeat cycle (days)	UNPERTURBED Orbital Ht.(km)	UNPERTURBED Period (mins)	D_N (km)	PERTURBED Orbital Ht.(km)	PERTURBED Period (mins)
214	$13\,^{6}/16$	8					
215	$13\,^{7}/16$	(16)	1095.331 <7473.494>	107.163	2990.509	1051.501 <7429.664>	106.222
216	$13\,^{8}/16=^{27}/2$	2					
217	$13\,^{9}/16$	(16)	1049.325 <7427.488>	106.175	2962.938	1004.779 <7382.942>	105.221
218	$13\,^{10}/16=^{109}/8$	8					
219	$13\,^{11}/16$	(16)	1004.018 <7382.181>	105.205	2935.869	958.750 <7336.913>	104.239
220	$13\,^{12}/16=^{55}/4$	4					
221	$13\,^{13}/16$	(16)	959.417 <7337.580>	104.253	2909.302	913.422 <7291.585>	103.274
222	$13\,^{14}/16=^{111}/8$	8					
223	$13\,^{15}/16$	(16)	915.479 <7293.642>	103.318	2883.210	868.753 <7246.916>	102.327
224	$14=^{14}/1$	1					
225	$14\,^{1}/16$	(16)	872.210 <7250.373>	102.400	2857.592	824.749 <7202.912>	101.396
226	$14\,^{2}/16=^{113}/8$	8					
227	$14\,^{3}/16$	(16)	829.570 <7207.733>	101.498	2832.410	781.369 <7159.532>	100.482
228	$14\,^{4}/16=^{57}/4$	4					
229	$14\,^{5}/16$	(16)	787.500 <7165.663>	100.611	2807.668	738.567 <7116.730>	99.582
230	$14\,^{6}/16=^{115}/8$	8					
231	$14\,^{7}/16$	(16)	746.100 <7124.263>	99.740	2783.361	696.398 <7074.561>	98.698

Table 5-4 CHARACTERISTICS OF A SUN SYNCHRONOUS
16-DAY REPEAT ORBIT
< > = semimajor axis

e=.002	UNPERTURBED				PERTURBED		
# Revs 16 days	Orbital Ht.(km)	Period (mins)	Inclination (degs)	D_N (km)	Orbital Ht.(km)	Period (mins)	Inclination (degs)
215	1095.331 <7473.494>	107.163	99.918	2990.509	1106.610 <7484.773>	107.406	99.971
217	1049.325 <7427.488>	106.175	99.704	2962.938	1060.486 <7438.649>	106.414	99.756
219	1004.018 <7382.181>	105.205	99.497	2935.869	1015.062 <7393.225>	105.441	99.547
221	959.417 <7337.580>	104.253	99.296	2909.302	970.344 <7348.507>	104.486	99.345
223	915.479 <7293.642>	103.318	99.100	2883.210	926.294 <7304.457>	103.548	99.148
225	872.210 <7250.373>	102.400	98.912	2857.592	882.915 <7261.078>	102.627	98.958
227	829.570 <7207.733>	101.498	98.728	2832.421	840.166 <7218.329>	101.722	98.773
229	787.500 <7165.663>	100.611	98.550	2807.668	798.004 <7176.167>	100.832	98.594
231	746.100 <7124.263>	99.740	98.377	2783.361	756.481 <7134.644>	99.958	98.420

CHAPTER VI

GEOSYNCHRONOUS ORBITS

6.1 Geosynchronous Orbits

Geosynchronous satellites orbit approximately 36,000 km above the surface of the Earth at a speed of 3.07 km/sec. The term *geosynchronous* refers to an orbit that has a period equal to the period of rotation of the Earth relative to an inertial system. Consequently, the satellite is at rest with respect to the rotating Earth. This type of orbit is mainly used for communications missions, but has also been used by some Earth–observation missions and scientific missions.

A perfectly geosynchronous orbit would only be achievable if the Earth were perfectly symmetrical and no other forces were acting on the satellite except the central gravity attraction of the Earth. However, additional forces acting on the satellite do change the shape of the orbit, the orientation of the orbital plane, and the longitude. These changes can only be compensated for by active orbit control.

As of January 1, 1985, there were approximately 185 satellites that are considered near-stationary. These satellites are near–circular ($e \leq 0.1$), near–equatorial ($i \leq 10^\circ$), and have an orbital period close to one mean sidereal day (0.9 rev/day $\leq n \leq 1.1$ rev/day) [3].

6.2 Fundamentals

With the origin of the coordinate system at the center of mass of the Earth the

gravitational potential (2.11) can be expanded to include tesseral harmonics which are due to longitudinal variations in the shape of the Earth.

$$U = \frac{-\mu}{r} \left[1 - \sum_{n=2}^{\infty} J_n \left(\frac{R_e}{r}\right)^n P_n (\sin \phi) + \sum_{n=2}^{\infty} \sum_{m=1}^{\infty} J_{nm} \left(\frac{R_e}{r}\right)^n P_{nm}(\sin \phi) \right.$$

$$\left. \times \cos m(\theta - \theta_{nm}) \right] \qquad (6.1)$$

The double summation includes the longitude-dependent terms: r is the geocentric distance, θ is the geographic longitude, ϕ is the latitude, R_e is the mean equatorial radius of the Earth, θ_{nm} is the longitude in the direction of the principal axis of symmetry of the Earth's distribution accounted for by the nm harmonic, P_{nm} is the associated Legendre polynomial, and J_{nm} is the numerical coefficient characterizing the Earth's mass distribution [4].

Using a spherical coordinate system (figure 6.1) that is rotating at the same rate as the angular velocity of the Earth (ω_c) the force field F of the Earth on a point mass is:

$$\bar{F} = F_r \hat{e}_r + F_\phi \hat{e}_\phi + F_\theta \hat{e}_\theta \qquad (6.2)$$

where $\hat{e}_r$, $\hat{e}_\phi$, and $\hat{e}_\theta$ are unit vectors in their respective directions.

$$F_r = m \frac{\partial U}{\partial r} \qquad (6.3a)$$

$$F_\phi = \frac{m}{r} \frac{\partial U}{\partial \phi} \qquad (6.3b)$$

$$F_\theta = \frac{m}{r \cos \phi} \frac{\partial U}{\partial \theta} \qquad (6.3c)$$

91
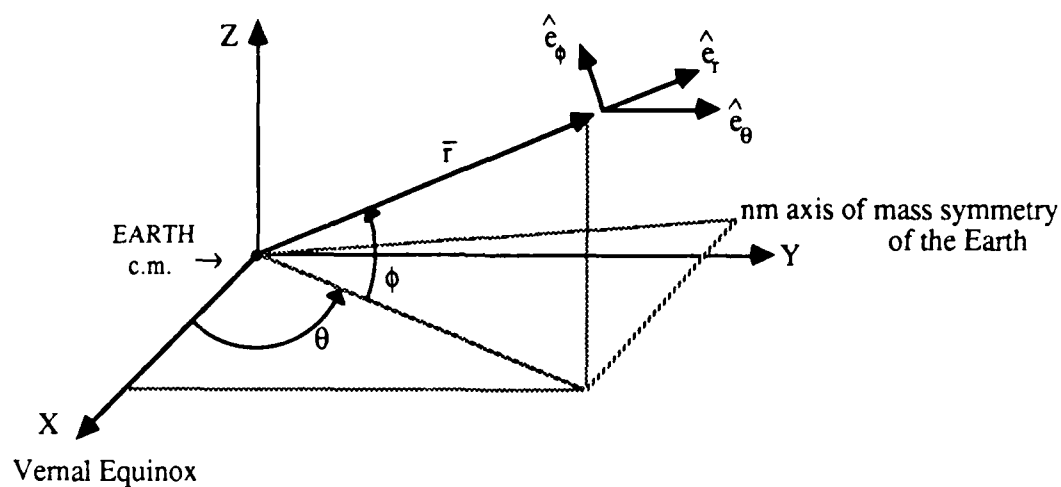
Figure 6.1   THE COORDINATE SYSTEM
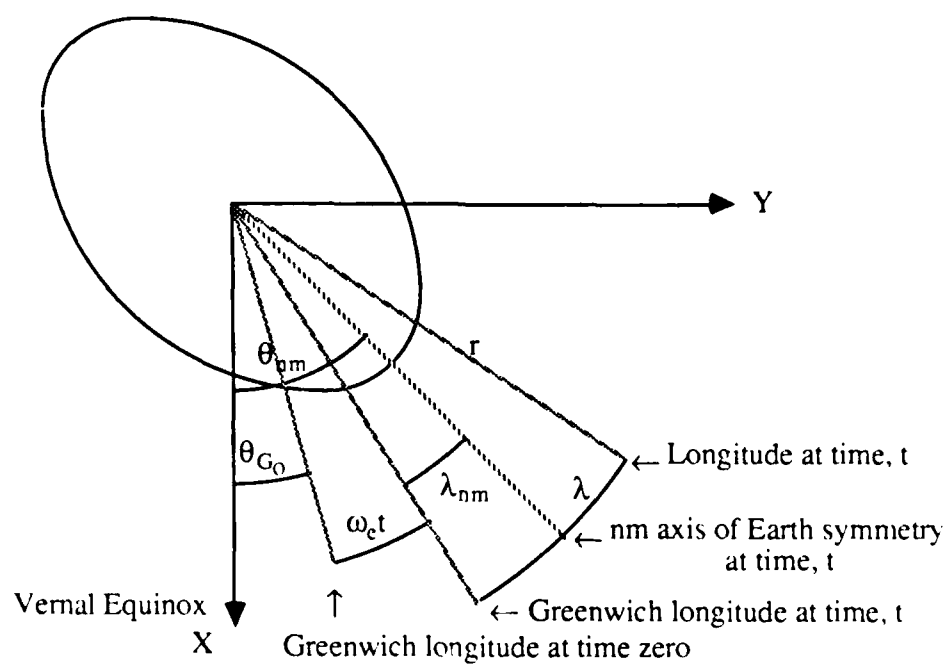
Figure 6.2   THE EARTH ELLIPSOID'S EQUATOR
WITH LONGITUDE REFERENCES
(North Pole looking south)

Figure 6.2 shows the ellipticity of the Earth's equator. λ is the geographic longitude of the satellite while λ_{nm} is the geographic longitude of the principal nm axis of Earth symmetry. It's seen that

$$\theta_{nm} = \theta_{G_o} + \omega_e t + \lambda_{nm} \qquad (6.4)$$

and $\qquad \lambda - \lambda_{nm} = \theta - \theta_{nm} \qquad (6.5)$

6-3 Equatorial Near–Circular Orbits

The short–period variations in r, ϕ, and θ are small for a geosynchronous orbit. On the equatorial plane there is a contribution to F_ϕ from the J_n terms with n odd and the J_{nm} terms with (n-m) odd. The effect is to displace the orbital plane slightly from the equatorial plane. The displacement due to J_3 is approximately 50 cm southwards from the equator. From this fact, F_ϕ can be ignored without introducing any meaningful error [41].

In addition, F_R can be ignored for this study. The effect of the zonal harmonics can be observed using (6.3a) The semimajor axis corresponding to synchronous motion is reduced by only .5 km if J_2 is ignored [41].

The tesseral harmonics primarily affect the tangential force F_θ. Although these forces are small, their long–term effects can be large when the motion of the satellite is commensurable with the Earth's rotation rate.

Employing an approach used by Allan (1963) the longitude acceleration can be determined. The total unperturbed energy of the satellite in a spherical Earth gravity field is

$$E = {}^{-\mu}/2a$$

therefore $\qquad dE = {}^{\mu}/2a^2 \ da \qquad (6.6)$

The energy change caused by the force acting on the satellite each day is approximately constant

$$dE = \int_0^{2\pi} \bar{F} \cdot a d\theta = 2\pi a \, \bar{F} \qquad (6.7)$$

For an orbit that is near–circular the averaged force ($\bar{F}$) per orbit is mainly the tangential perturbation force F_θ.

Substituting $F_\theta = \bar{F}$ in (6.7) and then equating the result with (6.6)

$$\mu/2a^2 \; da = 2\pi a \, F_\theta \qquad (6.8)$$

Solving (6.8) for da, recalling $\mu = n^2 a^3$, and using an orbital period of 1 sidereal day

$$da = {}^2/n \; F_\theta \qquad (6.9)$$

Starting with $\mu = n^2 a^3$ and using implicit differentiation

$$\dot{a} = {}^{-2\dot{n}a}/3n \qquad (6.10)$$

Differentiating $\dot{\theta} = n - n_o$ \qquad (6.11)

where n is the true mean motion and n_o is the mean angular velocity of the Earth

$$\ddot{\theta} = \dot{n} \qquad (6.12)$$

Substituting (6.12) in (6.10) and combining with (6.9)

$$\ddot{\theta} = {}^{-3}/a \ F_\theta \qquad\qquad (6.13)$$

It is seen from this equation that the apparent long–period acceleration θ is always opposite to the longitudinal force. Equation (6.9) shows that if the force is in the direction of motion (i.e. +) then the semimajor axis is increasing as is the energy. At the same time the mean motion and $\dot{\theta}$ are decreasing.

Since F_θ gives the long–period change in the semimajor axis, it also changes the period of the satellite. From Kepler's third law, the period of a 24-hour orbit is

$$T = 2\pi \ (a^3/\mu)^{1/2} \qquad\qquad (6.14)$$

Therefore

$$dT = 3\pi \ (^a/\mu)^{1/2} \ da \qquad\qquad (6.15)$$

Substituting (6.9) for da in (6.15) the change in period each day of a 24–hour near–circular orbit is given by

$$dT = 12\pi^2 \ (a^7/\mu^3)^{1/2} \ F_\theta \qquad\qquad (6.16)$$

If the present investigation is restricted to the dominant J_{22} term $m = n = 2$ in (6.1) and (6.3c) then substituting into (6.13) with $\phi = 0$, $r = a$, and $n = 2\pi$

$$\ddot{\theta} = A_{22} \sin 2 \ (\theta - \theta_{22}) \ {}^{rad}/\text{sid.day}^2 \qquad (6.17)$$

where $\qquad A_{22} = -72\pi^2 \ J_{22} \ (^{R_c}/a)^2$

The coefficient A_{22} is always positive if all the tesseral $J_{nn.}$ terms in the gravity potential are arbitrarily assigned as negative numbers. Equation (6.17)

represents the drift acceleration as a function of the longitude in a second-order gravity field for an equatorial synchronous satellite where F_θ is constant at every point in the orbit. Satellite data has shown that for eccentricities as high as .0012 the equation is extremely accurate. If θ is taken as the mean longitude of the ascending and descending nodes (6.17), with reasonable accuracy, represents the 24-hour drift regime for eccentricities as high as 0.3 [49].

The results of this approach compare exactly with those of the method completed by Kaula [12] in which the following resonating disturbing function was used

$$R = \sum_{(n-m)_{even}} Q_{nm} \cos m \left(\omega + M + \Omega - \lambda_{nm} - \theta_{G_0} \right) \qquad (6.18)$$

where Q_{nm} is a polymonial function of inclination, eccentricity, semimajor axis, and respective spherical harmonics (see page 50, reference 12). R can be exercised in the Lagrange planetary equation

$$\frac{da}{dt} = \frac{2}{na} \frac{\partial R}{\partial M}$$

The change in semimajor axis will cause an acceleration in the satellite's longitude which is defined by $\quad \lambda = \omega + M + \Omega + \theta_{G_0} \qquad (6.19)$

Using Kepler's law

$$M = ndt \implies \ddot{M} = \frac{dn}{dt}$$

Therefore

$$\ddot{\lambda} = \ddot{M} = \frac{\partial n}{\partial a} \frac{da}{dt} = \frac{2}{na} \frac{\partial n}{\partial a} \frac{\partial R}{\partial M} = \frac{-3}{a^2} \frac{\partial R}{\partial M} \qquad (6.20)$$

Taking the partial of R (6.18) with respect to M, using (6.19) and substituting in (6.20) the result is

$$\ddot{\lambda} = \frac{3}{a^2} \sum_{(n-m)_{even}} m \, Q_{nm} \sin m \, (\lambda - \lambda_{nm})$$

when $n = m = 2$

$$\ddot{\lambda} = \frac{6}{a^2} Q_{22} \sin 2 \, (\lambda - \lambda_{nm}) \qquad (6.21)$$

$$Q_{22} = 3n^2 \, a^2 \, J_{22} \, (R_{e/a})^2 \quad @ \quad i = 0° $$

letting $n^2 = 4\pi^2$

$$Q_{22} = -12\pi^2 \, a^2 \, J_{22} \, (R_{e/a})^2 \qquad (6.22)$$

Substituting (6.21) and (6.5) in (6.20)

$$\ddot{\theta} = \ddot{\lambda} = -72\pi^2 \, J_{22} \, (R_{e/a})^2 \sin 2 \, (\theta - \theta_{nm}) \qquad (6.23)$$

which is equivalent to (6.17).

Using (6.10) and (6.11)

$$\dot{\theta} = {}^{-3n/2a} \, da \qquad (6.24)$$

Solving (6.8) for da and substituting in (6.24) with $n = 2\pi$

$$\dot{\theta} = \frac{-12\pi^2 a^2}{\mu} F_\theta$$

Substituting for F_θ to second-order with $\phi = 0°$

$$\dot{\theta} = -24\pi^2 J_{22} (R_{e/a})^2 \sin 2 (\theta - \theta_{22})$$

$$\dot{\theta} = A_{22}/3 \sin 2 (\theta - \theta_{22}) \ ^{rad}/\text{sid. day} \qquad (6.25)$$

This represents the apparent net longitudinal drift rate of the 24-hour equatorial near-circular orbit's ground track with respect to the surface of the Earth.

6.4 Stable and Unstable Equilibrium Points

The actual tangential force on the satellite from (6.13) and (6.17) is

$$F_\theta = {}^{-a}/3 \ \ddot{\theta} = {}^{-a}/3 \ A_{22} \sin 2 (\theta-\theta_{22}) \qquad (6.26)$$

It is seen from this equation that the force vanishes when $\theta - \theta_{22} = {}^\pi/2 \ 1$ where $1 = 0$, 1, 2, and 3. These values correspond to the major and minor axes of the equatorial ellipse. The force is directed towards the nearest end of the major axis with the maximum value at the 45° points between the axes.
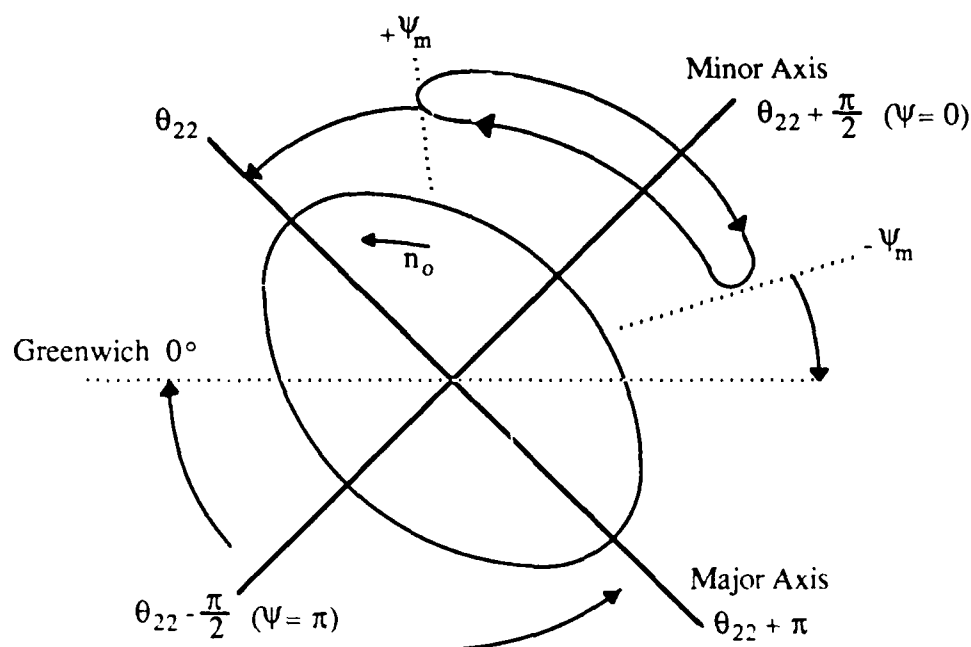
Figure 6.3 THE EQUILIBRIUM POINTS

Blitzer, et al., provided a mathematical derivation demonstrating that the two points on the minor axis are positions of stable equilibrium while those on the major axis are unstable points [39]. Later, Blitzer showed that when the entire spectrum of tesseral harmonics is included the equilibrium points were no longer symmetrically located on the extensions of the principal axes of the equatorial ellipse. The radial and latitudinal displacements from the symmetrical positions are negligible while the

longitudinal deviations can vary by $3°$ or more. The dominance of the J_{22} term still limits the number of equilibrium positions to four [44]. The stable longitudes are near $75°E$ and $105°W$ whereas the unstable longitudes are approximately $165°E$ and $15°W$ [41,75].

Since the stable equilibrium points exist along the minor axes, it is convenient to change the origin (see figure 6.3). Thus,

$$\psi = \theta - \theta_{22} \pm \pi/2$$

Equation (6.17) becomes

$$\ddot{\psi} = -A_{22} \sin 2\psi \qquad (6.27)$$

Multiplying (6.27) by $\dot{\psi}$ leads to a first integral which can be written as [41]

$$\dot{\psi}^2 - 2A_{22} \cos^2 \psi = C \qquad (6.28)$$

C is a constant of the motion which is determined by the initial conditions. From (6.28) it follows that $C \geq -2A_{22} \cos^2 \psi_0$. If the initial conditions are such that C is small, then ψ cannot go through a full cycle. If C is such that there is a maximum departure of ψ_m which is captured between $-\pi/2$ and $\pi/2$ then $\psi_m = 0$.

Therefore, from (6.28)

$$C = -2A_{22} \cos^2 \psi_m$$

and

$$\cos \psi_m = (C/-2A_{22})^{1/2} \qquad (6.29)$$

If the maximum value ψ_m achieves is $\pi/2$ then C must equal zero. If ψ_m is less than $\pi/2$ then $C < 0$.

Referring back to (6.28) with $C \leq 0$

$$\dot{\psi}_o{}^2 - 2A_{22} \cos^2 \psi_o \leq 0$$

Therefore,

$$|\dot{\psi}_o| < |(2A_{22})^{1/2} \cos \psi_o| \qquad (6.30)$$

If this condition is satisfied the satellite will oscillate in longitude about the stable equilibrium point. If not satisfied, the satellite circulates continuously around the Earth's longitudes. In addition, the maximum angle, $\pm\psi_m$, to which the satellite is confined in its oscillation is found from

$$\dot{\psi}_o{}^2 - 2A_{22} \cos^2 \psi_o = -2A_{22} \cos^2 \psi_m$$

Therefore,

$$\psi_m = \cos^{-1} \left[(\cos^2 \psi_o - \frac{\dot{\psi}_o{}^2}{2A_{22}})^{1/2} \right]$$

$$(6.31)$$

Using (6.28) with $\dot{\psi}_m = 0$

$$\dot{\psi}^2 = 2A_{22} (\cos^2\psi - \cos^2\psi_m) \qquad (6.32)$$

To find the period of the oscillation proceed in the following manner: substitute $\cos^2\psi = 1 - \sin^2\psi$ in (6.32) and solve for $\dot{\psi}$

$$\dot{\psi} = (2A_{22})^{1/2} (\sin^2\psi_m - \sin^2\psi)^{1/2}$$

let $\qquad k^2 = {}^1/\sin^2\psi_m$

therefore,

$$\dot{\psi} = d\psi/dt = (2A_{22})^{1/2} ({}^1/_{k^2} - \sin^2\psi)^{1/2}$$

$$(6.33)$$

Following the procedure used by Kaula [12] shift dt and functions of ψ to opposite sides of the equation

$$dt = \frac{k}{(2A_{22})^{1/2}} \left[1 - k^2 \sin^2 \psi\right]^{-1/2} d\psi$$

integrating

$$t = \frac{k}{(2A_{22})^{1/2}} \int_0^\psi \frac{d\psi}{[1 - k^2 \sin^2 \psi]^{1/2}} = \frac{k}{(2A_{22})^{1/2}} F(k, \psi)$$

$$(6.34)$$

where F is an elliptic integral of the first kind. The period of a complete oscillation becomes

$$T = \frac{4k}{(2A_{22})^{1/2}} F(k, \psi_m) \qquad (6.35)$$

As ψ_m approaches the unstable point of equilibrium the period increases with amplitude.

Since $\quad k = \dfrac{1}{\sin \psi_m} \qquad \Rightarrow \qquad k > 1$

In order to evaluate the resulting integral the following transformation can be used [76]

$$F(k, \psi_m) = k^{-1/2} F(^1/k, \sin^{-1} (k^{1/2} \sin \psi_m)) \qquad (6.36)$$

Substituting (6.36) in (6.35)

$$T = (^{8k}/A_{22})^{1/2} F(^1/k, \sin^{-1} (k^{1/2} \sin \psi_m))_{sid.days} \qquad (6.37)$$

Table 6-1 PERIOD OF OSCILLATION ABOUT THE STABLE EQUILIBRIUM POINT

$J_{22} = -1.7 \times 10^{-6}$ $\dot{\psi}_o = 0 \Rightarrow \psi_o = \psi_m$ (see 6.31)

$a = 42,163$ km $\gamma = \sin^{-1} (k^{1/2} \sin \psi_m)$

$i = 0°$ $A_{22} = 2.764 \times 10^{-5}$ rad/sid.day

ψ_m (deg)	γ (deg)	$(^{8k}/A_{22})^{1/2}$	F	T (days)
10	24.627	1291.041	.4299	555.03
20	35.791	919.916	.6292	578.79
30	45.000	760.833	.8044	612.01
40	53.297	671.023	.9839	660.19
50	61.073	614.676	1.1890	730.85
60	68.529	578.108	1.4507	838.66
70	75.784	554.991	1.8256	1013.21
80	82.920	542.117	2.4965	1353.40

6.5 Inclined Near–Circular Geosynchronous Orbits

This type of orbit has the following particular characteristics:

(1) The satellite crosses the equator twice a day
    – at the ascending and descending nodes.

(2) Excluding perturbations, the ground track is repeated.

(3) The ground track is a closed curve.

For an inclined 24–hour satellite the energy changing force on the satellite is no longer constant over a single orbit. A satellite in a near–circular orbit now describes a closed figure eight path over the Earth's surface centered on the equator.
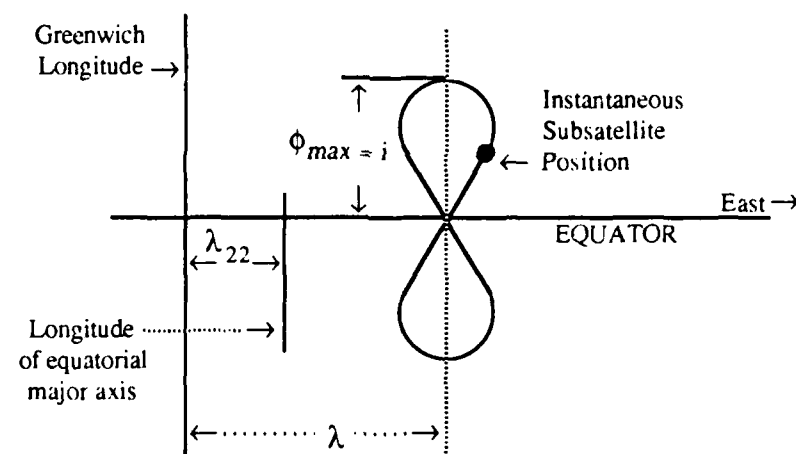
Figure 6.4 SATELLITE GROUND TRACK

At each point on the path the tangential force varies, as both the longitude and latitude change during the daily excursion. The force along the track is now composed of contributions from both latitude and longitude gravity perturbation forces. The zonal gravity forces have no net daily energy effect. For the inclined orbit the drift equations of motion will contain many small, short–period alterations introducing difficult non–linearities. To arrive at a theory for long–term drift motion Wagner [49] used a first approximation perturbation technique which smooths out the short–period effects and averages over the 24–hour period.

Using the tangential perturbing force (F_T) in place of F_θ in (6.13)

$$\ddot{\theta} = {}^{-3}/a \; F_T \qquad\qquad (6.38)$$

where $\qquad F_T \approx F_\phi \cos \propto + F_\theta \sin \propto$

$\propto$ = angle between a meridian plane and the orbital plane

and proceeding on the basis of the orbit–averaging theory established by Wagner in reference 49 an inclination factor can be determined. This factor is applied to the zero inclination regime to get the proper acceleration for the inclined satellite. The simple factor which is independent of the longitude is used to modify the equatorial regime.

The orbit–averaging modification gives the complete drift through $m = n = 4$ as

$$\ddot{\lambda} = -12\pi^2 \sum_{n=2}^{4} \sum_{m=1}^{n} C_{nm} F(i)_{nm} J_{nm} (\frac{R_e}{r})^n \sin m (\lambda - \lambda_{nm})^{rad}/{\rm sid.\ day}^2$$

$$(6.39)$$

where $C_{22} = 6$ $\qquad F(i)_{22} = \dfrac{(1+\cos i)^2}{4}$

$\qquad C_{31} = \dfrac{-3}{2}$ $\qquad F(i)_{31} = \dfrac{(1+\cos i)}{2} - \dfrac{5\sin^2 i\,(1+3\cos i)}{8}$

$\qquad C_{33} = 45$ $\qquad F(i)_{33} = \dfrac{(1+\cos i)^3}{8}$

$\qquad C_{42} = -15$ $\qquad F(i)_{42} = \dfrac{(1+\cos i)^2}{4} - \dfrac{7\sin^2 i\,\cos i\,(1+\cos i)}{4}$

$\qquad C_{44} = 420$ $\qquad F(i)_{44} = \dfrac{(1+\cos i)^4}{16}$

The contribution to the longitude acceleration of the inclined 24–hour near–circular orbit due to the 32, 41, and 43 harmonics is zero.

As was demonstrated in section 6.4 (see Table 6-1) the amplitude of the oscillation depends on the initial longitude. Figure 6.5 shows the amplitudes of the oscillations for orbits with an initial longitude of 75° from the stable point on the minor axis (75°E). The effect of inclination is to reduce the rate of change of the mean longitude and as a result, increase the period of the oscillation.
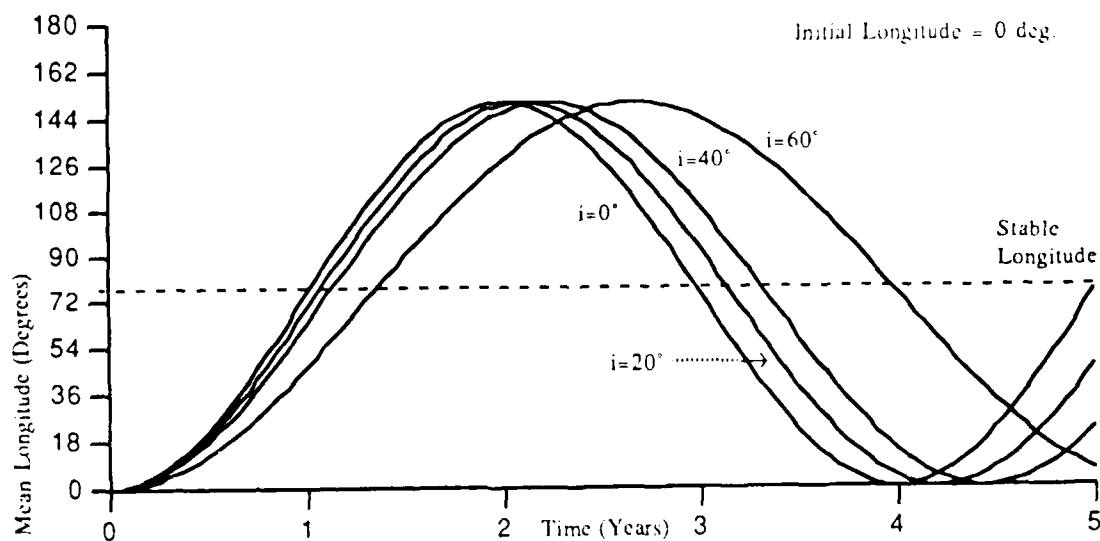
Figure 6.5 MEAN LONGITUDE VS. TIME [75]

Because of the increasing number of applications of the geosynchronous orbit, available space in the orbital arc is being depleted. The NASA Space Transportation System is expected to launch approximately 160 geosynchronous satellites between 1980 and 1990 [76]. These satellites need to have the proper separation to avoid physical and/or radio frequency interference. The geosynchronous arc of interest to the domestic U.S. is 55°W longitude and 135°W longitude. Extensive future traffic and the large amounts of arc needed for certain projects, such as space manufacturing, will promote the use of the inclined orbit. In addition, inclined geosynchronous orbits are useful for applications where there must be extended viewing time [75].

An enormous advantage of the inclined geosynchronous orbit is it allows several satellites to have the same figure eight ground track. They will cross the equator at the same longitude, called the *gateway*. The gateway may require only a few degrees of the geosynchronous arc, while accommodating up to 10-12 satellites [75].

6.6 Velocity Requirements for Orbit Maintenance

To maintain a satellite in a synchronous position other than the two stable positions it is necessary to do so with propulsion. To determine the ΔV required to offset the orbit perturbation consideration will be given only to in–plane corrections. The following assumptions are made for this study: (1) the orbit is near–circular so that ΔV in the radial direction is negligible as compared to the tangential component, and (2) there is no coupling between the in-plane and out–of–plane perturbations.

The orbit–averaged longitude drift of an inclined near–circular orbit to $O(J_{22})$ is obtained from (6.39)

$$\ddot{\lambda} = D_{22} \sin 2 (\lambda - \lambda_{22}) \; ^{rad}/sid.day^2 \qquad (6.40)$$

where

$$D_{22} = -72\pi^2 \, (R_{e/r})^2 \, J_{22} \, F(i)_{22}$$

Following the approach used in references 49 and 75 the above equation can be linearized in terms of the variation $\Delta\lambda$ defined by

$$\lambda = \lambda_s + \Delta\lambda \qquad (6.41)$$

where λ_s is the desired mean longitude of the ascending node. Substituting (6.41) into (6.40) and assuming $\Delta\lambda$ is small the result is

$$\ddot{\Delta\lambda} - [2D_{22} \cos 2(\lambda_s - \lambda_{22})] \, \Delta\lambda = D_{22} \sin 2(\lambda_s - \lambda_{22}) \qquad (6.42)$$

The complete solution to (6.42) is

$$\Delta\lambda = A \cos wt + B \sin wt - \tfrac{1}{2} \tan 2(\lambda_s - \lambda_{22}) \qquad (6.43)$$

where A and B are constants and $w = [-2D_{22} \cos 2(\lambda_s - \lambda_{22})]^{1/2}$.

To find the constants of integration it is assumed that there is no orbit injection error (i.e. $\Delta\lambda = 0$ and $\dot{\Delta\lambda} = 0$ at $t = 0$). The solution (6.43) becomes

$$\Delta\lambda = \tfrac{1}{2} \tan 2(\lambda_s - \lambda_{22})[\cos wt - 1] \qquad (6.44)$$

Equation (6.44) can be simplified by expanding cos wt and inserting the expression for w. The result is

$$\Delta\lambda = \frac{D_{22}\, t^2 \sin 2(\lambda_s - \lambda_{22})}{2} \tag{6.45}$$

In reference 49 it is shown that the rate of change of the near–circular radial distance satisfies the equation

$$\dot{r} = B_{22} \sin 2(\lambda - \lambda_{22}) \text{ length units}/\text{sid.day} \tag{6.46}$$

where

$$B_{22} = 24\pi r \,(R_{e/r})^2\, J_{22}\, F(i)_{22}$$

Equation (6.46) can be linearized in terms of the variation Δr defined by

$$r = r_s + \Delta r \tag{6.47}$$

Substituting into (6.46) the expressions for Δr and $\Delta\lambda$ and assuming $\Delta\lambda$ to be small

$$\Delta\dot{r} = B_{22} \sin 2(\lambda_s - \lambda_{22}) + 2B_{22} \cos 2(\lambda_s - \lambda_{22})\, \Delta\lambda \tag{6.48}$$

Substituting (6.45) into (6.48) and solving the differential equation

$$\Delta r = B_{22} \sin 2(\lambda_s - \lambda_{22}) \,[1 + \tfrac{1}{3}\, D_{22}\, t^2 \cos 2(\lambda_s - \lambda_{22})] \tag{6.49}$$

(the constant of integration is zero since $\Delta r = 0$ at $t = 0$).

To determine the ΔV required for station keeping (6.45) is used to compute the time of drift. At that time it will have a radial distance of $r_s + \Delta r$. For a near–circular orbit the velocity relative to inertial space is given by

$$V_1 = (r_s + \Delta r)\, \omega_e - r_s\, \dot{v} \tag{6.50}$$

where ω_e = Earth rotation rate

$\dot{v}$ = rate of change in true anomaly

To return the satellite to the original value of λ_s it will be necessary to transfer a near–circular orbit radius $r_s - \Delta r$ with a velocity V_2 relative to the inertial space given by

$$V_2 = (r_s - \Delta r)\,\omega_e + r_s\,\dot{v} \qquad (6.51)$$

Minimum energy expenditure would be achieved by a Hohmann transfer with $r_s + \Delta r$ being the apogee distance and $r_s - \Delta r$ the perigee distance. The transfer can be accomplished by applying an impulse ΔV_1 at time t_o.

$$\Delta V_1 = V_1 \left[\left(\frac{r_s - \Delta r}{r_s}\right)^{1/2} - 1 \right]$$

Since $\Delta r / r_s \ll 1 \Rightarrow \Delta V_1 \approx {}^{-1}/_2 V_1 \,\Delta r / r_s \qquad (6.52)$

At time t_o plus one half of a sidereal day a second impulse ΔV_2 is applied to slow the vehicle down to the desired velocity V_2.

$$\Delta V_2 = V_2 \left[1 - \left(\frac{r_s + \Delta r}{r_s}\right)^{1/2} \right] \approx {}^{-1}/_2 V_2 \,\Delta r / r_s \qquad (6.53)$$

The vehicle will move back towards the initial position λ_s as Δr increases to zero.

Substituting (6.50) into (6.52) and (6.51) into (6.53) and neglecting second and higher order terms of the small variations the following results

$$\Delta V_1 \approx {}^{-1}/_2 \,\Delta r \omega_e$$
$$\Delta V_2 \approx {}^{-1}/_2 \,\Delta r \omega_e$$

Therefore, the required ΔV for station keeping is

$$\Delta V = | \Delta V_1 | + | \Delta V_2 | = | \Delta r \omega_e | \qquad (6.54)$$

The period for the complete cycle can be determined from (6.45)

$$T = 2 \left[\frac{2\Delta\lambda}{D_{22} \sin 2(\lambda_s - \lambda_{22})} \right]^{1/2} \qquad (6.55)$$

Using (6.49), while neglecting the second term (due to order of magnitude), (6.45), (6.54) and (6.55) the velocity change per unit of operating time is therefore

$$\frac{\Delta V}{T} = \frac{\omega_e B_{22} \sin 2(\lambda_s - \lambda_{22})}{2} \qquad (6.56)$$

Figure 6.6 shows the in-plane velocity corrections necessary to compensate for longitude drift.
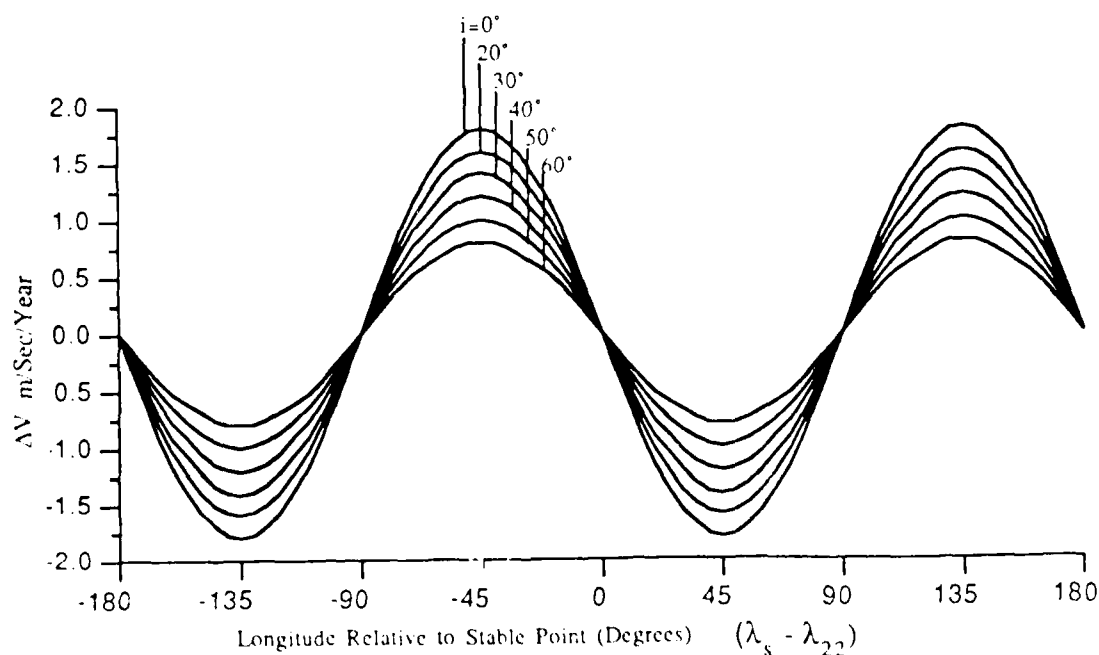
Figure 6.6 IN-PLANE VELOCITY CORRECTION
FOR LONGITUDE DRIFT

6.7 Solar Radiation Effects

This section is not intended to be a comprehensive study of the effects of solar radiation but rather an introduction to the complexity of the topic. Although the non-gravitational perturbation is usually small, for geosynchronous satellites with large solar collectors it could be substantial. For the Solar Power Satellite (SPS), the perturbation due to solar radiation was of the order of magnitude of gravitational terms due to the Sun, the Moon, and J_2. The major effect of this perturbation is oscillation of the eccentricity [37, 69, 77].

The perturbation equation for eccentricity in the Gaussian form is

$$\frac{de}{dt} = \frac{(1-e^2)^{1/2}}{na} \left[\sin v \, f_1 + \frac{2 \cos v + e(1+\cos^2 v)}{1+e \cos v} f_2 \right] \qquad (6.57)$$

where f_1 and f_2 are the radial and transverse components of the disturbing acceleration.

For near-circular orbits, $na \approx V$ (the velocity of the satellite) and since $e \ll 1$ (6.57) becomes

$$de/dt \approx {}^1/V \left[\sin v \, f_1 + (2 \cos v + e - e \cos^2 v) f_2 \right] \qquad (6.58)$$

To determine the value of f_1 and f_2 the following assumptions are made:

(1) the distance between the Sun and satellite is infinite; the parallax of the Sun is therefore negligible.

(2) the solar flux is constant along the orbit when there is no shadow; it is time independent.

(3) There is no re-radiation from the surface of the Earth.

The pressure, P, exerted by the electromagnetic radiation from the Sun is approximately 4.5×10^{-6} newton/m^2 [37]. The electromagnetic radiation pressure

exerts a force on the satellite proportional to its cross–section/mass ratio. Accurate modeling of the solar radiation acceleration is very difficult because the cross–section exposure to sunlight varies along the orbit. In addition, the acceleration ceases each time the satellite passes through the shadow of the Earth.

A convenient parameter to use is the *effective cross–section/mass ratio* defined by

$$\sigma = A/m \ (1+\epsilon) \qquad \text{typical values are of the magnitude } 10^{-2} m^2/kg$$
where

A = cross–sectional area

m = mass

ϵ = a factor determined from empirical data

Therefore,

$$f_1 = -P\sigma \cos s \sin i'$$

$$f_2 = P\sigma \sin s \sin i'$$

where s = the sidereal angle of the Sun

i' = angle between the direction of the Sun

and the orbit normal

Equation (6.58) becomes

$$de/dt = P\sigma/V \ [-\sin v \cos s \sin i' + (2 \cos v + e - e \cos^2 v) \sin s \sin i']$$

$$(6.59)$$

the factor P/V is approximately 1.298×10^{-4} kg/m^2

To use (6.59) the true anomaly at which the satellite enters and leaves the Earth's shadow must be known. The change in eccentricity over a period of time can then be obtained by numerical integration of the orbit. For the Solar Power Satellite with an area to weight ratio of 1.73 m^2/kg the max change in eccentricity over a year

varies between .025 and .042 depending upon inclination angle and the ascending node (see reference 75 for detailed figures and results). The motion of eccentricity is periodic with a period of one year.

To compensate for the change in eccentricity a variety of burn cycles can be used. If judiciously selected the burns can be accomplished in conjunction with the tangential burns (see section 6.6) performed for longitude station keeping.

REFERENCES

1. Danby, J.A. <u>Fundamentals of Celestial Mechanics</u>, The Macmillan Co., 1962.

2. Geyling, F.T. and Westerman, H.R., <u>Introduction to Orbital Mechanics</u>, Addison- Wesley Publishing Co., 1970.

3. Taff, L.G., <u>Celestial Mechanics, A Computational Guide for the Practitioner</u>, John Wiley and Sons, Inc., 1985.

4. Fitzpatrick, P.M., <u>Principles of Celestial Mechanics</u>, Academic Press, Inc., 1970.

5. Greenwood, D.T., <u>Principles of Dynamics</u>, Prentice-Hall, Inc., 1965.

6. Bate, R.R., Mueller, D.D., and White, J.E., <u>Fundamentals of Astrodynamics</u>, Dover Publications, Inc., 1971.

7. Herrick, S., <u>Astrodynamics, V1</u>, Van Nostrand Reinhold Co., 1971.

8. Smart, W.M., <u>Celestial Mechanics</u>, Longmans, Green and Co., 1953.

9. Sterne, T.E., <u>An Introduction to Celestial Mechanics</u>, Interscience Publishers, Inc., 1960.

10. McCuskey, S.W., <u>Introduction to Celestial Mechanics</u>, Addison-Wesley Publishing Co., 1963.

11. Brouwer, D. and Clemence, G.M., <u>Methods of Celestial Mechanics</u>, Academic Press, 1961.

12. Kaula, W.M., <u>Theory of Satellite Geodesy</u>, Blaisdell Publishing Co., 1966.

13. Musen, P., "The Influence of Solar Radiation Pressure on the Motion of an Artificial Satellite", <u>J. Geophys. Res.</u>, Vol. 65, 1960, p. 1391.

14. Jeffreys, H., <u>The Earth</u>, Cambridge University Press, London, 1952.

15. O'Keefe, J.A., Eckels, A., and Squires, R.K., "The Gravitational Field of the Earth", <u>The Astronomical Journal</u>, Vol. 64, No. 7, Sep. 1959, p. 245.

16. Tisserand, F., <u>Traité de Méchanique Céleste</u>, Vol. I, 1889.

17.   Kozai, Y., "The Motion of a Close Earth Satellite", The Astronomical Journal, Vol.64, Oct. 1959, p. 367.

18.   Kozai, Y., "The Gravitational Field of the Earth Derived From Motions of Three Satellites", The Astronomical Journal, Vol. 66, Feb. 1961, p. 8.

19.   King-Hele, D.G., "The Earth's Gravitational Potential, Deduced from the Orbits of Artificial Satellites", Geophys. Journal, Vol. 4, 1961, p. 3.

20.   King-Hele, D.G., Cook, G.E., and Rees, J.M., "Determination of the Even Harmonics in the Earth's Gravitational Potential", Geophys. Journal, Vol. 8, 1963, p. 119.

21.   King-Hele, D.G. and Cook, G.E., "The Even Harmonics of the Earth's Gravitational Potential", Geophys. Journal, Vol. 10, 1964, p. 17.

22.   King-Hele, D.G., Cook, G.E., and Scott, D.W., "Odd Zonal Harmonics in the Geopotential Determined Fourteen Well-Distributed Satellites", Planetary Space Sci., Vol. 15, 1967, p. 741.

23.   Kaula, W.M., "Determination of the Earth's Gravitational Field", Reviews of Geophysics, Vol. 1, No. 4, Nov. 1963, p. 507.

24.   Escobal, P.R., Methods of Orbit Determination, John Wiley and Sons, Inc., 1965.

25.   King-Hele, D.G., "The Gravity Field of the Earth", Royal Aircraft Establishment, Report No. TR78142, 1978.

26.   Brouwer, D. and Hori, G., "Theoretical Evaluation of Atmospheric Drag Effects on the Motion of an Artificial Satellite", The Astronomical Journal, Vol. 66, No. 5, June 1961, p. 193.

27.   Lane, M.H., "The Development of an Artificial Satellite Theory Using a Power-Law Atmospheric Density Representation", AIAA Paper No. 65-35, AIAA Second Aerospace Sciences Meeting, New York, N.Y., Jan. 25-27, 1965.

28.   Lane, M.H. and Cranford, K.H., "An Improved Analytical Drag Theory for the Artificial Satellite Problem", AIAA Paper 69-925, AIAA/AAS Astrodynamics Conference, Princeton, N.J., Aug. 20-22, 1969.

29.   King-Hele, D.G., Theory of Satellite Orbits In An Atmosphere, Butterworth and Co. Ltd., 1964.

30.   Zee, C.H., "Trajectories of Satellites Under the Combined Influence of Earth Oblateness and Air Drag", Celestial Mechanics, Vol. 3, No. 2, 1971, p. 148.

31.   Hoots, F.R., "Theory of the Motion of an Artificial Earth Satellite", Celestial Mechanics, Vol. 23, No. 4, 1981, p. 307.

32. Musen, P., Bailie, A., and Upton, E., "Development of the Lunar and Solar Perturbations in the Motion of an Artificial Satellite", NASA TN D - 494, Jan. 1961.

33. Kaula, W.M., "Development of the Lunar and Solar Disturbing Functions of a Close Satellite", The Astronomical Journal, Vol. 67, No. 5, 1962, p. 300.

34. Giacaglia, G.E.O., "Lunar Perturbations of Artificial Satellites of the Earth", Celestial Mechanics, Vol. 9, No. 2, 1974, p. 239.

35. Kozai, Y., "Effects of Solar-Radiation Pressure on the Motion of an Artificial Satellite", Smithsonian Astrophys. Obs. Special Report, No. 56, 1961.

36. Wyatt, S.P., "The Effect of Radiation Pressure on the Secular Acceleration of Satellites", Smithsonian Astrophys. Obs. Special Report, No. 60, 1961.

37. Soop, E.M., "Introduction to Geostationary Orbits", European Space Agency, Report No. 1053, 1983.

38. Cook, G.E., "Luni-Solar Perturbations of the Orbit of an Earth Satellite", Geophys. Journal, Vol. 6, 1962, p. 271.

39. Blitzer, L., Boughton, E.M., Kang, G., Page, R.M., "Effect of Ellipticity of the Equator on 24–Hour Nearly Circular Satellite Orbit", Journal of Geophysical Research, Vol. 67, No. 1, 1962, p. 329.

40. Iszak, I.G., "A Determination of the Ellipticity of the Earth's Equator from the Motion of 2 Satellites", The Astronomical Journal, Vol.66, No.5, 1961, p.226.

41. Allan, R.R., "Perturbations of a Geostationary Satellite by the Longitude-Dependent Terms in the Earth's Gravitational Field", Planetary Space Sci., Vol. 2, 1963, p. 1325.

42. Wagner, C.A., "The Drift of a 24–Hour Equatorial Satellite Due to an Earth Gravity Field Through 4th Order", NASA TN D-2103, Feb. 1964.

43. Wagner, C.A., "Determination of the Ellipticity of the Earth's Equator from Observations on the Drift of the Syncom II Satellite", NASA TN D-2759, May 1965.

44. Blitzer, L., "Equilibrium Positions and Stability of 24–Hour Satellite Orbits", Journal of Geophysical Research, Vol. 70, No. 16, 1965, p. 3987.

45. Frick, R.H., "Perturbations of a Synchronous Satellite Due to Triaxiality of the Earth", Journal of Aerospace Sciences, Vol. 29, 1962, p. 1105.

46. Blitzer, L., Kang, G., and McGuire, J.B., "The Perturbed Motion of 24–Hour Satellites Due to Equatorial Ellipticity", Journal of Geophysical Research, Vol. 68, 1963, p. 950.

47. Blitzer, L., "Satellite Resonances and Librations Associated with Tesseral Harmonics of the Geopotential", Journal of Geophysical Research, Vol. 71, No. 14, 1966, p. 3557.

48. Cook, G.E., "Perturbations of Near-Circular Orbits by the Earth's Gravitational Potential", Planetary Space Sci., Vol. 14, 1966, p. 433.

49. Wagner, C.A., "The Drift of an Inclined–Orbit 24–Hour Satellite in an Earth Gravity Field Through Fourth Order", NASA TN D-3316, 1966.

50. Merson, R.H., "The Motion of a Satellite in an Axi–Symmetric Gravitational Field", Geophys. Journal, Vol. 4, 1961, p. 17.

51. Kaplan, M.H., Modern Spacecraft Dynamics and Control, John Wiley and Sons, 1976.

52. Hoots, F.R., and Major, P E., "The Generalized Method of Averaging", CCZ Technical Note 76-1, Office of Astrodynamic Publications, 1976.

53. Garfinkel, B., "The Global Solution of the Problem of the Critical Inclination", Celestial Mechanics, Vol. 8, No. 1, 1973.

54. Liu, J.F., "A Second–Order Theory of an Artificial Satellite Under the Influence of Oblateness of the Earth", AIAA Paper No. 74-166, Feb. 1974.

55. Hassett, P.J., and Johnson, R.L., "Landsat-5 Orbit Adjust Maneuver Report", Computer Sciences Corporation Report TM-84/6075, 1984.

56. Cutting, E., Born, G.H., and Frautnick, J.C., "Orbit Analysis for SEASAT-A", The Journal of the Astronautical Sciences, Vol. 26, No. 4, 1978, p. 315.

57. Nickerson, K.G., Herder, R.W., and Glass, A.B., "Application of Altitude Control Techniques for Low Altitude Earth Satellites", AAS/AIAA Astrodynamics Conference, Grand Teton National Park, Wyoming, Sept. 7-9, 1977.

58. King-Hele, D.G. Theory of Satellite Orbits in an Atmosphere, Butterworth Mathematical Texts, London, 1964.

59. Wertz, J.R., Spacecraft Altitude Determination and Control, D. Reidel Pub. Co., 1984.

60. U.S. Standard Atmosphere, 1976, National Oceanic and Atmospheric Administration, 1976.

61. Vinh, N.X., Busemann, A., and Culp, R.D., Hypersonic and Planetary Entry Flight Mechanics, University of Michigan Press, 1980.

62. Hoots, F.R., "Theory of the Motion of an Artificial Earth Satellite", Celestial Mechanics, Vol. 23, 1981, p. 307.

63. Handbook of Mathematical Functions, U.S. Department of Commerce, National Bureau of Standards, 10th printing, December 1972.

64. Kalil, F., "Minimum Altitude Variation Orbits about an Oblate Planet", AIAA Journal, Vol. 1, No. 7, 1963, p. 1655.

65. Citron, S.J., _Elements of Optimal Control_, Holt, Rinehart, & Winston, Inc, 1969.

66. _Orbital Flight Handbook_, NASA SP-33, National Aeronautics and Space Administration, 1963.

67. Davies, R., Scott, M., Mitchell, C., and Torbett, A., "User Data Dissemination Concepts for Earth Resources", NASA CR-137904, 1976.

68. Duck, K.I., "Long–Period Nodal Motion of Sun Synchronous Orbits", Goddard Space Flight Center, 1975.

69. "Earth Observatory Satellite System Definition Study", Grumman Aerospace Corp., Bethpage, N.Y., 1974.

70. Musen, P., Bailie, A., and Upton, E., "Development of the Lunar and Solar Perturbations in the Motion of an Artificial Satellite", NASA TN-494, 1961.

71. Kaula, W.M., "Development of the Lunar and Solar Disturbing Functions for a Close Satellite", _The Astronomical Journal_, Vol. 67, No. 5, 1962.

72. Born, G.H., "The Derivaton of a General Perturbation Solution and Its Application to Orbit Determination", Aug. 1968.

73. Cooley, J.L., "Orbit Selection Considerations for Earth Observatory Satellites", Goddard Space Flight Center Report X-551-72-145, 1972.

74. Frautnick, J.C., and Cutting, E., "Flight Path Design Issues for the TOPEX Mission", AIAA-83-0197, Jan. 1983.

75. Graf, O.F., and Wang, K.C., "Mission Analysis Data for Inclined Geosynchronous Orbits,", _Analytical and Computational Mathematics, Inc._, NASA-CR-160702, 1980.

76. "NASA STS Mission Model: Payload Descriptions and Space Transportation System Cargo Manifests", Johnson Space Center Report JSC-13829, Oct. 1977.

77. Graf, O.F., "Orbit Motion of the Solar Power Satellite", ACM Technical Report TR-105, May 1977.

APPENDIX A

Table of First Ten Bessel Coefficient Derivatives:

$$2 J_1' (e) = 1 - \frac{3e^2}{8} + \frac{5e^4}{192} - \frac{7e^6}{9,216} + \frac{e^8}{81,920}$$

$$J_2' (2e) = e(1 - \frac{2e^2}{3} + \frac{e^4}{8} - \frac{e^6}{90} + \frac{e^8}{1,728})$$

$$J_3' (3e) = \frac{27e^2}{16} \left(1 - \frac{15e^2}{16} + \frac{189e^4}{640} - \frac{243e^6}{5,120} + \frac{2,673e^8}{543,440}\right)$$

$$J_4' (4e) = \frac{8e^3}{3} \left(1 - \frac{6}{5}e^2 + \frac{8e^4}{15} - \frac{8e^6}{63}\right)$$

$$J_5' (5e) = \frac{3,125}{768} e^4 \left(1 - \frac{35e^6}{24} + \frac{375}{448} e^8\right)$$

$$J_6' (6e) = \frac{243}{40} e^5 \left(1 - \frac{12e^2}{7} + \frac{135}{112} e^4\right)$$

$$J_7' (7e) = \frac{7(343)^2}{92,160} e^6 \left(1 - \frac{63e^2}{32} + \frac{3,773e^4}{2,304}\right)$$

$$J_8' (8e) = \frac{4,096e^7}{315} \left(1 - \frac{5e^2}{2} + \frac{32e^4}{15}\right)$$

$$J_9' (9e) = \frac{9^{10} e^8}{2^9 \, 9!} \left(1 - \frac{99e^2}{40}\right)$$

$$J_{10}' (10e) = \frac{9,765,625}{362,880} e^9$$

APPENDIX B

The Upper Atmosphere of the Earth [60]

ALTITUDE (km)	DENSITY (kg/km^3)	SCALE HEIGHT	ALTITUDE (km)	DENSITY (kg/km^3)	SCALE HEIGHT
150	2.076	16.321	480	7.208	61.543
160	1.233	19.194	490	6.127	62.047
170	7.815 -1	21.838	500	5.215	62.682
180	5.194	24.477	510	4.446	63.268
190	3.581	26.891	520	3.796	63.887
200	2.541	29.147	530	3.246	64.527
210	1.846	31.295	540	2.780	65.074
220	1.367	33.288	550	2.384	66.038
230	1.029	35.207	560	2.049	66.518
240	7.858 -2	37.086	570	1. ‹3	67.427
250	6.073	38.807	580	1..0	68.307
260	4.742	40.421	590	1.313	69.482
270	3.738	42.033	600	1.137	70.129
280	2.971	43.544	610	9.859 -5	71.428
‑90	2.378	44.915	620	8.571	72.591
300	1.916	46.291	630	7.468	73.913
310	1.552	47.461	640	6.523	75.320
320	1.264	48.717	650	5.712	76.842
330	1.035	50.030	660	5.015	78.616
340	8.503 -3	51.945	670	4.416	80.477
350	7.014	52.857	680	3.900	82.342
360	5.805	53.779	690	3.454	84.849
370	4.820	54.574	700	3.070	86.820
380	4.013	55.377	710	2.736	89.907
390	3.350	56.094	720	2.448	92.439
400	2.803	56.729	730	2.197	95.692
410	2.350	57.955	740	1.979	98.528
420	1.975	58.781	750	1.788	102.629
430	1.662	59.171	760	1.622	106.017
440	1.402	59.915	770	1.476	110.236
450	1.184	60.438	780	1.348	114.219
460	1.002 -3	60.719	790	1.235	119.677
470	8.492 -4	61.001	800	1.136	124.023

APPENDIX C

Lunar Gravitational Effect on Near–Circular Orbits

n	m	p	h	j	S (deg/day)	n	m	p	h	j	S (deg/day)
2	0	0	0	-1	$-.34637 \times 10^{-12}$	2	0	2	2	-1	$-.242457 \times 10^{-11}$
2	0	0	0	0	$.12618 \times 10^{-10}$	2	0	2	2	0	$.126178 \times 10^{-10}$
2	0	0	0	1	$.242457 \times 10^{-11}$	2	0	2	2	1	$-.346367 \times 10^{-12}$
2	0	0	1	-1	$.6670473 \times 10^{-11}$	2	1	0	0	-1	$-.795364 \times 10^{-11}$
2	0	0	1	0	$.810008 \times 10^{-10}$	2	1	0	0	0	$.289748 \times 10^{-9}$
2	0	0	1	1	$.6670473 \times 10^{-11}$	2	1	0	0	1	$.556755 \times 10^{-10}$
2	0	0	2	-1	$.2424568 \times 10^{-11}$	2	1	0	1	-1	$-.228331 \times 10^{-10}$
2	0	0	2	0	$.1261799 \times 10^{-10}$	2	1	0	1	0	$-.277267 \times 10^{-9}$
2	0	0	2	1	$-.346367 \times 10^{-12}$	2	1	0	1	1	$.761104 \times 10^{-11}$
2	0	1	0	-1	$.0$	2	1	0	2	-1	$-.239822 \times 10^{-11}$
2	0	1	0	0	$.0$	2	1	0	2	0	$-.124809 \times 10^{-10}$
2	0	1	0	1	$.0$	2	1	0	2	1	$.342603 \times 10^{-12}$
2	0	1	1	-1	$.0$	2	1	1	0	-1	$-.512061 \times 10^{-6}$
2	0	1	1	0	$.0$	2	1	1	0	0	$.186543 \times 10^{-4}$
2	0	1	1	1	$.0$	2	1	1	0	1	$.358442 \times 10^{-5}$
2	0	1	2	-1	$.0$	2	1	1	1	-1	$-.147001 \times 10^{-5}$
2	0	1	2	0	$.0$	2	1	1	1	0	$-.178506 \times 10^{-4}$
2	0	1	2	1	$.0$	2	1	1	1	1	$-.147001 \times 10^{-5}$
2	0	2	0	-1	$.34637 \times 10^{-12}$	2	1	1	2	-1	$-.15440 \times 10^{-6}$
2	0	2	0	0	$-.12618 \times 10^{-10}$	2	1	1	2	0	$-.803530 \times 10^{-6}$
2	0	2	0	1	$-.242457 \times 10^{-11}$	2	1	1	2	1	$.220570 \times 10^{-7}$
2	0	2	1	-1	$-.667047 \times 10^{-11}$	2	1	2	0	-1	$.570057 \times 10^{-11}$
2	0	2	1	0	$-.810008 \times 10^{-10}$	2	1	2	0	0	$-.207669 \times 10^{-9}$
2	0	2	1	1	$-.667047 \times 10^{-11}$	2	1	2	0	1	$-.399039 \times 10^{-10}$

n	m	p	h	j	S (deg/day)
2	1	2	1	-1	$.163651 \times 10^{-10}$
2	1	2	1	0	$.198724 \times 10^{-9}$
2	1	2	1	1	$.163651 \times 10^{-10}$
2	1	2	2	-1	$-.170333 \times 10^{-11}$
2	1	2	2	0	$-.886448 \times 10^{-11}$
2	1	2	2	1	$.243332 \times 10^{-12}$
2	2	0	0	-1	$-.144043 \times 10^{-10}$
2	2	0	0	0	$.524742 \times 10^{-9}$
2	2	0	0	1	$.100830 \times 10^{-9}$
2	2	0	1	-1	$.372278 \times 10^{-11}$
2	2	0	1	0	$.452065 \times 10^{-10}$
2	2	0	1	1	$.372278 \times 10^{-11}$
2	2	0	2	-1	$.187086 \times 10^{-12}$
2	2	0	2	0	$.973635 \times 10^{-12}$
2	2	0	2	1	$-.267265 \times 10^{-13}$
2	2	1	0	-1	$.776574 \times 10^{-5}$
2	2	1	0	0	$.2829024 \times 10^{-3}$
2	2	1	0	1	$.543602 \times 10^{-4}$
2	2	1	1	-1	$.200705 \times 10^{-5}$
2	2	1	1	0	$.243720 \times 10^{-4}$
2	2	1	1	1	$.200705 \times 10^{-5}$
2	2	1	2	-1	$.100863 \times 10^{-6}$
2	2	1	2	0	$.524913 \times 10^{-6}$
2	2	1	2	1	$-.144089 \times 10^{-7}$

n	m	p	h	j	S (deg/day)
2	2	2	0	-1	$-.197649 \times 10^{-10}$
2	2	2	0	0	$.720029 \times 10^{-9}$
2	2	2	0	1	$.138355 \times 10^{-9}$
2	2	2	1	-1	$.510825 \times 10^{-11}$
2	2	2	1	0	$.620305 \times 10^{-10}$
2	2	2	1	1	$.510825 \times 10^{-11}$
2	2	2	2	-1	$.256711 \times 10^{-12}$
2	2	2	2	0	$.133598 \times 10^{-11}$
2	2	2	2	1	$-.366730 \times 10^{-13}$

END

DTIC

9 – 86